CHALMERS
UNIVERSITY OF TECHNOLOGY

Offshore Wind Turbine Substructures at Intermediate Sea Depths

Preliminary design of a floating substructure and comparison with a fixed substructure

Master's thesis in Master Program Structural Engineering and Building Technology

Sofie Skorsdal
Daniel Tärbo

Department of Architecture and Civil Engineering

CHALMERS UNIVERSITY OF TECHNOLOGY
Gothenburg, Sweden 2023
www.chalmers.se

Master's thesis ACEX30

Offshore Wind Turbine Substructures at Intermediate Sea Depths

Preliminary design of a floating substructure and comparison with a fixed substructure

SOFIE SKORSDAL
DANIEL TÄRBO

CHALMERS
UNIVERSITY OF TECHNOLOGY

Department of Architecture and Civil Engineering
Division of Building Technology
Building Physics Group
Chalmers University of Technology
Gothenburg, Sweden 2023

Offshore Wind Turbine Substructures at Intermediate Sea Depths
Preliminary design of a floating substructure and comparison with a fixed substructure

SOFIE SKORSDAL & DANIEL TÄRBO

Supervisors: Christoffer Svedholm, ELU Konsult AB
Alexandre Mathern, NCC AB
Examiner: Rasmus Rempling, Department of Architecture and Civil Engineering

Department of Architecture and Civil Engineering
Division of Building Technology
Building Physics Group
Chalmers University of Technology
SE-412 96 Gothenburg
Sweden
Telephone +46 31 772 1000

Cover: Figure shows offshore wind turbines (Dingley, 2012)

Department of Architecture and Civil Engineering
Gothenburg, Sweden 2023

Offshore Wind Turbine Substructures at Intermediate Sea Depths
Preliminary design of a floating substructure and comparison with a fixed substructure

SOFIE SKORSDAL & DANIEL TÄRBO
Department of Architecture and Civil Engineering
Division of Building Technology
Building Physics Group
Chalmers University of Technology

Abstract

The demand for electricity is increasing and offshore wind farms have great potential to bridge this void. This thesis explores the potential of having floating offshore wind turbine substructures at sea depths between 30 and 60 m because of the limited studies in this area.

The study will provide a comparative analysis of a fixed lattice-based substructure and a floating semi-submersible substructure for a 5 and a 15 MW wind turbine. Furthermore, this thesis will address the various factors that need to be considered in the selection of the solutions and will cover a preliminary design of the two substructures. The preliminary design is based on simplified methods that can be used in the early stages. Focus lies on the analysis of global response and structural resistance as well as a brief frequency observation. Due to the complexity of the floating solution, this thesis aims to summarize and clarify the main theory behind them. In comparison to the floating substructure, the design method for the jacket substructure is more straightforward and well-documented. The main purpose of the preliminary design of the jacket substructure is to compare the material consumption and how it changes with the intermediate sea depths.

The results from the design iteration provide a deeper understanding of the overall behavior of the substructure and validate the applied simplified methods. Furthermore, the results show the need for design changes for varying depths for floating and fixed substructures. A floating substructure of the type semi-submersible is possible at intermediate sea depths. However, according to the preliminary design of this particular semi-submersible, it was less material efficient than the fixed jacket substructure.

Keywords: Substructures, Offshore wind turbine, Preliminary design, Intermediate depths, Floating substructure, Fixed substructure, Comparison, Jacket, Semi-submersible

Acknowledgements

As the culmination of our Master Programme in Structural Engineering and Building Technology at Chalmers University of Technology, this master thesis represents the final milestone. The research has been conducted in collaboration with ELU Konsult AB, NCC AB, and the Division of Building Technology at Chalmers University of Technology.

We would like to express our gratitude to Rasmus Rempling, our examiner at the Department of Architecture and Civil Engineering, for the opportunity to undertake this thesis.

We extend a special appreciation to our supervisor at ELU Konsult AB, Christoffer Svedholm, and to Alexandre Mathern from NCC AB for their invaluable support. Christoffer's extensive experience as a consultant and expertise in dynamic problems have greatly contributed to our project. Additionally, Alexandre's expertise in offshore wind turbines and simulation software has been important in our project. We would like to express our gratitude to ELU for granting us the use of their office space. Furthermore, we are grateful for the support given in the software Ashes by the developers from Simis.

Finally, we would like to praise our opponents for their commendable collaboration during the spring season. Your valuable feedback has significantly contributed to the enhancement of this thesis.

Sofie Skorsdal & Daniel Tärbo, Gothenburg, June 2023

Contents

List of Figures

List of Tables

List of Acronyms

1P	Rotor induced vibrations at hub level
3P	Blade shadowing effect
ALS	Accidental limit state
BEM	Beam Element Momentum
CC	Center-to-center
DNV	Det Norkse Veritas
EOG	Extreme operating gust
ESS	Extreme sea state
ETM	Extreme turbulence model
EWC	Extreme wind conditions
EWH	Extreme wave height
FEM	Finite Element Method
FLS	Fatigue limit state
HHT	Hillber-Hughes-Taylor
IEA	International Energy Agency
IEC	International Electrotechnical Commission
ISO	International Organization for Standardization
NREL	National Renewable Energy Laboratory
NSS	Normal sea state
NTM	Normal turbulence model
NWC	Normal wind conditions
OC3	Offshore Code Comparison Collaboration 3
OC4	Offshore Code Comparison Collaboration 4
OWT	Offshore wind turbine
PSD	Power spectral density
RNA	Rotor-nacelle assembly
RPM	Revoulutions per minute
SLS	Service limit state
SSS	Severe sea state
TLP	Tension-leg platform
TP	Transistion piece
ULS	Ultimate limit state

List of Notations

Roman upper case letters

A	Cross-sectional area	m^2
A_n	Amplitude of wave	m
A_γ	Normalizing factor	$-$
A_R	Rotor swept area	m^2
A_w	Water plane area	m^2
C_a	Wave added mass coefficient	$-$
$C_{D.wind}$	Wind drag coefficient	$-$
$C_{D.wave}$	Wave drag coefficient	$-$
C_m	Wave inertia coefficient	$-$
C_r	Restoring coefficient	Nm
C_T	Thrust coefficient	$-$
D	Diameter	m
E	Young's modulus	Pa
F_{1P}	Mass imbalance force	N
F_{3P}	Drag force from 3P load	N
F_B	Buoyancy force	N
F_{drag}	Drag force	N
F_g	Gravitational force	N
F_{Th}	Thrust force	N
F_{wave}	Wave force per unit length	N
H	Wave height	m
H_s	Significant wave height	m
I_m	Mass imbalance	$kg \cdot m$
I_T	Transversal moment of inertia	m^2
L	Line length	m
L_U	Integral scale length	m
M_{heel}	Heel moment	Nm
R	Radius to hub	m
R_m	Anchor radius	m
R_{max}	Longest anchor radius length	m
R_{mean}	mean anchor radius length	m
R_{min}	Shortest anchor radius length	m

S_{1P}	1P spectral density	W/Hz
S_{3P}	3P spectral density	W/Hz
S_J	JONSWAP spectral density	W/Hz
S_member	Stiffness spring member	N/n
S_node	Stiffness spring node	N/m
S_{PM}	Pierson-Moskowitz spectral density	W/Hz
S_U	Kaimal spectral density	W/Hz
T	Wave period	s
Th_{dyn}	Dynamic thrust force	N
Th_{stat}	Static thrust force	N
$V_{submerged}$	Submerged volume	m^3
$\overline{U}$	Mean wind speed, 10 min	m/s
$U(z)$	Wind profile along z-axis	m/s
U_r	Relative velocity of flow	m/s
U_{ref}	Reference wind speed	m/s
$\dot{U}_S$	Acceleration of the structure	m/s^2
$\dot{U}U_W$	Acceleration of flow	m/s^2

Roman lower case letters

d	Sea depth	m
$f_{1P.max}$	Maximum frequency in rotor rpm range	Hz
f_y	Yield strength	Pa
g	Gravitational constant	m/s^2
h	Sea depth between fairlead and seabed	m
h_f	Fairlead height	m
h_{sea}	Sea depth	m
k	Wave number	$-$
m	Mass	kg
r	Radius	m
t	Time	s
u	Fluctuating wind speed component	m/s
x	Distance of wave propagation	m
z	Position along z-axis	m
z_B	Center of buoyancy	m
z_g	Center of mass	m
z^n_{node}	Distance from node to sea surface	m
z^{tot}_{node}	Sum of distance from two nodes	m
z_r	Hub height	m
z_s	Distance positive upwards from the mean free surface elevation	m

Greek lower case letters

α	Power law exponent	-
ϵ	Phase angle	deg
ϵ_a	Energy tolerance	$-$
η	Mean free surface elevation	m
λ	Wave length	m
λ_R	Proportional stiffness Rayleigh damping	$-$
μ_R	Proportional mass Rayleigh damping	$-$
ρ_a	Density of air	kg/m^3
ρ_w	Density of seawater	kg/m^3
σ	Spectral width parameter	$-$
σ_U	Standard deviation of wind speed	m/s
θ_{heel}	Steady-state pitch	deg
γ	Non-dimensional peak shape parameter	$-$
ω	Angular wave frequency	rad/s
ω_p	Angular spectral peak frequency	rad/s

1
Introduction

This report is a master thesis in the master program Structural Engineering and Building Technology at Chalmers University of Technology. The project has been carried out at ELU Konsult AB and together with NCC AB.

1.1 Background

The demand for electricity is rising rapidly and the global need for increased electricity supply remains a significant concern. Global electricity consumption was 23 031 TWh in the year 2018 (International Energy Agency, 2019). IEA also states that the demand is expected to increase by 30 % to 2030 and 20 % between 2030 and 2040. Because of the consumption increase as well as the transition from non-renewable energy sources the demand for renewable energy sources is high on the agenda.

One of the most common renewable energy sources is wind power which has grown rapidly since the beginning of the 21 century (International Renewable Energy Agency, 2019a). The development has mainly been for onshore wind turbines but looking forwards, offshore have the greatest possibilities for many reasons. One of the advantages is more consistent wind and higher wind speed which leads to an increase in the production of electricity (Bureau of Ocean Energy Management, 2023). The total global offshore turbine capacity currently under operation is about 50.6 GW (Musial et al., 2022a). To put this into perspective, the offshore turbine capacity in 2018 was 4 % of the onshore capacity (International Renewable Energy Agency, 2019b). The estimation for 2024 is that offshore turbine capacity has increased to 10 % of onshore capacity.

Another advantage is the development of larger wind turbines. The electricity output has increased from 0.2 MW in 1990 and up to 4 MW in 2020 for onshore wind turbines (Hartman, 2022). Hartman claims that the reward for larger wind turbines is higher offshore and today 6 MW turbines are common and 17 MW turbines are expected in the near future. Figure 1.1 shows a 5 MW turbine and a 15 MW turbine along with the Eiffel tower as a reference to easier comprehend the sizes of the wind turbines. To grasp the magnitude in capacity, a 17 MW offshore wind turbine provides electricity to approximately 17 000 households under a year.

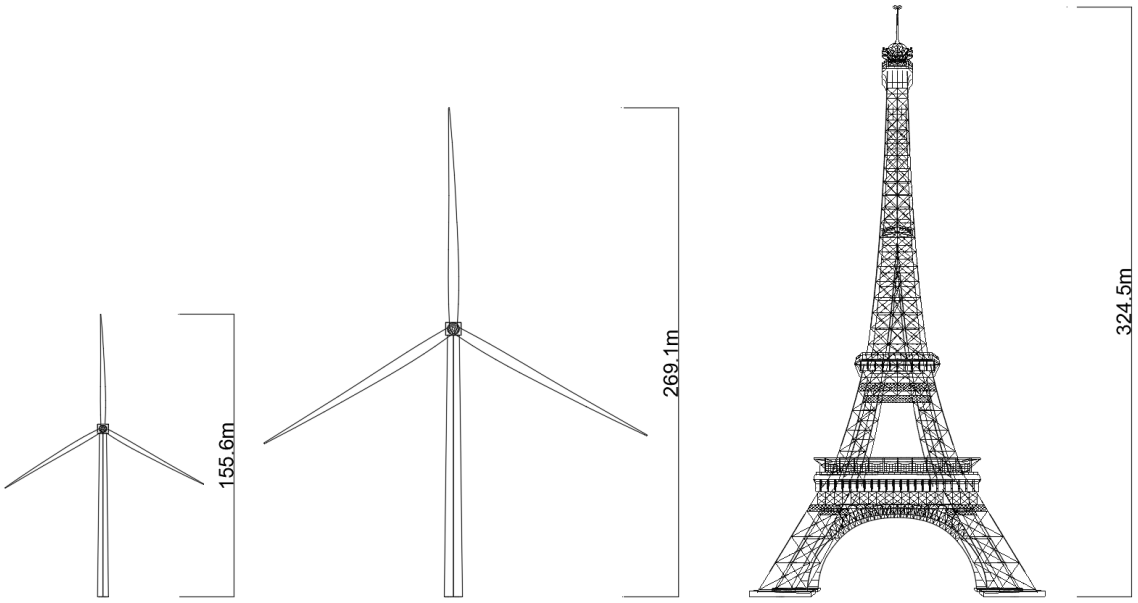

Figure 1.1. *Size comparison for, from left to right, a 5MW OWT, a 15 MW OWT and the Eiffel tower.*

The open ocean also provides large new areas where possible wind farms can be installed, which won't cause disturbance to the local population when it comes to not only noise but also the view of the landscape. This makes offshore wind turbines more acceptable by Society. In a study in Ireland the conclusion was that 87 % of the people who participated in the study were positive or neutral to offshore wind turbines (Cronin et al., 2021). Another study presents that offshore turbines are more accepted by public opinion according to results from Sweden and Denmark (Lamy et al., 2020). These studies show that offshore wind turbines have an edge compared to onshore wind turbines.

An offshore wind turbine (OWT) consists of three main components, a turbine, a substructure and a foundation. The OWT substructures can be categorized into two different systems: fixed and floating. Within these categories, there are several different types and each has its own benefits for different sea depths and environmental aspects such as soil conditions. The fixed types are typically gravity, pile, or lattice-based, while the floating can be sorted into groups of buoyancy, tension mooring lines, and ballast.

The choice between fixed and floating substructure is highly dependent on the sea depth. In the published book that concerns the design of offshore wind turbines does professor Bhattacharya (2019) outline the water depth and different types within the categories that are commonly applied today, but highlight that there are site-specific factors that influence which type of support are most suitable. The limit between fixed and floating is about 60 m today, even though floating types are able to be installed at lower depths. This limit builds on two main reasons; the feasibility of the fixed substructure where it gets oversized for larger depths than 60 m and

the higher expenses the floating supports generates, due to the more complex infrastructure the solution needs to support them. There is limited research on additional factors influencing the adaptability of floating substructures at depths below 60 m.

The sea depth for floating substructures is in principle only limited to their draft, which would make some of the substructure types suitable for lower depths than 60 m. Many sites around the world have depths far greater than 60 m and are forced to go for the floating solution, as the demands goes up the expenses will go down. With a broaden knowledge of floating substructures, increased manufacturing and overall widened infrastructure concerning the floating solution will reduce the overall expenses of floating substructures. This can be seen in the project of Hywind Scotland, where it was achieved a 60-70 % cost reduction compared to the Hywind Demo project in Norway (Equinor, 2022). Reuters Events (2019) writes that the petroleum refining company Equinor estimated in 2019 that the next project Hywind Tampen will reduce the cost by a further 40 % compared to Hywind Scotland which has been operating since 2017. Musial et al. (2022b) have summarized global prediction of the LCOE (Levelized Cost of Energy) for floating wind projects from 2020 onward to 2035 where reduction is even above 40 %.

When planning for future investments in OWT farms there is of essence to look at the influencing factors concerning economics as well as sustainability. The main components influencing the finances of an OWT are the turbine, substructure, foundation, assembly and installation, electrical infrastructure, maintenance, and soft costs including for example contingency, and insurance. Where the substructure and foundation stand for between 20.1-27 % of the investment dependent on fixed or floating solution (Stehly et al., 2019).

There are several points of view to work towards a sustainable future for the OWT industry. Choosing the most suitable substructure and foundation to fit the site conditions is a major key to increase the material efficiency (Bhattacharya, 2019). Low maintenance on the substructure and foundation and a longer lifetime for the turbine will generate a more durable solution, this together with recycling will be of essence to keep the life cycle of OWT sustainable (Li et al., 2022).

1.2 Aim

The aim is to analyze the potential of floating substructures at intermediate water depths. Primarily in regard of structural mass (stel and concrete) in comparison to a fixed substructure. The analyze also aims to investigate how the design alters between different depths and turbine sizes.

1.3 Objectives

In order to compare the fixed and floating offshore wind turbine substructures the following objectives are established.

- Explore floating and fixed offshore wind turbine substructure and their differences at intermediate sea depth. Select one of each type for preliminary design.
- Review loads, theories, and models connected to offshore wind turbines.
- Establish design methods for preliminary design for each substructure type.
- Preliminary design of a substructure of each type at intermediate sea depths for a 5 MW turbine and at 40 m sea depth for a 15 MW turbine.
- Compare the floating and fixed substructure regarding structural mass

1.4 Limitations

The studied substructure types do not cover all possible different solutions. Comparison between the fixed and floating substructures is limited to examining one substructure from each category. Furthermore, the comparison between substructures is entirely based on the structural mass of the main components. The following limitations are applied in the preliminary design:

- One fixed substructure and one floating substructures are preliminary designed
- One design configuration of the selected substructures are preliminary designed
- No design in fatigue limit state and accidental limit state
- No detailing design, such as connections, welds, and reinforcement
- The loads applied are limited to wind, wave, 1P, and 3P
- Five simplified load cases are applied
- The preliminary design does not include a complete optimization of the main components in regard to material efficiency

1.5 Method

The thesis is divided into two parts where the first part includes a literature study and the second part includes a case study with numerical analysis.

In the first part, a literature study was performed that aimed to explore the field around OWTs. Particular focus was given to the various substructures. The study was done to map the existing types of solutions and understand the overall difference between them. Furthermore, the literature study continued with the aim to understand which loads, theories, and models are applicable for a preliminary design of OWT substructures.

The second part of this thesis was to perform a case study at a location with intermediate sea depths. Environmental data for the case study were established and tower data for the 5 and 15 MW turbines were defined. Furthermore, one substructure from each category of fixed and floating was selected. A design method for each of the substructures is established and contains several iterations. A reference case was used as an initial assumption in the design method as well as to verify the numerical model. The design method iteration included:

- Define an initial geometry based on a reference case, stability, and assumptions in MATLAB
- Simulate the OWT in a time domain analysis in Ashes
- Control the global response of the OWT in MATLAB
- Analyze the structural resistance of the substructure in MATLAB
- Study the natural frequencies of the substructures in Ashes

A convergence analysis was performed for the floating substructure. The purpose was to analyze which simplifications were possible in order to obtain a stable model as well as decrease computational time.

Finally, a comparison between the two types of substructures at intermediate sea depths was performed to compare the structural mass of a 5 MW turbine. A brief comparison was also performed for the substructures at 40 m sea depth with a 15 MW turbine.

2

Supportive structures for offshore wind turbines

This chapter will introduce the reader to the basic knowledge about OWTs. The first section describes the main components of an OWT. Moving forward the different foundations and substructures for fixed and floating substructures are described. The chapter ends with a definition of the degrees of freedom for a floating substructure and a summary of sea depths for the presented substructures.

2.1 Main components of an OWT

The main components of an OWT are a foundation, a substructure, and a turbine (Bhattacharya, 2019). The turbine itself consists of a tower and a rotor-nacelle assembly (RNA). The RNA typically consists of three blades attached to a hub which is connected to a gearbox and generator. These components are placed at the top of the tower i.e. the nacelle. The most common is to have a rotor that is horizontally mounted. Figure 2.1 shows the main components.

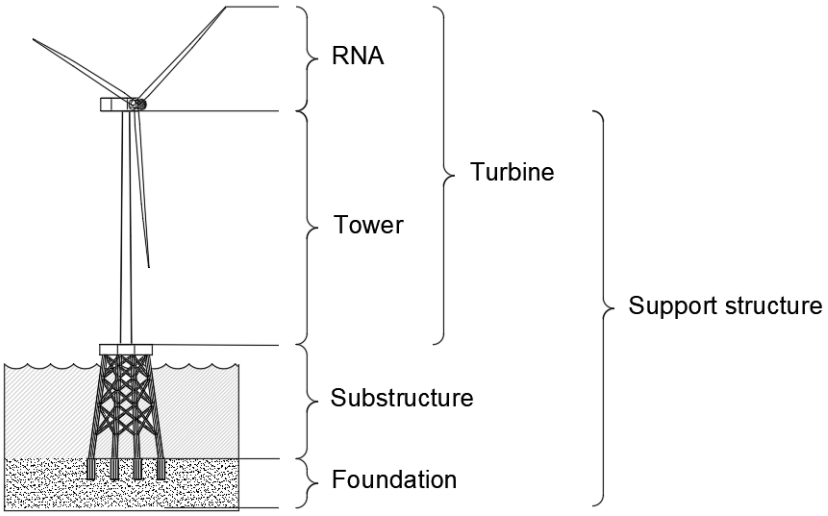

Figure 2.1. *Main components of a OWT: foundation, substructure, tower, and RNA.*

2.2 Foundation and substructure

The following sections describe the different foundations and substructures used for floating and fixed structures. The foundation and substructure are sometimes described as a whole unit but within this project, it's chosen to treat them separately. The foundation is regarding the structure below the seabed and the substructure

the supporting structure above the sea floor.

A challenge for foundations offshore is a phenomenon called scour, which happens because of the movement of water (van der Tempel et al., 2019). The water particles accelerate around foundations and bring small grains from the sea bed away from the foundation, resulting in a scour hole. Therefore most solutions demand scour protection, especially if the soil is erodible to ensure the stability of the support structure.

2.2.1 Foundation for fixed substructures

The fixed substructures have in principle three different types of foundations: pile, suction caissons/buckets, and shallow foundation(ICF, 2020). The shallow foundation, Figure 2.2a, is used for gravity-based substructures which basically rest on the seabed and withstand the overturning moments by their dead weight. The solution demands a solid and flat seabed to rest on. Suction bucket, Figure 2.2c, and suction caisson, Figure 2.2b (left), has the same appearance, a cylinder-shaped body which has a closed top where the substructure rests and an open bottom enabling the mounting into the seabed. They are inserted into the seabed by creating a vacuum within the base by removing water, which allows the ocean's hydrostatic pressure to push the suction bucket/caisson into the soil. The difference between the two is that the suction bucket works as a single unit, utilizing the diameter to resist the overturning moments, while the suction caisson works together in a group of smaller units(ICF, 2020). For some soil conditions foundation piles, Figure 2.2b (right), can be used instead of suction caissons. The pile foundation, Figure 2.2d, consists of a pile driven into the seabed where the vertical loads are resisted by soil friction and resistance, and the horizontal loads are supported by the pile's bending resistance and the soil's lateral resistance around the embedded portion of the pile.

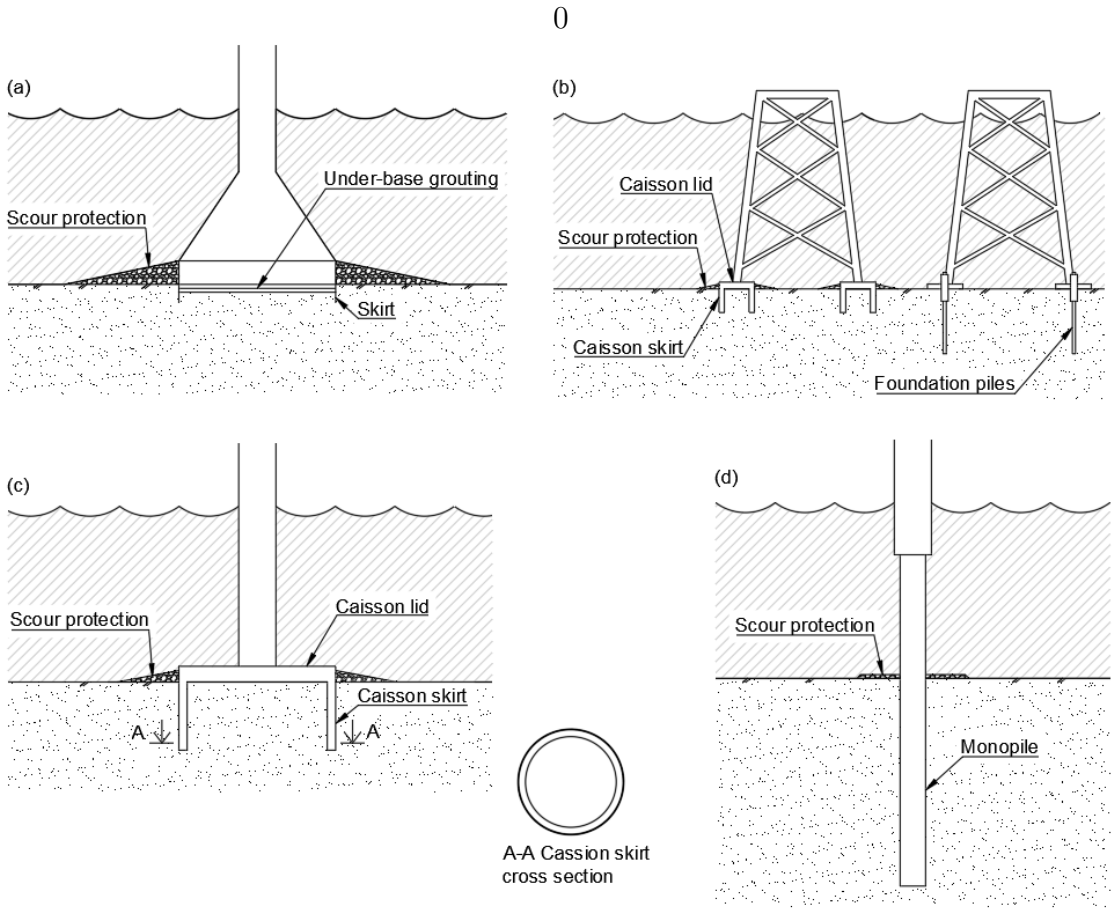

Figure 2.2. *Foundation types for fixed substructures: (a) shallow foundation, (b) from left: suction caisson and foundation piles, (c) suction bucket and (d) monopile foundation.*

2.2.2 Foundation for floating substructures

The floating substructures are anchored to the seabed, which can be done with either surface or embedded anchors. Suction caissons as described in Section 2.2.1 can also be used for anchoring floating substructures as illustrated in Figure 2.3a. Surface anchors, which are represented in Figure 2.3b, rest on the seabed with the help of their dead weight. There are several different types of embedded anchors such as the drag embedded anchor shown in Figure 2.3c, which is applied in the seabed by being pulled through the soil. Anchor piles can also be used as an embedded solution, Figure 2.3d. A solution leaving a low impact on the seabed is dynamically embedded anchors which are represented in Figure 2.3e. The procedure of deployment is that the installation device is withdrawn directly after mounting, leaving the anchor set in the soil.

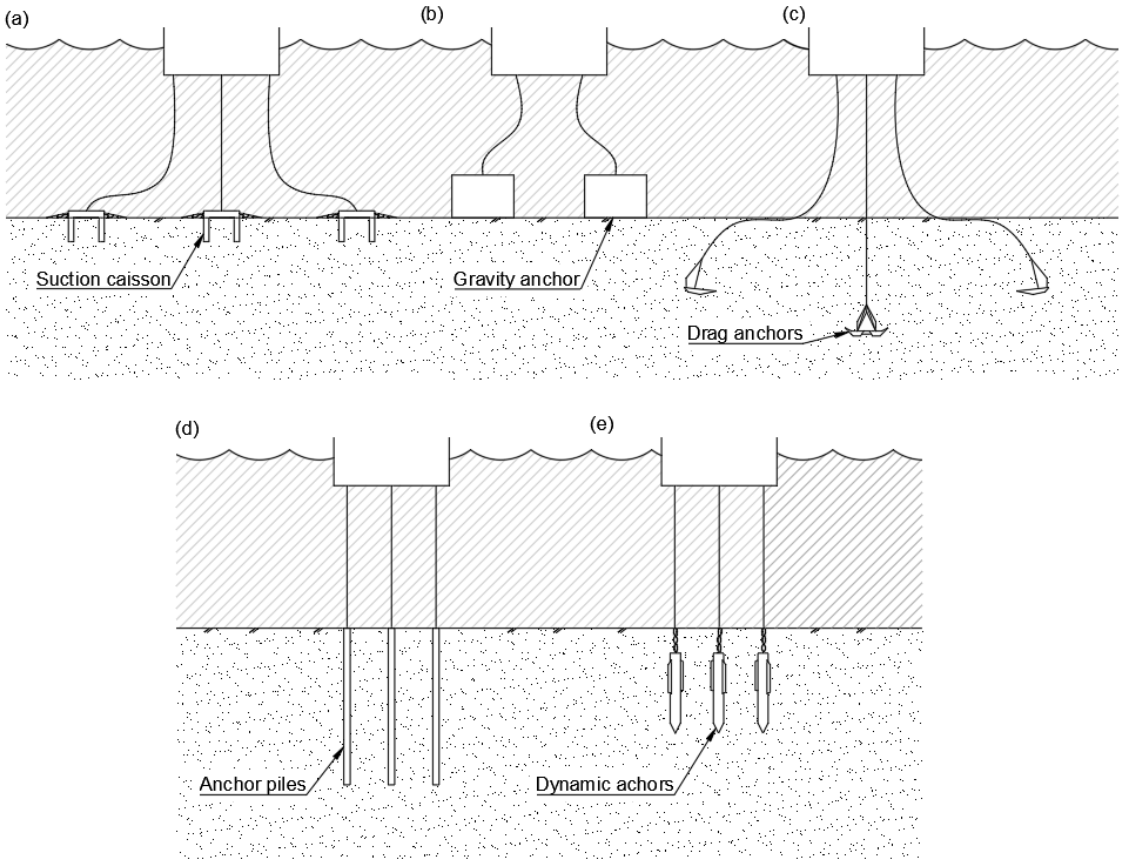

Figure 2.3. *Foundation types for floating substructures: (a) suction caissons, (b) gravity anchors, (c) drag anchors, (d) anchor piles, and (e) dynamic anchors.*

2.2.3 Fixed substructures

Grounded systems are the most common type of substructure used today for OWT. The characteristic of a fixed substructure is that its directly mounted to the sea bed. Fixed substructures are often used in water depths between 0-60 m but larger water depths are technically possible. There are a few different variants of substructures that can be broken down into, gravity-based, pile-based, and lattice-based. Gravity-based substructures are limited to a shallow foundation type but piled-based and lattice-based substructures can be installed with suction caisson/bucket or foundation piles.

Gravity

A gravity-based substructure has two main components, a wide base, and a cylindrical column. On top of the column, the turbine is attached and below the base, a foundation is constructed according to Section 2.2.1. To resist the forces from the turbine, this type of substructure relies on the gravitational theory to avoid uplift, sliding, or overturning (ICF, 2020). The contact between the wide base and the seabed handles the vertical forces. The overturning moment is resisted by the

self-weight of the OWT as well as additional ballast inside the substructure. The most common material for gravity substructures is reinforced concrete but steel is also possible. The construction is often performed onshore in a dry dock and then two options are viable for the transport. For substructures with enough buoyancy, a crane-free approach can be used by towing to the final position (Bhattacharya, 2019). The other option is to load the substructure on a ship or barge and then lift it off with a crane at the final position. In the final location, the structure is filled with ballast which causes it to sink. Gravity substructures have been used for turbines between 0.45-5 MW with a base diameter of 11-24 m and at water depths between 0-26m (ICF, 2020).

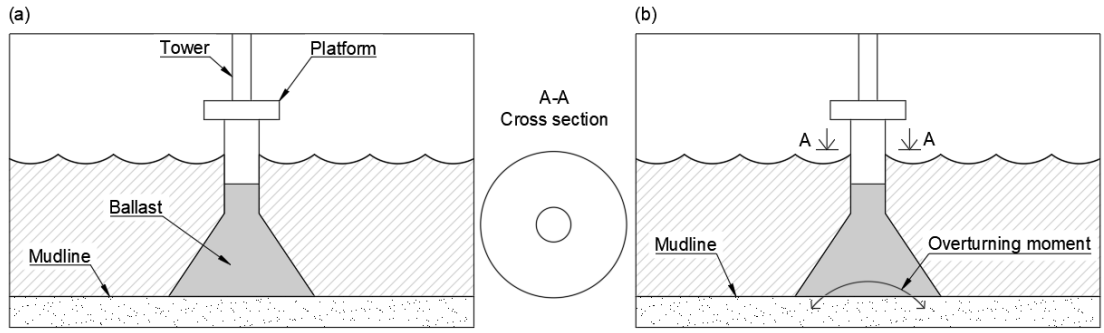

Figure 2.4. *Gravity substructure: (a) Main components, (b) Reaction forces.*

Monopile

The most common type of substructure is the monopile which consists of two main parts, a pile and a transition piece (ICF, 2020). Essentially, the pile is a large tube that is prefabricated and is often made of steel but concrete is possible as well. Monopiles have been used to support turbines between 1.5 to 9.5 MW with a diameter between 3-10 m at water depths up to 50 m. The pile acts as a substructure but also as a foundation described in Section 2.2.1, because the pile is inserted into the seabed approximately equal to the sea depth. The monopile can be driven, vibrated, or drilled into the seabed depending on the soil conditions. This requires a large floating vessel or a jack-up to be able to support the machine installing the pile. A drawback of the installation is often that the top of the pile is deformed and therefore a transition piece is attached on top of the pile.

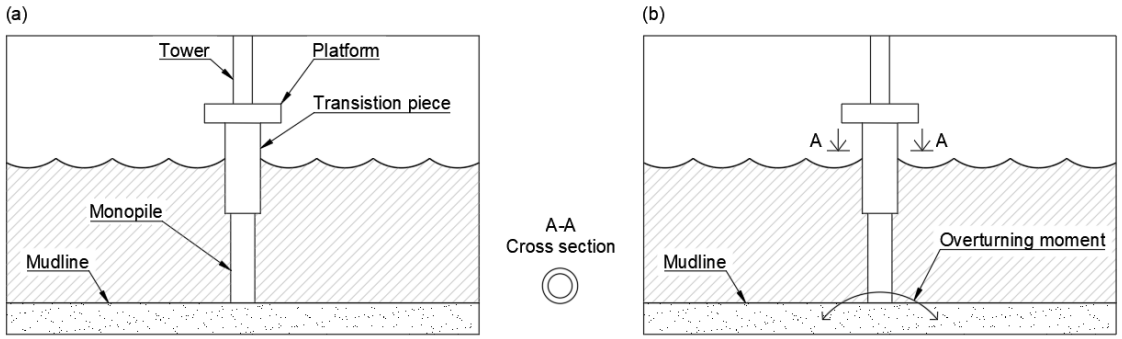

Figure 2.5. *Monopile substructure: (a) Main components, (b) Reaction forces.*

Jacket

A jacket substructure is a common type of lattice variant. The main components are a transition piece, a frame, and a foundation. Above the water, the transition piece is located and spreads the load from the turbine to the frame. The frame is tapered, largest at the base, and consists of legs which can differ in number but three and four are most common. Between the legs, a truss is formed with struts in a smaller dimension in order to stiffen the structure. The frame legs are then connected to the foundation which can be either suction caissons or foundation piles, see Section 2.2.1. Jackets used today have supported turbines between 3-6 MW at water depths between 20-50 m. Common diameter of the frame legs is 1-3 m and the base dimensions are approximately 20x20 m. The overturning moment located at the transition piece generates tension and compression in different frame legs. Jacket structures are made of steel but the transition piece can either be made of steel or concrete. The jacket structure is prefabricated onshore and is then transported to the site with large vessels or barges. At the site, a crane lifts the structure vertically and lowers it to the sea bed.

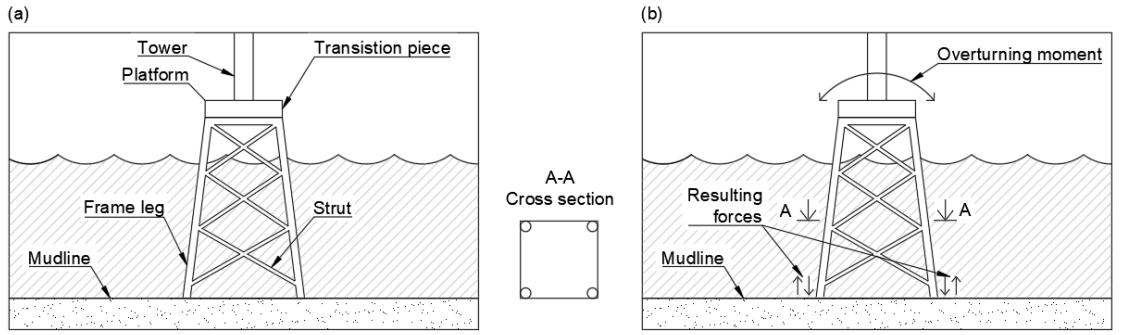

Figure 2.6. *Jacket substructure: (a) Main components, (b) Reaction forces.*

Tripod

Another lattice substructure is the tripod which is a combination of a monopile and a jacket. The main parts are a tubular pipe, three legs, bracing, and a foundation. As for the jacket structure, the foundation is either foundation piles or suction caissons,

see Section 2.2.1. The legs are arranged in a triangular pattern with sides of 20 m and the tubular pipe is placed in the middle and connected by struts that act as bracing. Tripods have been used for turbines between 3-5 MW and for water depths between 20-40 m. Common dimension for the legs is a diameter of 2-3 m and the tubular pipe is smaller than for an equivalent monopile. The overturning moment is resisted in the same way as for a jacket structure. Tripods are produced in steel onshore and follow the same installation process as the jacket structure.

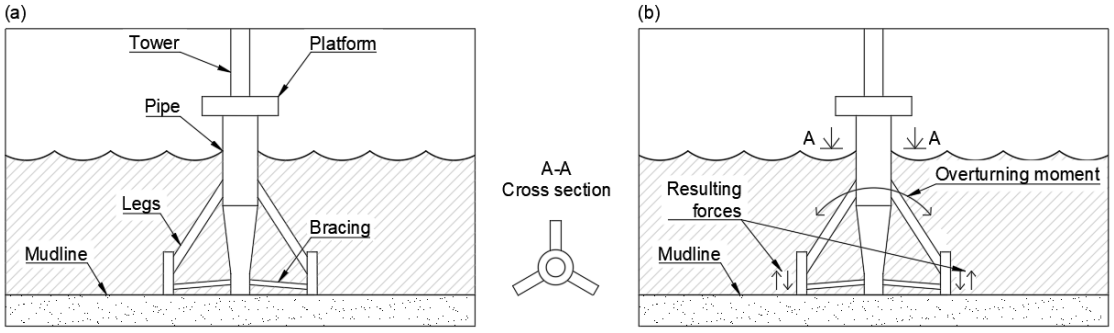

Figure 2.7. *Tripod substructure: (a) Main components, (b) Reaction forces.*

2.2.4 Floating substructures

There are several different types of floating substructures and even more are under development. There are three main principles within the floating substructures: buoyancy-based, tension-based, and ballast-based. This section will present one type from each principle that is most common in the industry today. To keep the floating substructure in place, mooring lines are used together with an anchorage system as described in Section 2.2.2.

Semi-submersible

Semi-submersible substructures are buoyancy stabilized, the stability is provided by the multiple struts bracing the submerged ballast-filled cylindrical hulls, which also provides buoyancy and keeps the structure vertical (ICF, 2020). This solution can be installed in a wide range of water depths from 30-1000 m (Vázquez et al., 2022b). To support a 5 MW turbine the cylindrical hull has a total height of 32 m, where 12 m is above and 20 m below the waterline (Robertson, Jonkman, Masciola, et al., 2014). The diameter of one bottom hull is 24 m and the distance between the hulls is 50 m. To station the semi-submersible substructure, mooring lines are connected to an anchoring system, typically suction caisson or drag anchors.

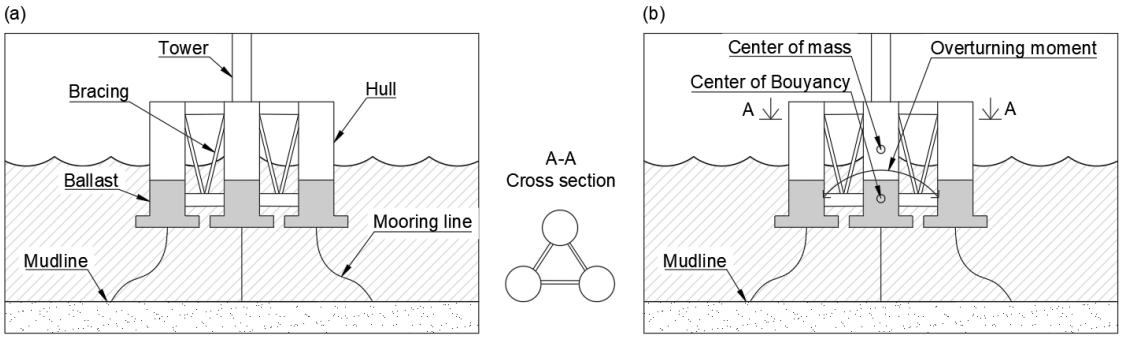

Figure 2.8. *Semi-submersible substructure: (a) Main components, (b) Reaction forces.*

Tension-leg platform

Tension-leg platform (TLP) is a buoyant floating rig. In opposite to the semi-submersible that mainly is moored for station keeping this solution also provides additional vertical stability (Speight, 2015). The additional downward and stabilizing force is achieved by the tendons that are anchored just beneath the platform. The solution also gives restraint rotationally i.e pitch and roll, see Section 2.3. Therefore global pitch and heave are carried directly by the tendons. The system does allow for motions in surge and sway. Since the solution is self-buoyant it can be towed to the site.

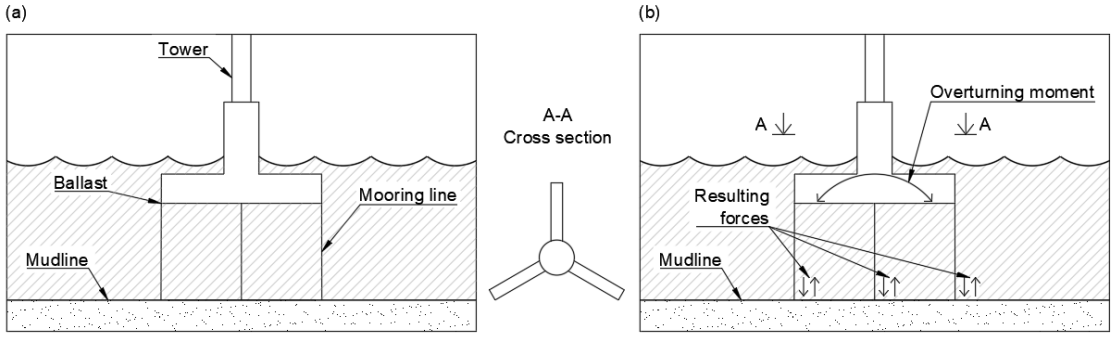

Figure 2.9. *Tension-leg substructure: (a) Main components, (b) Reaction forces.*

Spar-buoy

Spar-buoy is a ballast-based solution, consisting of a single cylindrical hull, which is kept upright by the dead weight the ballast provides in the bottom part of the hull, while the upper part maintains the buoyancy (ICF, 2020). Since its one single hull which keeps the substructure upright, it extends deeper down in the water than the semi-submersible solution which makes it suitable for deeper waters, 60-1000 m (Vázquez et al., 2022b). If there is an additional need to prevent the overall tilt of the system, motion controlled stabilizer can be used, attached below the hull (Bhattacharya, 2019).

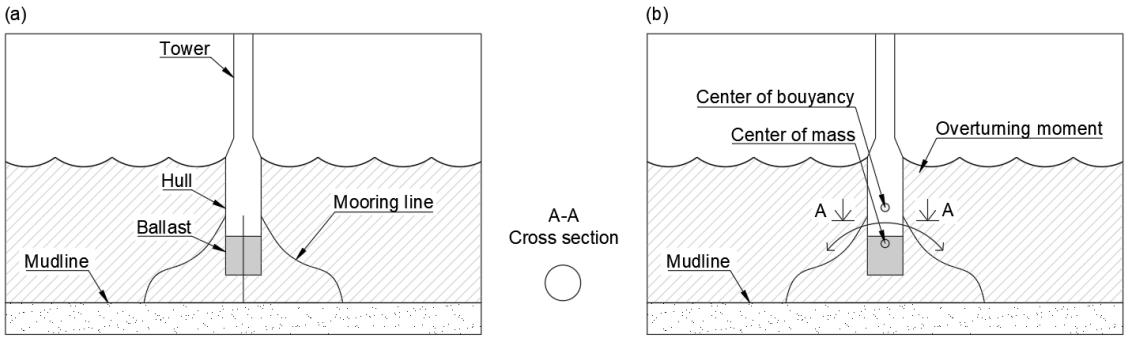

Figure 2.10. *Spar-bouy substructure: (a) Main components, (b) Reaction forces.*

2.3 Degrees of freedom for floating substructure

Regardless of substructure type, the floating systems have six degrees of freedom. The first three are translations and are called sway, surge, and heave. The last three are rotations about each axis and are defined as pitch, roll, and yaw. An illustration of the degrees of freedom together with a commonly chosen coordinate system x, y, and z are presented in Figure 2.11. This system is also used within this thesis.

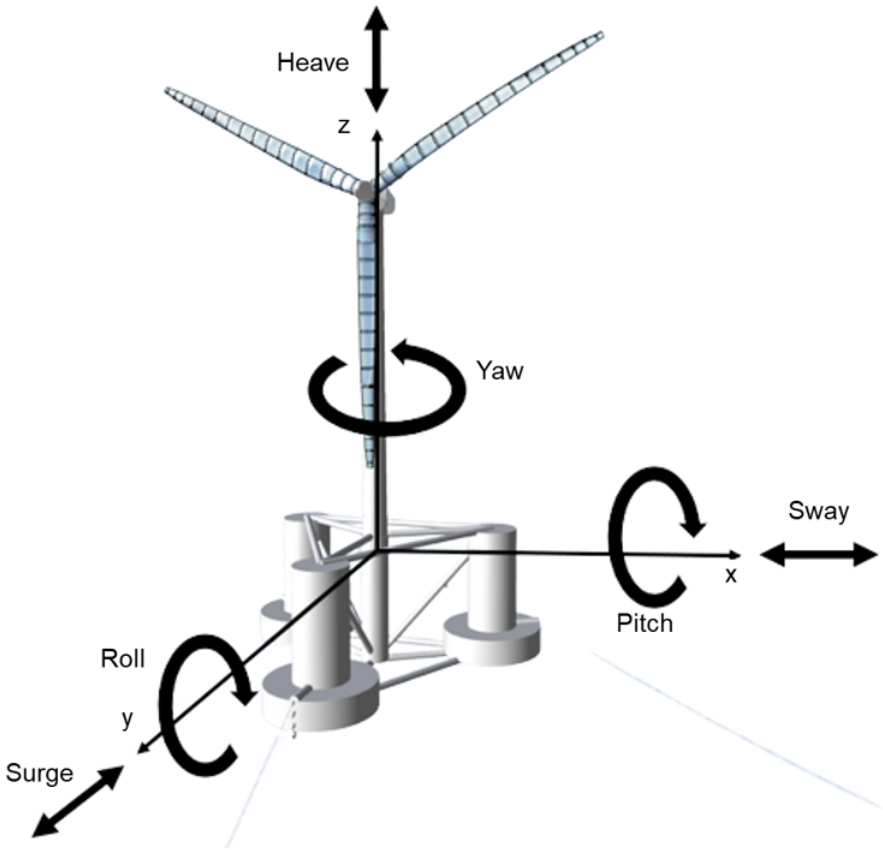

Figure 2.11. *Definition of degrees of freedom and coordinate system for a floating substructure.*

2.4 Sea depths for different substructures

One of the main factors in the selection of substructure is the sea depth. A summary of the spans of sea depth for each substructure from some offshore wind parks currently in operation is presented in Figure 2.12. As Bhattacharya (2019) concludes the limit between the fixed and floating are today roughly about 60 m. Contradictory to previous choices of substructures in regard to sea depth several sources argue that some of the floating substructures can be well suited for below 40 m sea depth (Vázquez et al., 2022a).

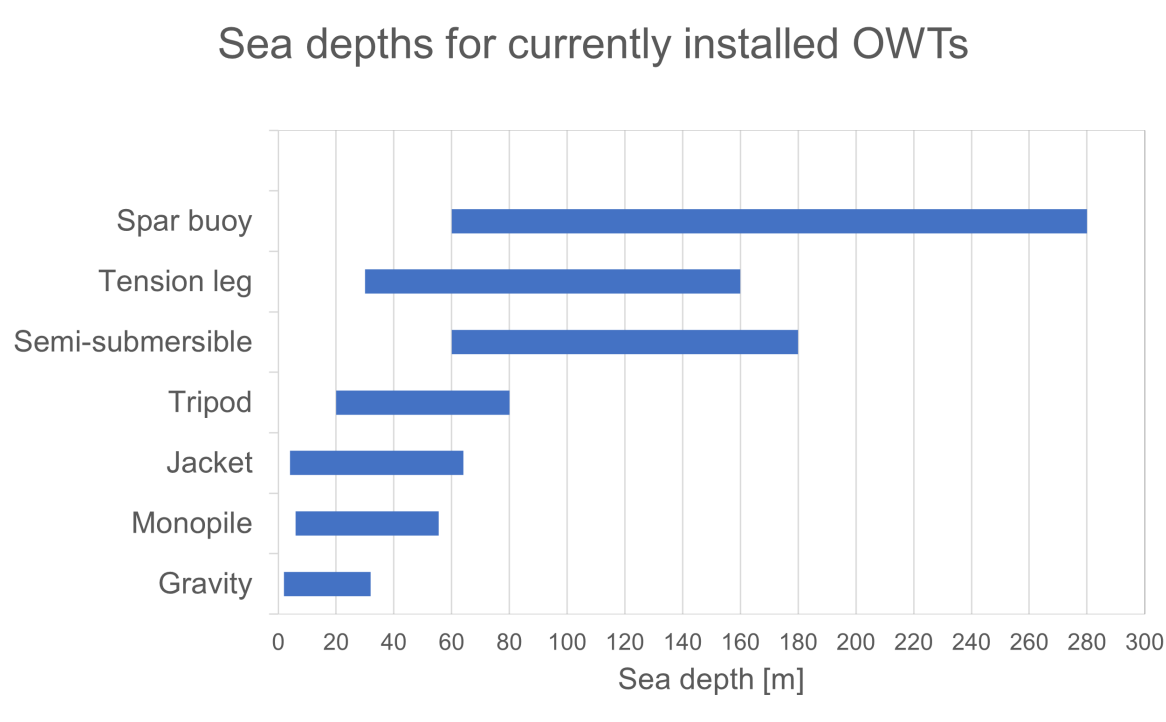

Figure 2.12. *Collected data of sea depths for the different substructures from several sources for currently installed offshore wind parks (Bhattacharya, 2019; ICF, 2020; Malhotra, 2007; Wang et al., 2018).*

3

Loads, theories and models connected to OWTs

This chapter will walk through the main loads and load cases in the early stages of preliminary design. Furthermore, the theory and models used for the static and time-dependent case are presented. Section 3.3 explains how to obtain the frequencies from the loads analytically and how to assemble them to find the target frequency. This frequency range is used when designing the structure's natural frequency also described in Section 3.3. The final section in this chapter describes the necessary theory to comprehend how the floating substructure behaves with regard to stability.

The OWT is designed for the ultimate limit state (ULS) which in the preliminary design includes control of the structural resistance and assures that the fixed substructure can resist the overturning moment and that the floating substructure avoid capsizing. Serviceability limit state (SLS) is also regarded in the preliminary design in terms of vibrations, by assuring that the structure is not in resonance due to the cyclic loads. Therefore the frequency from the loads should not collide with the natural frequency of the structure. Fatigue limit state (FLS) and Accidental limit state (ALS) are important design conditions for this type of structure but are not in the scope of this thesis.

It can be a challenge to select the best-suited standards and regulations when designing offshore wind turbines. Partly due to its different main components but also due to its location at sea. Within this thesis, it is chosen to follow guidelines and documents provided by DNV (Det Norske Veritas), which is one of the certification organ for OWTs. In their documents, they also provide recommendations and guidance to other standards, norms, and documents covering all parts of the OWT. Some of the organs referred to in DNV are IEC (International Electrotechnical Commission), ISO (International Organization for Standardization), and Eurocode.

3.1 Main loads and load cases

This section covers the main loads used in the preliminary design of the substructures. Other loads that need to be accounted for in a detailed design are briefly stated. The second part defines different load conditions for wind and waves. Lastly, five different loads cases are presented for an OWT that can be applied in the early stages of preliminary design.

3.1.1 Loads acting on the OWT

OWTs are subject to a number of different loads and the main loads can be summarized in two types of groups, static and dynamic loads (Bhattacharya, 2019). The

static load is the dead weight of the whole structure and the definition of a static load is that it is applied slowly and remains constant in time. Dynamic loads are the other group whose primary loads are wind, waves, 1P, and 3P (Bhattacharya, 2019). The definition of a dynamic load is that it is applied rapidly or changes with time. The main loads acting on the OWT are illustrated in Figure 3.1.

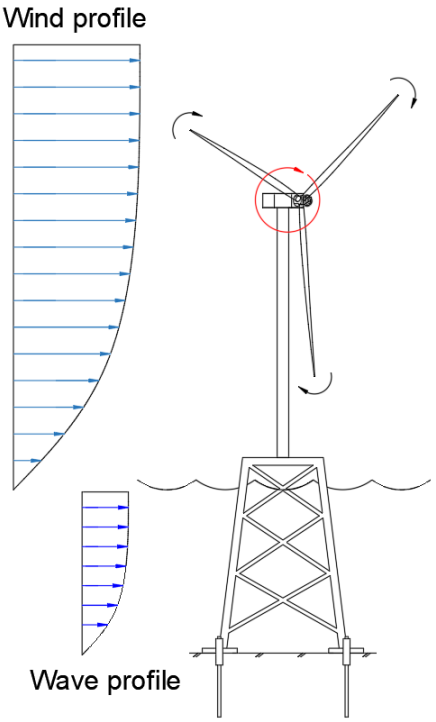

Figure 3.1. *Environmental loads acting on OWT together with the vibration loads 1P and 3P.*

Wind on turbine

The wind load on the turbine can be described as two parts, a thrust created by the rotation of the blades and a drag on the tower (Bhattacharya, 2019). The thrust depends on the wind speed and its variation as well as the operating wind turbine characteristics and size of the turbine. Due to this thrust, a lateral load is created at the hub level. The drag depends on the wind speed and its variations and creates a lateral load along the tower.

Waves on substructure

The substructure is subjected to a lateral load induced when waves are hitting the substructure (Bhattacharya, 2019). The magnitude of the wave load is dependent on the wave height, wave period, and sea depth.

1P (Rotor induced vibrations at hub level)

1P load is an effect of imbalances inside the rotor and simultaneously due to differences in the pitch of individual blades which creates vibrations in the RNA (Bhattacharya, 2019). These vibrations have a specific frequency that is equal to the rotational frequency of the rotor. Modern wind turbines are capable of operating at different speeds and therefore the 1P frequency is a span between the lowest and highest speed. The 1P load generates a lateral load as well as an overturning moment.

3P (Blade shadowing effect)

As an effect of the 1P load, the so-called 3P load is generated. When the blades of the rotor pass the tower a shadowing effect appears (Bhattacharya, 2019). The result of this is a reduction in the thrust acting on the tower. Similar to the 1P load, the 3P load is a vibration with a three times higher frequency and generates a lateral load and an overturning moment.

Other loads

A few other common loads that affect the OWT in the group of cyclic/dynamic loads (Bhattacharya, 2019) are stated below. One of these is the effect of wind-induced current or tidal current which leads to drag on the substructure. Another load that is special for OWTs is marine growth. When plants, animals, and bacteria grow on the substructure it increases the weight and therefore the vertical loads (DNV, 2021c). The growth also increases the diameter of the different members and therefore wave and current loads increase over the first years. It also affects the dynamic response, accessibility, and corrosion rate. Typical values of marine growth are 100 mm in the Baltic Sea with a density of 1325 kg/m^3.

Furthermore, ice loads are a load that is relevant for OWTs in the Baltic Sea. Ice loads can appear in many forms and create horizontal and vertical loads on the structure (Lindblom & Ånger, 2022). Example of horizontal loads is thermal expansion, drifting ice and pack ice. Water level changes can create horizontal loads but also vertical loads such as uplifting. Other examples of loads are ice on the turbine blades, ship impacts, start-up, emergency shutdown, and emergency fault of the turbine as well as seismic loads. One also needs to consider the effects of installation errors and residual stresses.

3.1.2 Load cases used for OWT design

Load cases combine different types of environmental loads to reflect typical conditions to which the structure is exposed. In order to ensure the structural integrity of an OWT, it is necessary for it to withstand these load conditions. There are a vast amount of load cases according to DNV which considers ultimate loads and fatigue

loads. The load cases are built up by different categories of wind and wave loads.

Wind loads are separated into two types of categories, normal wind conditions (NWC) and extreme wind conditions (EWC) (DNV, 2021c). NWC is used for fatigue calculations and maximum wind loads on operating wind turbines and EWC is for peak wind speeds and changes in direction and speed. Furthermore, wind turbulence can be divided on the same basis as the normal turbulence model (NTM) and extreme turbulence model (ETM). Wind turbulence models create a wind field of velocities that varies in space and time. The difference between NTM and ETM is that the standard deviation is calculated differently. The ETM model results in a larger standard deviation and therefore larger difference in wind velocity. Another category is the extreme operating gust (EOG) which is a fast change in wind speed (Bhattacharya, 2019). The difference compared to the turbulence model is that the velocity changes in time but not in space. Common for all three models is that the wind is modeled with the same wind profile which is described in Equation 3.4.

Wave loads are separated into four different categories (DNV, 2021c):

- Normal sea state (NSS). Significant wave height is concurrent with a 10-minute mean wind speed. They are used for ultimate loads and fatigue loads.
- Severe sea state (SSS). Significant wave height is extrapolated to achieve a load effect in combination with the 10-minute mean wind speed which has a return period of 50 years. Used for ultimate loads and fatigue loads.
- Extreme sea state (ESS). Significant wave height is determined from the distribution of the annual maximum significant wave height for either a 1-year or 50-year return period.
- Extreme wave height (EWH). Maximum wave height is determined by the distribution of the annual maximum wave height.

With the wind and wave states described above a few simplified load cases can be created for the design of substructures (Bhattacharya, 2019). The load cases are reduced in the number of cases, number of loads, and number of angles the load is applied at the structure. In load case 5 the wind and waves are misaligned which means that the wave direction rotated 90 degrees. The load cases that was used in the thesis are presented in Table 3.1.

Table 3.1. *Simplified load cases used for the design of substructures (Bhattacharya, 2019).*

Name	Load case	Wind model	Wave model	Alignment
Normal operational	1	NTM at U_{mean}	1-year ESS	Collinear
Extreme wave load	2	ETM at U_{mean}	50-year EWH	Collinear
Extreme wind load	3	EOG at U_{mean}	1-year EWH	Collinear
Extreme operating gust	4	EOG at U_{out}	50-year EWH	Collinear
Wind-wave misalignment	5	ETM at U_{mean}	50-year EWH	Misaligned

3.2 Static and time dependant models

The static model follows the simplified analytical calculations explained according Bhattacharya (2019). This model are used in the early stages of preliminary dimensioning and later as a reference comparing results to the numerical model from a time-dependent simulation software. The numerical models and theories implemented in the simulation software can account for non-linearity's and reflect the more realistic cyclic behavior of the loads.

3.2.1 Static model

The static model can have two different setups as presented in Figure 3.2. In the first setup, the drag force (F_{drag}) is acting on the full tower as seen in Figure 3.2a. In the second setup, the blade is shadowing the tower and instead, the force of 3P is used as seen in Figure 3.2b. Equation 3.1 - 3.5 defines each load indicated in the figure.

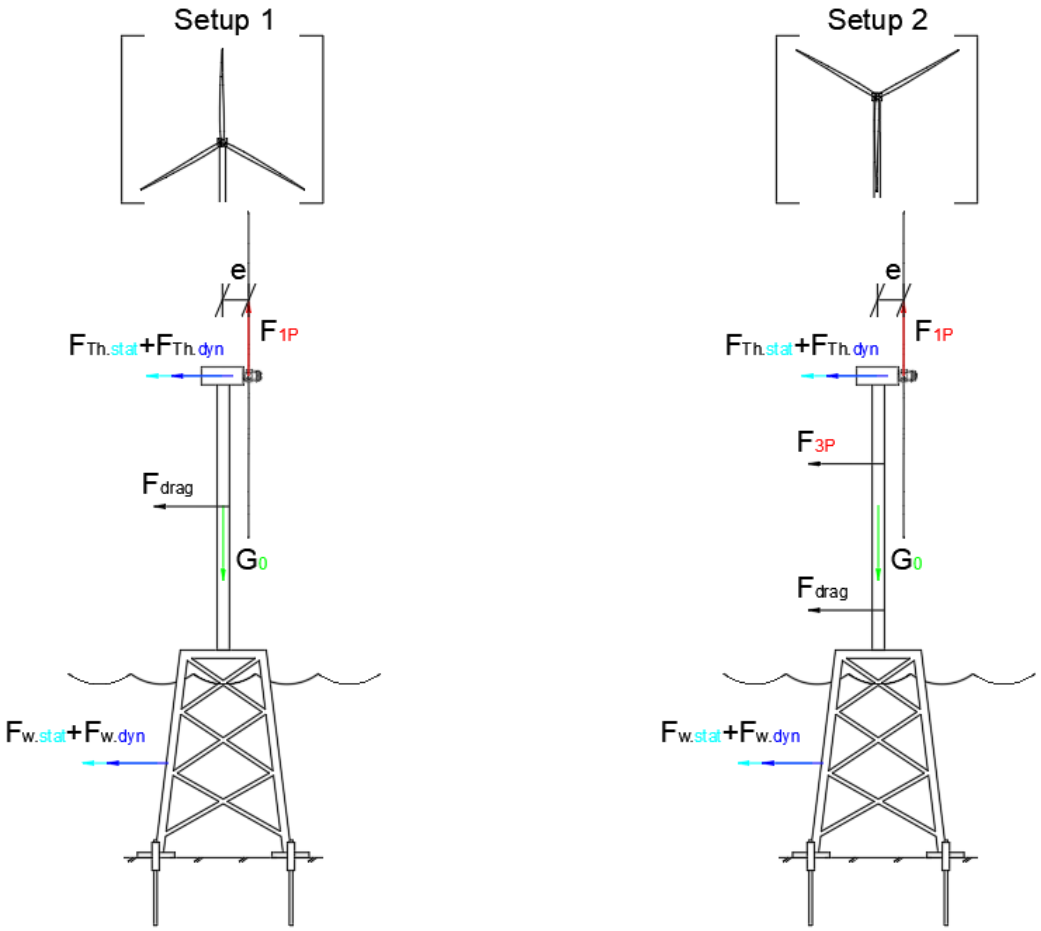

(a) *Setup 1 with drag force acting on the full tower.*

(b) *Setup 2 with the blade shadowing the tower.*

Figure 3.2. *Static model with the two different setups depending on the blade position.*

Thrust force

The wind load acting on the RNA is translated to a resulting thrust force, F_{Th}, acting on the rotor. The thrust force is the summation of a static wind load (Th_{stat}) and a fluctuating dynamic wind load (Th_{dyn}) at a given wind speed. This simplified analytical translation is built from the Morrison equation and expressed according to Bhattacharya (2019) as:

$$F_{Th} = Th_{stat} + Th_{dyn} = \frac{1}{2}\rho_a A_R C_T \overline{U}^2 + \frac{1}{2}\rho_a A_R C_T (2\overline{U}u + u^2) \tag{3.1}$$

Where ρ_a is the density of air, A_R is the swept area of the rotor, and C_T is the thrust coefficient which is dependent on the wind related to the operating wind speeds in the RNA. $\overline{U}$ is the mean wind speed over a 10 min interval at hub height and depends on the load case. The turbulence is estimated with the component u, which is the fluctuation of the wind speed. This component varies with the turbulence

intensity and are therefore load case dependent.

Mass imbalance force (F_{P1})

The imbalance induced by pitch difference in the blades and imbalances in the rotor can in a simplified matter be translated to a centrifugal force. By adding one lumped mass on the rotor with a certain distance R from the hub in the swept rotor area and at a distance b from the center of the tower, called rotor overhang (Bhattacharya, 2019). The centrifugal force can be expressed according to equation 3.2.

$$F_{1P} = 4\pi^2 I_m f^2 \tag{3.2}$$

Where I_m is the product of the lumped mass and the radius (R) to the hub, and f is the maximum frequency obtained in the rotor rpm range. To obtain the moment this force is generating this expression is multiplied with the rotor overhang.

Tower drag force and blade passing force (F_{P3})

There are two different setups when the wind is hitting the tower. Either the tower is fully exposed to the wind which is resulting in the total drag force acting on the tower which can be expressed with the following equation:

$$F_{drag} = \int_0^H \frac{1}{2}\rho_a C_{D.wind} D(z) U(z)^2 \tag{3.3}$$

where $C_{D.wind}$ is the drag coefficient. $D_{tower}(z)$, accounts for the change of the cross-section diameter, and the wind profile $U(z)$, is expressed with the following power law:

$$U(z) = U_{ref}\left(\frac{z}{z_r}\right)^{\alpha} \tag{3.4}$$

where U_{ref} is the reference wind speed at hub height and z_r is the height of the hub. The power law exponent α determines the shape of the wind distribution.

The second setup is where one blade is in the location of the tower i.e shadowing the tower. This force (F_{3P}) is expressed as the drag force but only integrated over the area that the blade covers, where the area of the blade can be approximated as trapezoids. This force has a small influence in the static model and can be assumed as beneficial in comparison to the first setup. The dynamic influence is though of essence which is described in Section 3.3.1. Therefore the total drag force (F_{drag}) is used for analytical calculations. The shadowing effect has a larger influence regarding the vibrations it contributes to.

Wave loading

Different models are applicable to calculate the loads on a given structure. One model is the Morison equation which is suitable for slender structures (International

Electrotechnical Commission, 2019b). The purpose is to calculate the forces from viscous drag and inertia loading. A limitation of the model is that if the cross-section of the structure is large compared to the wavelength, typically $D > 0.2\lambda$ where D is the diameter and λ is the wavelength, the model isn't applicable. The general formula for Morison´s equation is presented below:

$$F = \frac{1}{2} C_d \rho_w D \mid U_r \mid U_r + C_m \rho_w A \dot{U}_W - C_a \rho_w A \dot{U}_S \tag{3.5}$$

Where F is the force per unit length of the member, C_d is the drag coefficient, usually between (0.7-1.2), C_m is the inertia coefficient, usually between (2.5-3), ρ_W is the density of seawater, D is the diameter, A is the cross-section area, U_r is the relative velocity of the flow normal to the member, see Equation 3.6, $\dot{U}_W$ is the acceleration of the flow resolved normal to the member, see Equation 3.7, $\dot{U}_S$ is the acceleration of the structure resolved to the member and C_a is the added mass coefficient, usually between (1.5-2).

$$U_r = \frac{\pi H}{T} \frac{cosh[k(z_s + d)]}{sinh(kd)} cos\left(\frac{2\pi t}{T} - kx\right) \tag{3.6}$$

$$\dot{U}_W = \frac{\pi^2 H}{T^2} \frac{cosh[k(z_s + d)]}{sinh(kd)} cos\left(\frac{2\pi t}{T} - kx\right) \tag{3.7}$$

Where H is the wave height, T is the wave period, k is the wave number, see Equation 3.8, z_s is the distance positive upwards from the mean free surface elevation, see Equation 3.9 and Figure 3.3, d is the sea depth, t is the time and x is the distance of propagation.

$$\omega^2 = gk \cdot tanh(kd) \tag{3.8}$$

Where $\omega = \frac{2\pi}{T}$.

$$\eta = \frac{H}{2} cos\left(\frac{2\pi t}{T} - kx\right) \tag{3.9}$$

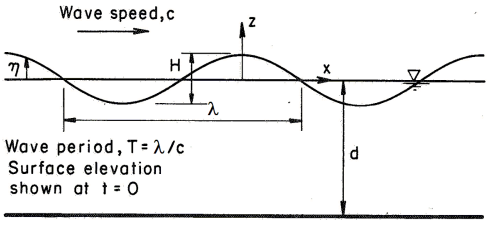

Figure 3.3. *Illustration of mean free surface elevation and the distance z_s (DNV, 2021a).*

A requirement for the models to work is a choice of wave theory. The selection of wave theory is based on the sea depth, wave period, and wave height (DNV, 2021a). The simplest assumption is to use simple linear waves called (Airy). This theory is based on the fact that the wave height is much smaller than the sea depth and the wavelength. The Equations 3.6-3.9 is based on Airy theory and regular waves.

3.2.2 Time dependant model

To simulate the periodic loads such as wind and waves over time, it is needed to initiate a signal of the load over a frequency domain. The frequency domain for the different loads as described in Section 3.3 is thereby the different frequencies that make up the signal. The time domain is how the amplitude of the signal changes over time. With a Fourier transform it is possible to convert in between the spectrum and time domain. In other words, the environmental data is used to generate the load in the form of a spectrum and further on convert it into a time domain with a Fourier transform. The load's behavior in a time domain is illustrated in Figure 3.4.

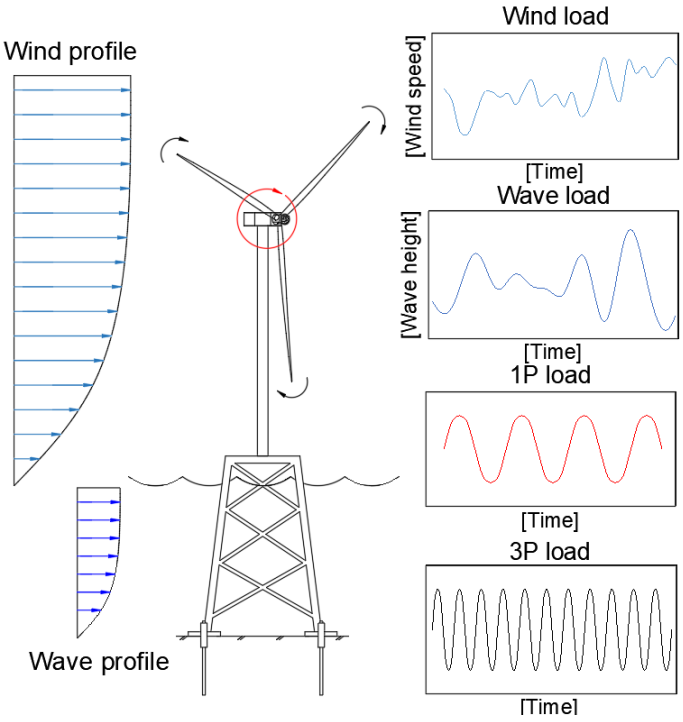

Figure 3.4. *Main loads acting on the OWT and their behaviour in a time domain.*

The time domain analysis is performed by solving the dynamic equation of motions at each time step (n) according to Equation 3.10.

$$M\ddot{d}_n + C\dot{d}_n + f_n^{int} = f_n^{ext} \tag{3.10}$$

$$f_n^{int} = \frac{\partial f^{int}}{\partial d}\Delta d_n = K_n^{int}\Delta d_n \tag{3.11}$$

$$f_n^{ext} = \frac{\partial f^{ext}}{\partial d}\Delta d_n = K_n^{ext}\Delta d_n \tag{3.12}$$

Where M is the mass matrix, C the damping matrix, d governs the displacement at each node, f_n^{int} the internal forces, and f_n^{ext} the external forces. As can be seen in Equation 3.11 and 3.12, the consistent tangent matrix K_n^{ext}, and the load stiffness matrix, K_n^{ext}, are dependant on the displacement, d, in a non-linear analysis.

The dynamic equation of motions is solved with the Newmark-Beta method with the possibility to include Hilbert-Hughes-Taylor (HHT) method which enables to include numerical damping. If the analysis is nonlinear, which results in a residual error, the Newton-Raphsson iteration method is used. This reduces the error until a set tolerance.

Aerodynamic loads

In a simulation software, the wind is modeled as a 3D wind field based on average wind speed, turbulence intensity, and a wind profile according to the power law. For load case category NTM and ETM, described in Section 3.1.2, a turbulence field is built up with the signal from either Kaimal or Mann spectrum and then converted into a time domain which will allow the wind field to vary in time. In order to model the wind field to vary in time and space there is a need for a stochastic turbulence simulator such as TurbSim (B. J. Jonkman & Kilcher, 2012). This allows for a second layer superimposed on the spectral layer. This will create the randomized structure of turbulence in all three dimensions. The data is applied onto each node at the wind fields mesh which is fixed in space for each time step. As for the category EOG, described in Section 3.1.2, the wind field is based on a wind profile and varies in time based on a sudden extreme event. An illustration of how the wind field can appear graphically in a simulation software is seen in Figure 3.5. The turbulent case (NTM/ETM) can be seen in Figure 3.5a and the extreme event (EOG) in Figure 3.5b.

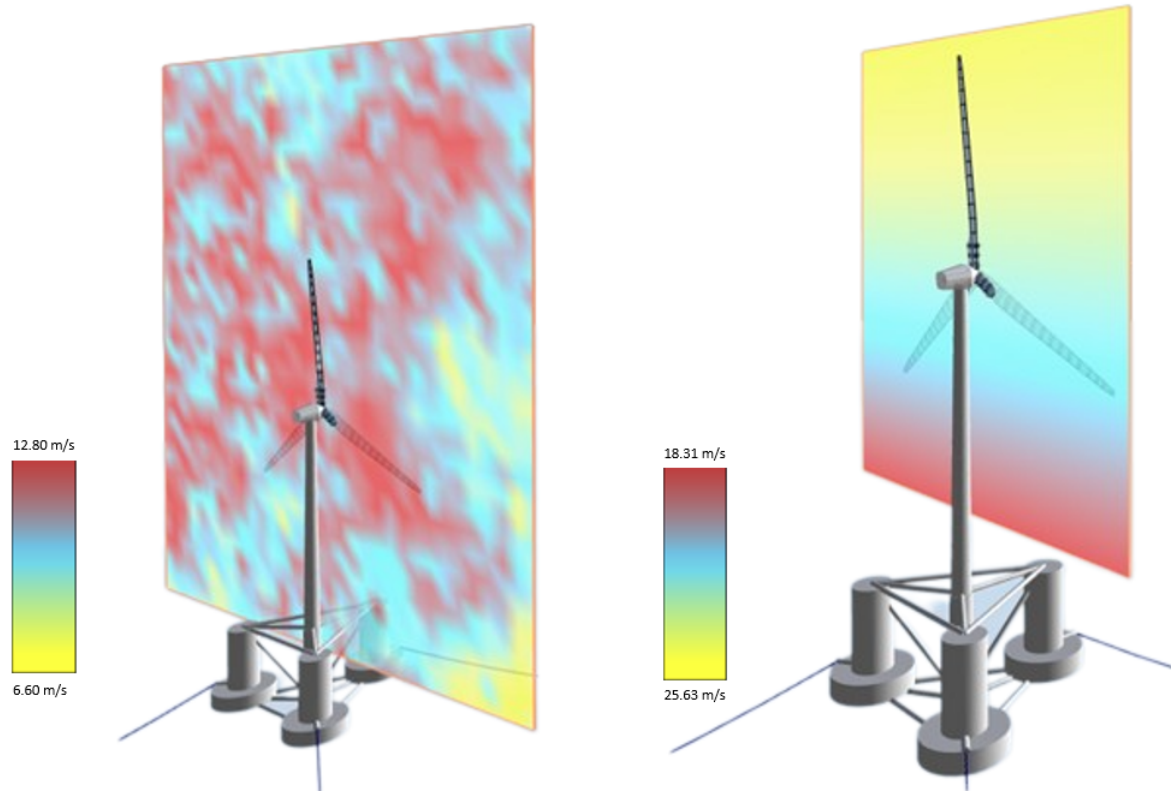

(a) *Wind field for a turbulent load case (NTM/ETM) including power law.*

(b) *Wind field for an extreme event load case (EOG) with solely power law.*

Figure 3.5. *Graphical visualization of wind fields in a simulation software.*

Numerically a common model to compute the aerodynamic loads on the rotor is the Blade Element Momentum (BEM) model. The BEM model is a combination of Blade Element Theory and Momentum Theory (Rogers et al., 2010). Blade Element Theorem considers the shape of the blades and computes lift and drag force acting on each blade element yielding to independent behavior of each other. The lift force acts perpendicular to the incoming wind velocity and the drag force is parallel. Momentum Theorem considers the flow of a medium passing through the turbine and results in a thrust and a torque. For the non-blade members of the structure such as the tower and substructure, the aerodynamic loads are computed with the term related to the drag in Morison's equation.

Wave loads

In a numerical model the Morrison equation described in Section 3.2.1 is used. If Morison´s equation isn't applicable a diffraction theory such as MacCamy-Fuchs needs to be used. The difference when the cross-section is large is that the structure modifies the wave pattern. The difference in modeling is an added boundary condition that there is no flow through the structure. The MacCamy-Fuchs model is an addition to Morison´s equation and reduces to Morison´s equation for long wavelength and small cross-sections. The addition to Morison´s equation is presented

below:

$$C_m = \frac{4}{\pi(kr)^2\sqrt{A_1}} \tag{3.13}$$

Where r is the radius, k is the wave number and A_1 comes from the Bessel function depending on k and r. A solution to a differential equation can be specified with a Bessel function of different orders (Britannica, 2023).

As described in Section 3.2.1 a simple linear wave model can be used but also more advanced models can be used depending on the sea conditions. Linear wave theory is applicable for intermediate to deep waters depending on the ratios between wave height and wave period on the y-axis and water depth and wave period on the x-axis, see Figure 3.6. If the ratio on the y-axis is large or the ratio on the x-axis is low a more advanced model such as Stokes's theory or Dean´s stream function can be used. These models often apply in shallow water or when the waves start to break.

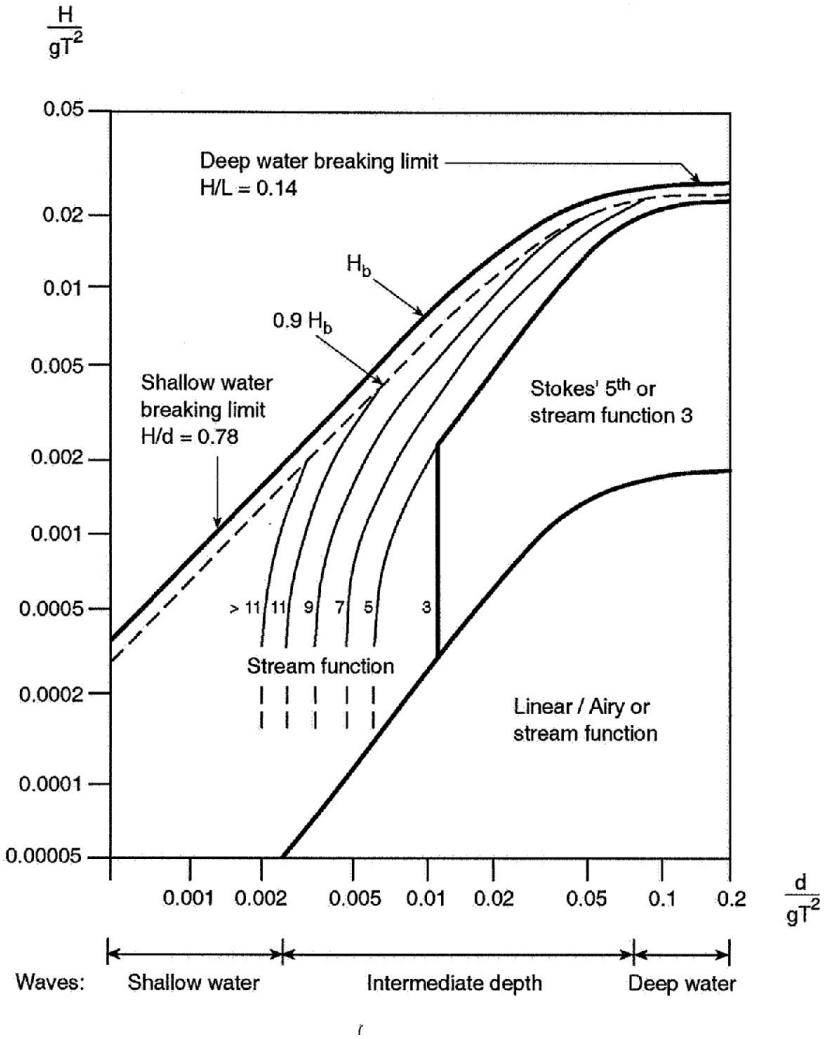

Figure 3.6. *Illustration of at which depth different wave models should be applicable (DNV, 2021a).*

The linear wave theory can be modeled as either regular or irregular waves. Irregular waves are a sum of different regular waves and the most simple expression can be defined as in Equation 3.14 (DNV, 2021a). This replaces the mean free surface elevation described in Equation 3.9 which are used in Equation 3.6 and 3.7.

$$\eta(t) = \sum_{n=1}^{N} A_n cos(\omega_n t - k_n x + \epsilon_n) \tag{3.14}$$

Where the subindex defines the wave component and N is the number of wave components. ω is the angular wave frequency, k is the wave number, ϵ is the phase angle and A is the amplitude of the wave which can be calculated with Equation 3.15.

$$\frac{1}{2}A_n^2 = S_J(\omega_n)\Delta\omega_n \tag{3.15}$$

Where $S_J(\omega_n)$ is the wave spectrum defined in Section 3.3.1 and $\Delta\omega_n = \omega_{n+1} - \omega_n$ is the difference between two successive frequencies.

3.3 Frequency

The OWT is dynamically sensitive due to its tall and slender shape as well as the additional weight and movement caused by the RNA on the top (Bhattacharya, 2019). Therefore, it is of essence to ensure that the natural frequency of the OWT doesn't collide with the frequency of the environmental and mechanical loads.

It is appropriate to analyze the issue in a frequency domain (Bhattacharya, 2019). The frequency domain can be set up by Power Spectral Density (PSD) functions. Each load generates a spectrum in the domain. By analyzing the combined normalized spectrums from each load one can establish design target frequency ranges. The aim is then to obtain a natural frequency (f_0) of the OWT that fits in this frequency range.

The following section describes how to find the target frequency connected to the loads and how the natural frequency is obtained.

3.3.1 Target frequency

An illustration of a PSD diagram including the spectrum from each load and the domain ranges possible for design (soft-soft, soft-stiff, and stiff-stiff) can be seen in Figure 3.7. The curves from each load are obtained analytically and described with Equation 3.16 - 3.20. A summary of the three possible design options and their frequency range is presented in Table 3.2.

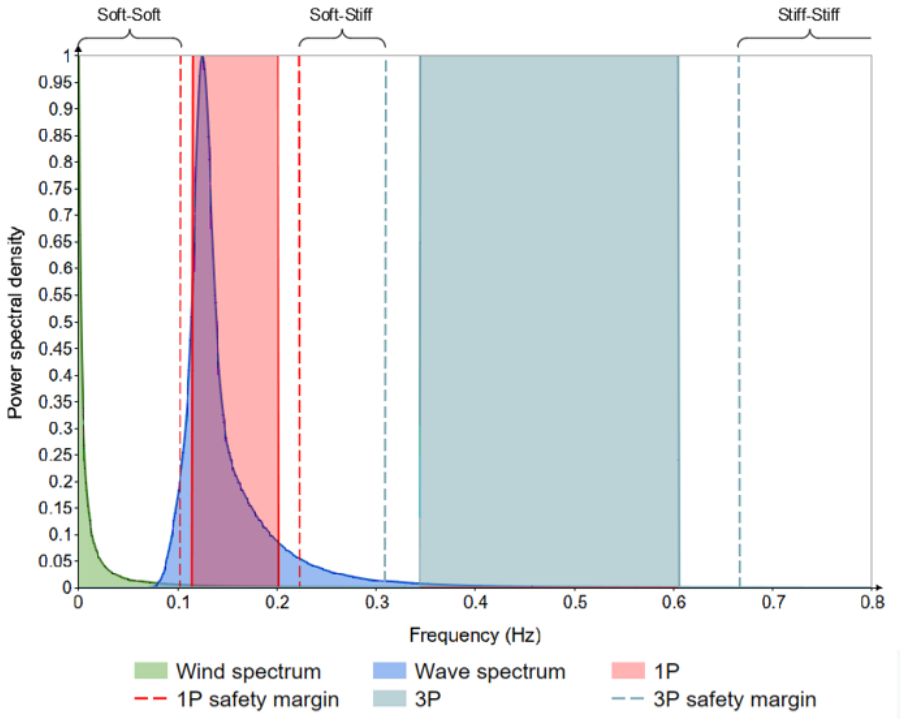

Figure 3.7. *Example of a PSD diagram including the spectrum from each load.*

Table 3.2. *Design options and their frequency range (Bhattacharya, 2019).*

Design	Frequency range	Range specifics
Soft-soft	$f_0 < f_{1P.min}$	f_0 located below 1P loading. A very flexible structure is needed to achieve a natural frequency within this low range.
Soft-stiff	$f_{1P.max} < f_0 < f_{3P.min}$	f_0 located in between the spectrum of 1P loading and 3P loading. Range suitable for most support structures
Stiff-stiff	$f_0 > f_{3P.max}$	f_0 located above the spectrum of 3P loading. To achieve a natural frequency in this high range a very stiff structure is needed.

Wind spectrum

In International Electrotechnical Commission [IEC], (2019a) there are two standard turbulence models presented, Kaimal spectral and exponential coherence model and Mann uniform shear model. DNV also refers to these two as commonly used. The Kaimal spectrum is suitable for atmospheric boundary layers and builds up on the frozen turbulence hypothesis and Kolmogrow's law. The Kaimal spectral density is described with the following expression according to DNV (2021a):

$$S_U(f) = \sigma_U^2 \cdot \frac{6.868 \cdot \frac{L_U}{U_{10}}}{\left(1 + 10.32 \cdot \frac{f \cdot L_U}{U_{10}}\right)^{\frac{5}{3}}} \tag{3.16}$$

Where σ_U is the standard deviation of wind speed. Which depends on the turbulence intensity, and the mean wind speed over 10 minutes intervals, $\overline{U}_{10}$. L_U is the integral scale length and corresponds to the specification in Eurocode 1.

Wave spectrum

A common spectrum for waves is Pierson-Moskowitz. This spectrum builds on the fact that the sea is fully developed. A fully developed sea can be characterized by a longer fetch length than 5000 wavelengths and the wind speed has been constant for 10 000 wave periods (Arany et al., 2015). The expression for the Pierson-Moskowitz spectrum is defined as (DNV, 2021a):

$$S_{PM}(\omega) = \frac{5}{16} \cdot H_s^2 \omega_p^4 \cdot \omega^{-5} exp\left(-\frac{5}{4}\left(\frac{\omega}{\omega_p}\right)^{-4}\right) \tag{3.17}$$

Where H_s is the significant wave height, ω_p is the angular spectral peak frequency and ω is the angular frequency.

If the sea isn't fully developed a modified version of this spectrum called JONSWAP can be used as suggested by DNV. The difference is that the JONSWAP spectrum handles different fetch lengths and therefore is more suitable for developing seas or seas with smaller fetch distances. The expression for the JONSWAP spectrum is:

$$S_J(\omega) = A_\gamma S_{PM}(\omega) \gamma^{exp\left(-0.5\left(\frac{\omega-\omega_p}{\sigma\omega_p}\right)^2\right)} \tag{3.18}$$

Where A_γ is a normalizing factor, $S_{PM}(\omega)$ is the Pierson-Moskowitz spectrum, γ is a non-dimensional peak shape parameter and σ is the spectral width parameter.

1P and 3P spectrum

The spectrum of 1P is simply generated from the operational revolutions per minute (rpm) range of the rotor where one rpm corresponds to 1/60 Hz. The spectrum of 3P loading is three times the rpm range of the rotor for a three-bladed rotor.

$$S_{1P} = rpm\frac{1}{60} \tag{3.19}$$

$$S_{3P} = 3 \cdot rpm\frac{1}{60} \tag{3.20}$$

3.3.2 Natural frequency

Natural frequencies are of importance for structures that are subjected to dynamic loads. The basic method of how to calculate these and the modes which are most critical for a fixed and a floating substructure is presented in the following sections.

Fixed substructure

The natural frequency for a jacket substructure can be solved with the eigenvalue problem showed in Equation 3.21.

$$(\mathbf{K} - \omega^2\mathbf{M})\mathbf{u} = 0 \tag{3.21}$$

Where $\mathbf{K}$ is the stiffness matrix, $\mathbf{M}$ the mass matrix and $\mathbf{u}$ the displacement vector.

There are two categories of modes for fixed substructures depending on the foundation and the stiffness/mass distribution of the turbine (Bhattacharya, 2019). The first category is sway-bending modes which are typical for foundations with high axial stiffness compared to the turbine. This is often the case for monopiles or jackets with piled foundations. The first mode of sway-bending can occur in two directions, tower side-to-side and tower fore-aft, illustrated in Figure 3.8.

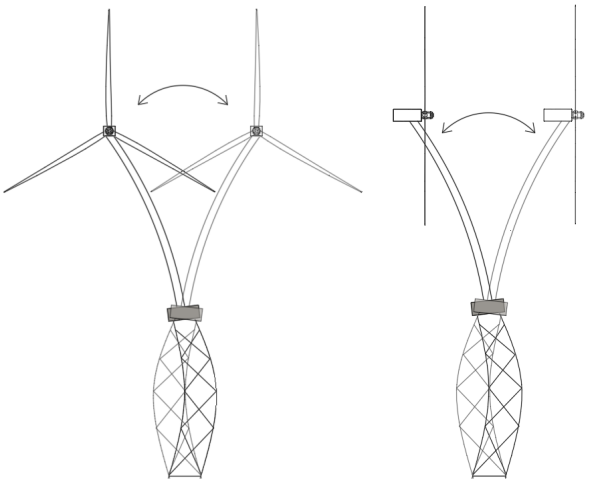

Figure 3.8. *Sway-bending modes for an OWT on a jacket substructure. From left to right: tower side-to-side mode and tower fore-aft mode.*

The second category is the rocking modes which occur for foundations that are less stiff in the axial direction (Bhattacharya, 2019). The first mode of rocking can occur in two directions, tower side-to-side and tower fore-aft, illustrated in Figure 3.9. The second mode of sway-bending and rocking is not of interest because their frequency is about four to six times higher than the first mode.

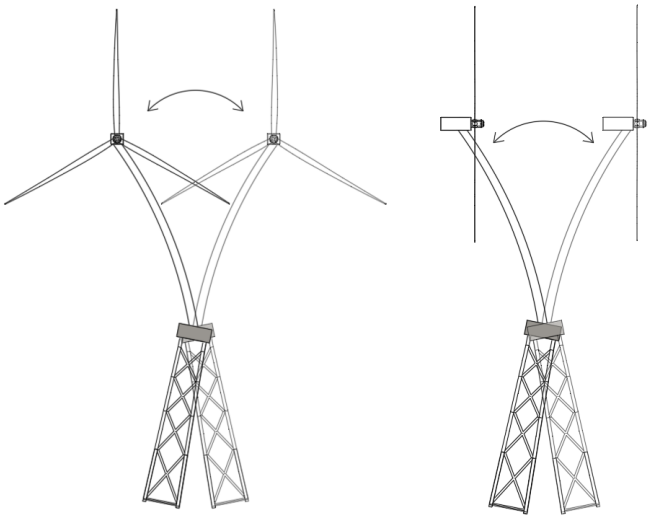

Figure 3.9. *Rocking modes for an OWT on a jacket substructure. From left to right: tower side-to-side mode and tower fore-aft mode.*

Floating substructure

The natural frequency for a floating body such as the semi-submersible can be derived by solving the eigenvalue problem expressed in Equation 3.22. The expression of motions builds on an undamped system and without excitation loads (Zhou et al., 2021).

$$\boldsymbol{\omega}^2 \ \mathbf{q}(\boldsymbol{\omega}) = [\mathbf{M} + \mathbf{A}(\boldsymbol{\omega})]^{-1}\mathbf{C} \ \mathbf{q}(\boldsymbol{\omega}) \tag{3.22}$$

Where $\mathbf{M}$ and $\mathbf{A}$ is the mass and added mass matrix. The added mass is a consequence due to the inertia from the water surrounding the structure, which forces the structure to oscillate with the frequency of the waves in a rigid body motion(Faltinsen, 1990). $\mathbf{q}$ is the platform motion vector and $\mathbf{C}$ the stiffness matrix of the structure, where one can include the stiffness of the mooring lines ($\mathbf{C} = \mathbf{C}_{structure} + \mathbf{C}_{mooring}$). Since all loads have different frequency ranges as shown in Section 3.3.1 there is of essence to avoid resonance by making sure the natural frequency is outside the range of the load that is causing the specific mode. There are typically three modes for a semi-submersible substructure that are critical: The tower side-to-side mode, tower for-aft mode, and heave mode where the waves forces the substructure to lift upwards. An illustration of these modes can be seen in Figure 3.10.

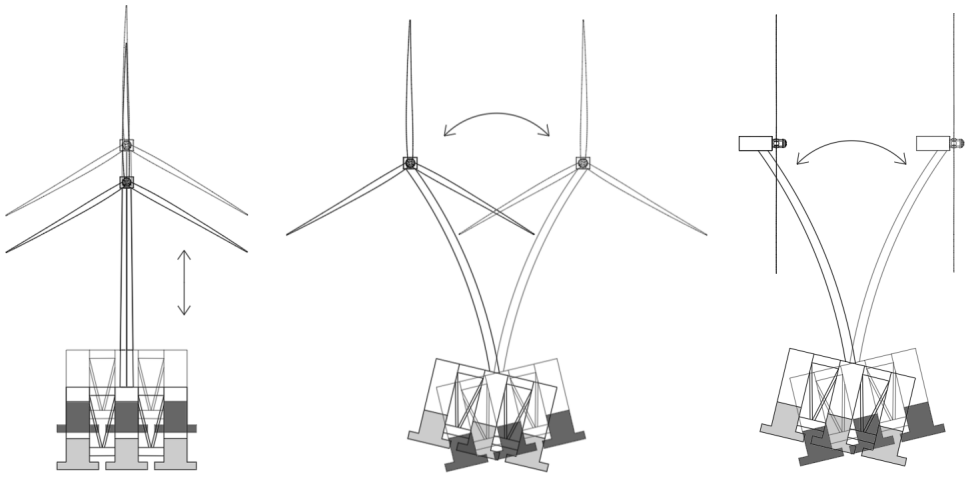

Figure 3.10. *Different critical modes for an OWT on a semi-submersible substructure. From left to right: heave mode, tower side-to-side mode, tower fore-aft mode.*

3.4 Stability for floating OWT

The following section describes the buoyancy and static stability of a floating substructure. A simplified method to analyze floating OWTs is to use a quasi-static method. For a structure subjected to dynamic loads, the assumption is that the deformation profile is time-independent (Ambrosio, 2001). The benefit of this is that the inertia forces coming from the dynamic load doesn't contribute to the deformation profile.

3.4.1 Floating equilibrium

The floating equilibrium is obtained by balancing the buoyancy force F_B and the gravitational force F_g. The buoyant force is the weight of water displaced by the submerged volume of the substructure according to Archimedes's principle. The gravitational force F_m comes from the total weight of the OWT. The balance is kept intact as long as the two forces are in equilibrium as shown in Equation 3.23.

$$F_B - F_g = \rho_w g V_{submerged} - m_{OWT}\ g = 0 \tag{3.23}$$

3.4.2 Static stability

Floating substructures should be able to have sufficient stability against disturbances such as wind, waves, and currents in order to not capsize. In calculations of static stability the buoyancy forces are summed up to one single vertical force acting upwards, the location of this force is called the center of buoyancy. In the same matter, the gravity force from the dead weight of the OWT is summed up to a vertical force acting downwards. In an upright position, the center of buoyancy and center of gravity are aligned and stable. As soon as a heel is introduced by the environmental loads, forcing the structure into a tilting position, the center of

buoyancy shifts position. This is due to the change of submerged volume which generates a lever arm to its original center. The reaction to this is then what is called a restoring moment. The different floating solutions described earlier achieve stability in different ways. The semi-submersible is much like a boat and has the center of buoyancy below the center of gravity, unlike the spar buoy which has the center of buoyancy above the center of gravity.

The thrust force is in magnitude the force generating the most heel, i.e. called heel moment, and has the lever arm from the center of the hub to the sea level. An illustration of different stability situations for increasing heel angle is presented in Figure 3.11. The heel moment reduces with increasing heel angle due to the reduced lever arm. The restoring moment increases up to a point where the center of buoyancy starts to shift in the opposite direction. If the system is in the region before the point of capsize it has the ability to retain its original upright position.

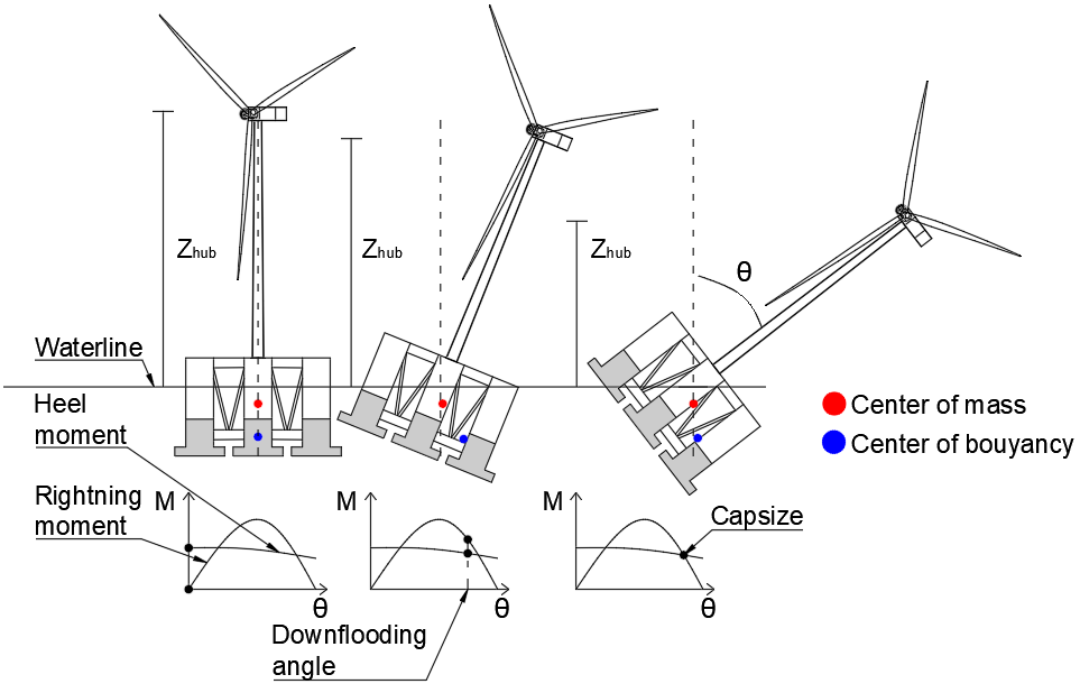

Figure 3.11. *Illustration of heel and righting moment curves for a semi-submersible substructure.*

The heel and restoring moment curve then indicates the heel angle of possible capsize and this can be used as a check in the time-domain analysis of the structure. In terms of the coordinate system, this heel angle refers to the pitch angle of the system. For column stabilized units such as semi-submersibles, DNV (2021b) require that the area under the righting moment should be equal to or 30% more than the area under the heel moment. In the early stages of preliminary design, it is convenient to set a maximum heel angle for a quasi-static stability case. This is typically set to a heel angle of 10° due to the reduced capacity in energy production and risk of blades colliding with the tower for angles above this limit (Chella et al., 2010;

Gilloteaux and Bozonnet, 2014; Huijs et al., 2014; Wayman et al., 2006). For small heel angles, the vertical distance between the center of gravity and the center of buoyancy can be assumed to be unchanged. With this in mind, one can set up the following relationship:

$$\theta_{heel} = \frac{M_{heel}}{C_r} \tag{3.24}$$

Where θ_{heel} is the steady-state pitch, limited to 10° in this case. M_{heel} is the product of the mean thrust force and its lever arm from the hub height to the sea level. C_r is the restoring coefficient and expressed according Equation 3.25.

$$C_r = F_B z_B - F_g z_g + \rho_w g I_T \tag{3.25}$$

where F_B is the buoyancy force and z_B center of buoyancy; F_g the total system gravity force and its mass center z_g; and the transversal moment of inertia of the substructure, I_T.

In the early design of a semi-submersible one can utilize previous expressions and extract the needed distance between the main column and the offset column to maintain stability. All of the previously described are for a quasi-static case where the floater is fixed in one position. There are "dynamic" effects that put the floater into a rolling motion which is not considered within the design phase in this thesis (Lee, 2019). This is because the contribution of potential energy is only affecting the initial and final state.

4

Case study

This chapter presents the case study for the comparison between a semi-submersible and a jacket substructure. The chosen simulation software and chosen substructures are presented. A reference case is introduced for verification and validation. The chapter ends with a description of the design method for the substructures to be designed.

4.1 Location, specifications and assumptions

The case study is located 70 km northeast of Gävle and 50 km north of Orskar in Uppsala county where the sea depth varies between 25-82 m with an average of 45 m (wpd, 2021). There is currently a project in early planning here called Fyrskeppet owned by the company wpd AG and the location can be seen in Figure 4.1.

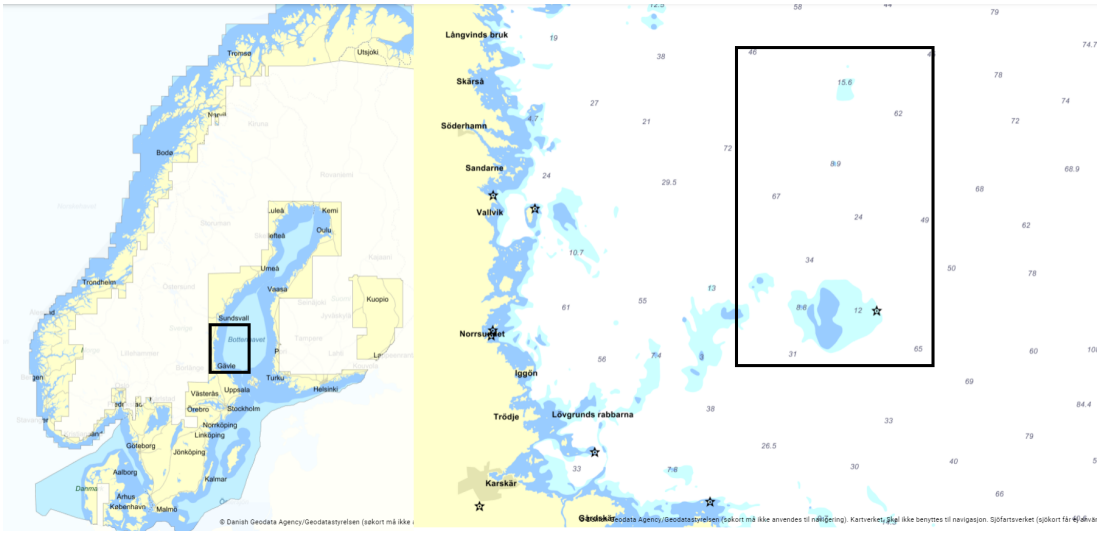

Figure 4.1. *Location where the wind farm is planned.* Eniro (2023). *Bothnian Sea Sweden.* Nautical chart [Cartographic material]. https://pasjon.eniro.se/ [27-03-2023].

Since data is yet to be collected regarding wind and waves at this location, assumptions have been made and gathered from other sites in the Baltic Sea and are therefore estimations for this project. The mean wind speed at a height of 150 m is estimated by Global wind atlas (https://globalwindatlas.info/en) to 9.3 m/s. All other environmental input needed for the case study is extracted from a site south of Sweden. The input is from a project called Krieger flak and will be estimations for the actual location (Bülow Jørgensen Ljjj & Gravesen, 2009). The environmental data for the five load cases are presented in Table 4.1. The calculated significant wave height, peak wave period, and peak-enhancement factor are specified in Appendix B.

Table 4.1. *Environmental data for the case study.*

Parameter			
Reference height	H_s	(m)	150.0
Mean wind speed[1]	U_{m150}	(m/s)	9.3
Load case 1			
Significant wave height[2]	$H_{s.1year}$	(m)	3.6
Peak wave period[2]	$T_{p.1year}$	(s)	8.0
Peak-enhancement factor[3]	$\gamma_{p.1year}$	(-)	2.462
Load case 3			
Significant wave height[2]	$H_{m.1year}$	(m)	7.0
Peak wave period[2]	$T_{m.1year}$	(s)	9.4
Peak-enhancement factor[3]	$\gamma_{m.1year}$	(-)	2.359
Load case 2, 4, 5			
Maximum wave height[3]	$H_{m.50year}$	(m)	10.1
Peak wave period[3]	$T_{m.50year}$	(s)	11.25
Peak-enhancement factor[3]	$\gamma_{m.50year}$	(-)	5

Note.
[1]Global wind atlas
[2]Bülow Jørgensen Ljjj and Gravesen, 2009
[3]Calculated Appendix B

As described in Section 3.2.2, a wind turbulence field is required. The wind field is created according to the specified load cases presented in Table 3.1 and the environmental data in Table 4.1. In this thesis, one seed is chosen for all iterations to remove the stochastic effect and therefore be able to study the effect of dimension changes more clearly. A seed is the initial value that set the stochastic effect. This assumption is also made for irregular waves where one seed is used in all iterations. Input files for the wind and wave files are found in Appendix G.1, G.2, and H. The requirements according to DNV (2021c) are that the wind turbulence field should be 10 minutes long and six different seeds should be used. Another assumption is that the wind and waves are only simulated to attack the structure from one angle, 0 deg. The exception is in load case 5 where the waves attack perpendicular to the wind direction, 90 deg. For the simulations in this thesis, the angle of 0 deg means that one column is at the front and two at the back. In a detailed design, these factors need to be considered with simulation for different seeds and different angles of attack.

The substructures will be designed and analyzed for two different sizes of wind turbines. The input data for the 5 MW and 15 MW wind turbines are presented in Table 4.2.

Table 4.2. *Input data for 5 MW wind turbine (J. Jonkman et al., 2009) and 15 MW wind turbine (Gaertner et al., 2020).*

Parameter		NREL 5 MW	IEA 15 MW
Rated power	(MW)	5.00	15.00
Rotor diameter	(m)	126.00	245.00
Rotor overhang	(m)	5.02	11.35
Blade length	(m)	60.00	120.00
Blade width root	(m)	3.54	5.20
Blade width tip	(m)	1.42	2.34
Hub height	(m)	90.00	150.00
Tower diameter bottom	(m)	6.00	10.00
Tower diameter top	(m)	3.87	6.50
RNA mass	(ton)	350.00	1017.00
Cut-In wind speed	(m/s)	3.00	3.00
Rated wind speed	(m/s)	11.40	10.59
Cut-Out wind speed	(m/s)	25.00	25.00
Cut-In speed	(rpm)	6.90	5.00
Rated speed	(rpm)	12.10	7.56

4.2 Simulation software

The study is based on one semi-submersible substructure and one jacket substructure. To investigate and design the substructures in a time domain a simulation software is used. These software are sometimes called “simulation codes” which can be mistaken for “design codes” which refer to rules and standards used within the industry. There are several different simulation software available on the market all with different functionalities, possibilities, and ways to design an OWT.

Mutungi and Faruk Halici (2016) have categorized common simulation software and its limitations, which is used to select appropriate simulation software for this project. The selection is based on the possibility to design fixed and floating substructures within the same software. Secondly, it is preferable that all types of substructures within fixed and floating substructures can be analyzed within the software. A third criterion is the availability of the software. Based on these criteria, the software Ashes was chosen.

One of the benefits of Ashes is the prebuilt reference cases from the OC4 project which is further described in Section 4.4. The advantage of Ashes is that the structural model for the chosen substructures already is correctly implemented and verified by the software developers. According to the OC4 comparison the results from Ashes corresponded well with other simulation software’s.

4.3 Selection of substructures to analyze

The selection of substructures is based on several design criteria. Firstly the solution needs to be technically feasible for the intermediate depths, 30-60 m. Further on, it is desirable to concentrate most of the construction work onshore in the harbour, to reduce costs and to obtain safer work sites. Therefore the draft in the harbour will influence the choice of the substructure for the floating substructures. Secondly, the selection is based on the most established substructure solutions currently in operation and the announced selection of substructure for future projects. These criteria are valued since extended knowledge and infrastructure around the specific solution will decrease expenses. A summary of the input needed for selecting the substructure type is presented in Table 4.3. The table shows the suitable sea depths for the fixed solutions, the possible sea depths and harbour depths for floating substructures and lastly the establishment of different substructures on the global market.

Table 4.3. *A summary of the input needed for selecting the substructure type.*

Substructure type	Suitable sea depth (m)	Possible sea depth[1] (m)	Harbour draft[2] (m)	Establishment: OP[3] (%)	FP[4] (%)
Fixed substructures					
Gravity	< 30			1.60	6.65
Monopile	< 50			65.60	56.95
Jacket	< 60			11.60	13.40
Tripod	$20 - 60$			2.09	0.11
Floating substructures					
Semi-Submersible		$> 30 - 40$	$10 - 12$	0.16	16.10
Tension leg		> 50	$10 - 12$	0.07	0.03
Spar-buoy		> 70	70		1.90

Note. In OP and FP, there is a certain amount not listed in the table which refers to substructure types not mentioned in this thesis or unreported.
[1]ETIPWind Executive Committee, 2020 Vázquez et al., 2022a
[2]Crowle and Thies, 2022
[3]Currently operating projects (Musial et al., 2022b)
[4]Announced future planned projects (Musial et al., 2022b)

Fixed substructure

The jacket and tripod are the fixed substructures that fit in the range of the intermediate water depth of 30-60 m. Since the jacket is more established in current operating and future planned projects, the selection for the fixed substructure is therefore the jacked substructure. The monopile could also be an alternative depending on the soil conditions for depths below 50 m. However, only one substructure is analyzed in this thesis, thereby the jacket substructure alone is selected.

Floating substructure

For the floating types, the intermediate depths are clearly to shallow for the spar-buoy and it can be seen with the 16 % that the semi-submersible solution is increasing in the future planned project. The semi-submersible substructure will therefore be used to dimension and analyze within this thesis.

4.4 Reference case

The project used for verification and validation is the OC4 project led by the International Energy Agency (IEA). OC4 was a continuation of an earlier project called OC3 and the purpose of the projects was to perform a code-to-code comparison of coupled simulation tools. The comparison was performed with one jacket structure and one semi-submersible structure. Input data from the OC4 load case 3.2 are used for validation and verification of the numerical model and can be seen in Table 4.4. The turbulent wind model used is the Mann model and the wave spectrum is JONSWAP. The turbine used was the NREL 5MW, which is presented in Table 4.2. Material data for the reference case and the case study is presented in Table 4.5.

The purpose with the reference case is to avoid to start from scratch with a initial geometry which is a time consuming process. Another intention is to compensate for the exclusion of FLS and ALS. Therefore the dimensions is not optimized according to the structural resistance controls described in Section 4.5.3.

Table 4.4. *Input data for validation and verification for semi-submersible substructure, from OC4 load case 3.2 (Robertson, Jonkman, Vorpahl, et al., 2014).*

Parameter		
Wind speed at hub height, V_{hub}	(m/s)	11.4
Significant wave height, H_s	(m)	6.0
Peak-spectral wave period, T_p	(s)	10.0
Enhancement factor/peakedness, γ	(-)	2.87

Table 4.5. *Material properties for steel used in the reference case as well as in the case study (Vorpahl et al., 2011).*

Material property		
Density, ρ	(kg/m^3)	7850.0
Young´s modulus, E	(GPa)	210.0
Yield strength, f_y	(MPa)	355.0
Poisson´s ratio, ν	(-)	0.3

4.4.1 Geometry semi-submersible

The main components and the design configuration of the OC4 semi-submersible designed for 200 m sea depth is illustrated in Figure 4.2. One of the main components in a semi-submersible substructure is the main column, which is located in the center of the substructure, below the tower. Below the offset columns, heave plates are installed to provide buoyancy and damping to the structure. To provide stability within the substructure bracing is used between the columns. Mooring lines are used for station keeping and does not provide stability. The anchor distance for the mooring lines is 837.6 m from the platform center line to the anchor. The draft at still water level (SWL) is 20 m and the elevation of the tower base is 10 m above SWL. A summary of the dimensions for the OC4 semis-submersible substructure is presented in Table 4.6.

The dimensions from the semi-submersible substructure are used as a validation for the structural model built in Ashes and for the convergence study.

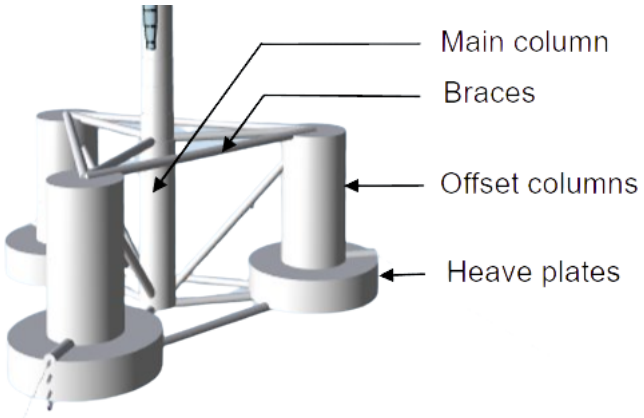

Figure 4.2. *Main components in the semi-submersible substructure: main column, braces, offset columns, and heave plates.*

Table 4.6. *Geometry for OC4 reference case (Robertson, Jonkman, Vorpahl, et al., 2014).*

Parameter	Length/ Height (m)	Diameter (m)	Thickness (mm)
Main column	30.0	6.5	30.0
Offset columns	26.0[1]	12.0	60.0
Heave plates	6.0	24.0	60.0
Brace		1.6	17.5
Mooring lines (unstretched)	835.5	0.0766	

[1]Set to 24 m as a simplification in the simulation model, as can be seen in Figure 4.2 there is no protrusion above the upper level of braces.

4.4.2 Geometry jacket

A jacket designed for 50 m sea depth is used in the OC4 project with a total height of 70 meters. The main components and the design configuration of the jacket are illustrated in Figure 4.3. Three main parts are the transition piece, the legs, and the X-braces. The transition piece is a concrete block that transfers the forces from the tower to the lattice structure and the dimensions are 9.6 x 9.6 x 4 with a weight of 666 000 kg (Vorpahl et al., 2011). Below the transition piece, four legs are connected and carry the load down to the foundation. The center-to-center distance between the legs is 8 m at the top and 12 m at the bottom. Between the legs, X-braces are attached in four levels to stabilize the substructure. A summary of the dimensions for the OC4 jacket substructure is presented in Table 4.7.

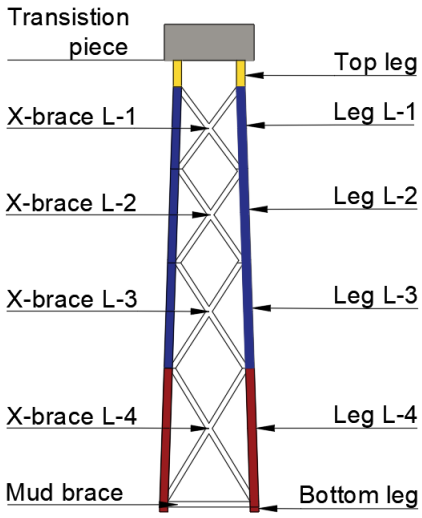

Figure 4.3. *Main components in the jacket substructure: transition piece, legs 1-4, X-braces 1-4, and mud brace.*

Table 4.7. *Dimensions for the OC4 jacket at 50 m sea depth (Vorpahl et al., 2011).*

Part	Color in figure	Diameter (m)	Thickness (m)
Truss and mud brace	White	0.8	0.020
Top leg	Yellow	1.2	0.040
Leg truss 1-3	Blue	1.2	0.035
Bottom leg and leg truss 4	Red	1.2	0.050

4.5 Preliminary design of the semi-submersible substructure

The preliminary design of the semi-submersible substructure has the same configuration as the reference case. This is to enable validation of results from the case study in comparison to the reference case. There might be more efficient and optimized designs, in regards of placement of the tower and stabilization of the columns but this is not investigated within this thesis.

4.5.1 Structural model

The structural model for the semi-submersible substructure is built with Euler-Bernoulli beam elements. Since the member types cross-sections are uniform along the length of the member the element size is chosen to 10 m. The buoyancy is modeled with a spring system which can be seen in Figure 4.4.

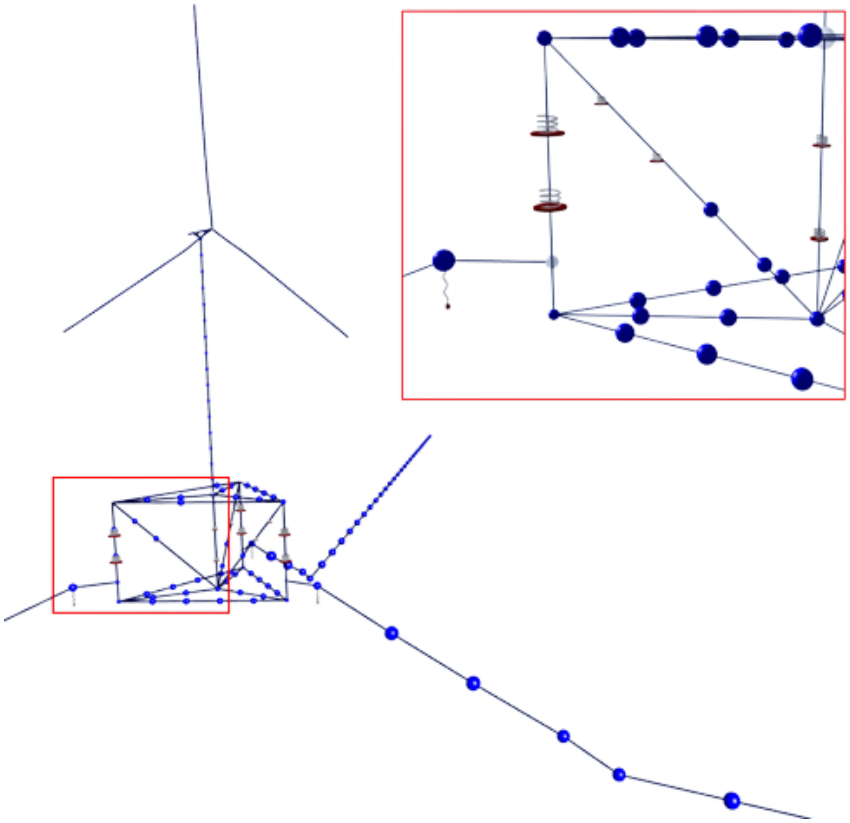

Figure 4.4. *Structural model for the semi-submersible substructure, showing the support system. Where the translational springs are placed in the columns and braces; rotational springs where the mooring lines are attached to the heave plates; and fixed to the seafloor in the opposite end.*

The translational spring is applied for one element and therefore placed in the ele-

ments two nodes. These springs are located in the offset columns, the main column, and in the diagonal braces. The translational springs are free to move in the x- and y-direction which allows the structure for motions caused by environmental loads. At the bottom edge of the heave plates where the mooring lines are attached, there are rotational springs providing stiffness in the yaw motion. The stiffness of these rotational springs are used as a calibration tool for improving the results closer to the reference case. Their stiffness is set to 3.278 GNm/rad The structure is then station kept by fixating the end of the mooring lines to the seabed. An overview of the support system can be seen in Table 4.8.

Table 4.8. *Structural model support system.*

Location	n	Purpose	Restrained coordinates/ motions	Support	n_{tot}
Offset column	2	Buoyancy	Heave	Spring ^{T}	6
Main column	2	Buoyancy	Heave	Spring ^{T}	2
Diagonal braces	2	Buoyancy	Heave	Spring ^{T}	6
Mooring $\leftrightarrow$ heave plate	1	Calibration	Yaw	Spring ^{R}	3
Mooring $\leftrightarrow$ sea bed	1	Station keeping	x, y, z	Fixed	3

Note.
^{T}Translational
^{R}Rotational
$\leftrightarrow$Connecting

The stiffness of a member's translational spring is calculated depending on the member area breaking through the undisturbed sea surface according to Equation 4.1. The resulting spring stiffness for one node is described with Equation 4.2.

$$S_{member} = A_w \cdot \rho_w \cdot g \tag{4.1}$$

Where A_w is the water plane area, ρ_w is the density of seawater, and g is the gravitational constant.

$$S_{node} = S_{member} \frac{z^n_{node}}{z^{tot}_{node}} \tag{4.2}$$

Where S_{member} is the stiffness equal to one spring for the element, z^n_{node} is the distance from a node to the sea surface, and z^{tot}_{node} is the sum of z^1_{node} and z^2_{node}.

As can be seen in the structural model in Figure 4.4, the braces are modeled from the center of the main column to the center of the offset column/heave plate. This differs compared to the geometry in reality illustrated in Figure 2.1 where the braces are connected between the edge of the heave plates and the edge of the columns. The reason for this simplification is the use of beam elements. This generates a moment stiff connection, ultimately also generating a longer distance than reality.

Therefore the check due to structural resistance will be based on longer braces which are on the safe side.

The resultant forces from the environmental loads acting on each element are applied to the element's two nodes. The wind velocity generates a lift and drag force on the blades shown in Figure 4.5a, these forces induce the thrust and torque illustrated in Figure 4.5b. The two force couples are acting on each element and are then combined with the BEM model described in Section 3.2.2. This generates one resulting force and moment applied on each of the two nodes in the blade element as can be seen in Figure 4.5c. A drag force is acting on each element of the tower which is calculated with Morrison's equation which also can be seen in Figure 4.5c.

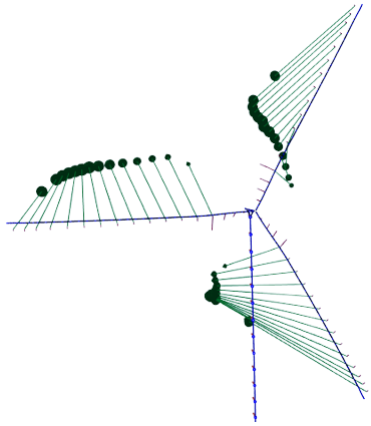

(a) *Lift (red) and drag (green).*

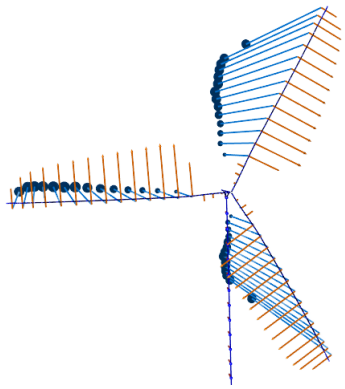

(b) *Thrust (blue) and torque (orange).*

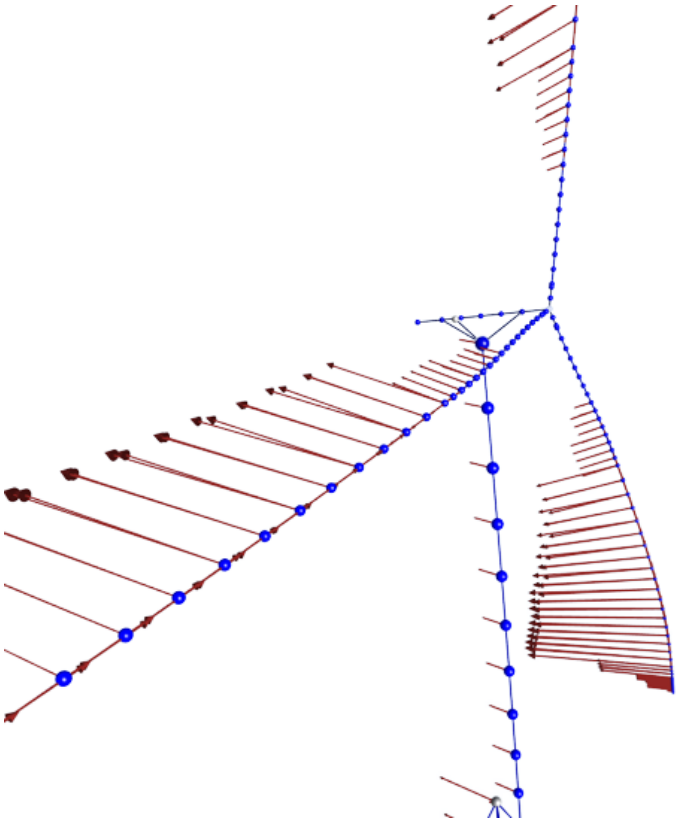

(c) *Resultant forces applied on the nodes.*

Figure 4.5. *(a) Lift and drag resultant force acting on each element on the blade. (b) Thrust and Torque force acting on the blade elements. (c) The resultant force and moment generated with BEM model applied on the nodes. Where the force acting outward from the blade and moment acting perpendicular to the blade cross-section. On the tower nodes resultant drag force is applied.*

Furthermore, the applied forces from the hydrodynamic loads are illustrated in Figure 4.6. The yellow arrows represent the buoyancy forces from the submerged volume of the elements. The arrows with two shades of red are the drag forces according to Morison's equation described in Section 3.2.1. In addition, the light blue and purple represent the inertia forces, and the blue and green represent the added mass term in Morison's equation.

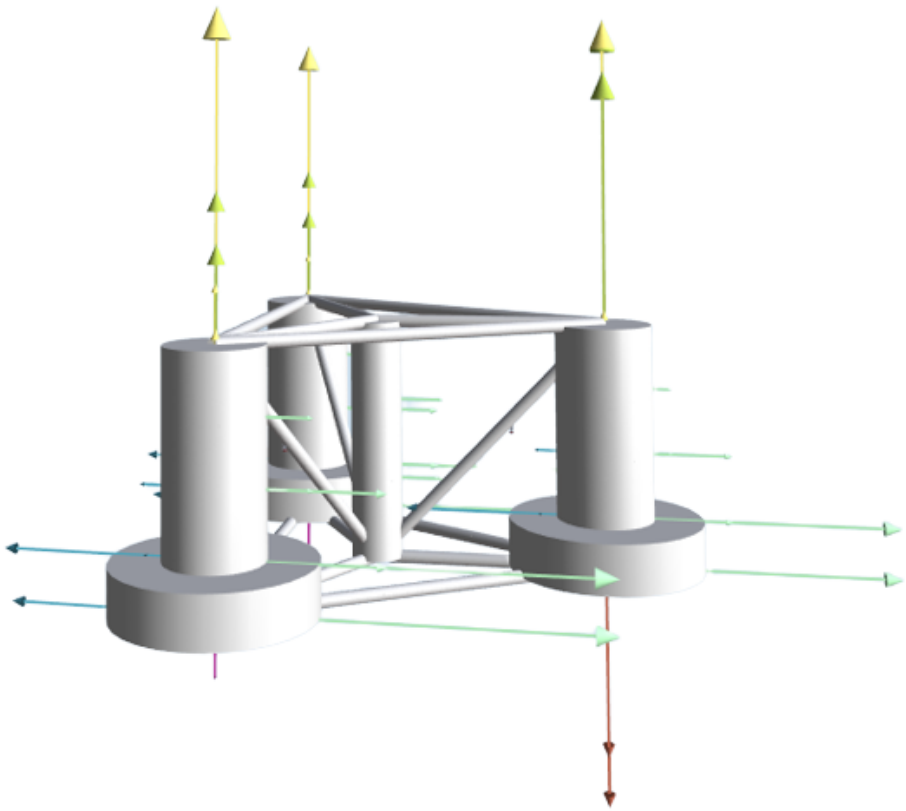

Figure 4.6. *Hydrodynamic loads acting on the structure.*

The effect of the water pressure at the bottom heave plate can be critical, due to its wide span. Since the model in Ashes is modelled with beam elements this is not captured within the software. The bottom heave plate is therefore analyzed in Abaqus where the von Mises stress is checked for two different configurations of internal supports. Configuration 1 is visualized in Figure 4.7a and shows the geometry according to the reference case and configuration 2 is shown in Figure 4.7b which is a new design, with simple internal support, to decrease stresses in the bottom heave plate. The boundary conditions are applied at the top of the offset column where it's locked in the x and the z direction. Three loads are applied in the model, water pressure from below acting on the bottom heave plate, water pressure from above acting on the upper heave plate, and water pressure on the inside of the bottom heave plate representing the ballast water. The magnitude of the loads is presented in Table 4.9. Additionally, the structural model is built with shell elements with a mesh size of 0.5 m. In the purpose of the rough control there was no need for convergence study of the mesh, since it will not change the conclusion of the study.

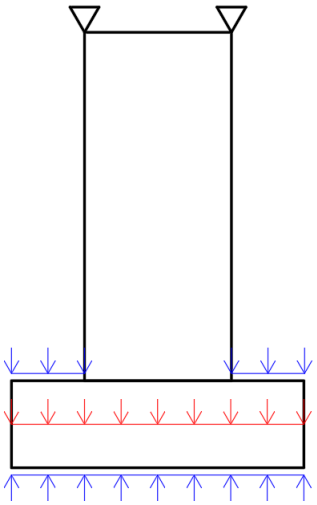

(a) *Configuration 1 according to OC4 where offset column are ending where heave plate starts.*

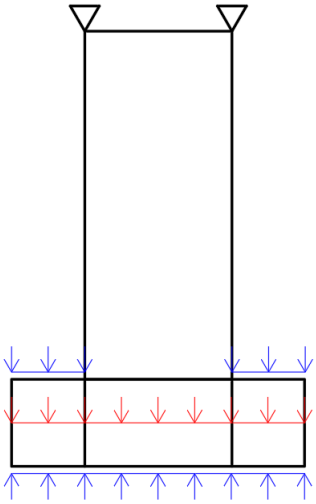

(b) *Configuration 2, new design with offset column extending to bottom heave plate to lower span length.*

Figure 4.7. *Structural models for the analysis of the heave plate.*

Table 4.9. *Load applied on the structural model for the analysis of the heave plate.*

Placement of distributed load	Sea depth (m)	Safety factor (-)	Water pressure (kPa)
Outside bottom	20	1.35[1]	270
Outside top	14	1.00[2]	140
Inside bottom	6	1.00[2]	60

Note.
[1]Unfavourable load
[2]Favourable load

4.5.2 Design choices and requirements

The semi-submersible substructure can have several different configurations and be designed in multiple ways. To enable more reliable results, which can be compared to the reference case OC4, it is chosen to have the same geometric shapes, keep the placement of the main column in the center of the substructure, and have the same stabilizing configuration of the bracing system between the columns.

Since the intermediate water depth of 30-60 meters limits the space available for the substructure it is set a maximum total height of 30 meters. Where 10 of these 30 meters are set to be above sea level, this design choice is regulated partly with buoyancy but also with ballast.

To limit the number of design parameters, the diameter of the heave plate is set to two times the offset column. The CC-distance between the main column and

the offset columns is limited to 29 meters maximum, which is in line with the OC4 design. Furthermore, the main column diameter is set to match the diameter of the tower base. The thickness is equal for the members of the same type and is therefore not optimized, similar to the OC4 design. Dimensions that are analyzed and enabled for changes are listened below:

- Offset column: diameter and thickness
- Heave plate: thickness
- Brace: diameter and thickness
- Main column: thickness

The heel angle that the structure is allowed to tilt is set to 10°. This requirement is conservative and sets the boundary for the static stability calculations. The lowest value allowed for the tilt is set to 9.5° to minimize dimensions. The max structural resistance utilization is set to 90 %. Finally, it is aimed to keep the dimensions of each member at a feasible size for simplified manufacturing and transportation.

Since mooring design isn't a focus in this thesis the dimensions are based on a study comparing non-linear and linear modeling of mooring lines at lower sea depth (Xu & Michailides, 2015). In Figure 4.8 the mooring line and the parameters used for design are visualized. The line lengths for different depths according to the study are presented in Table 4.10.

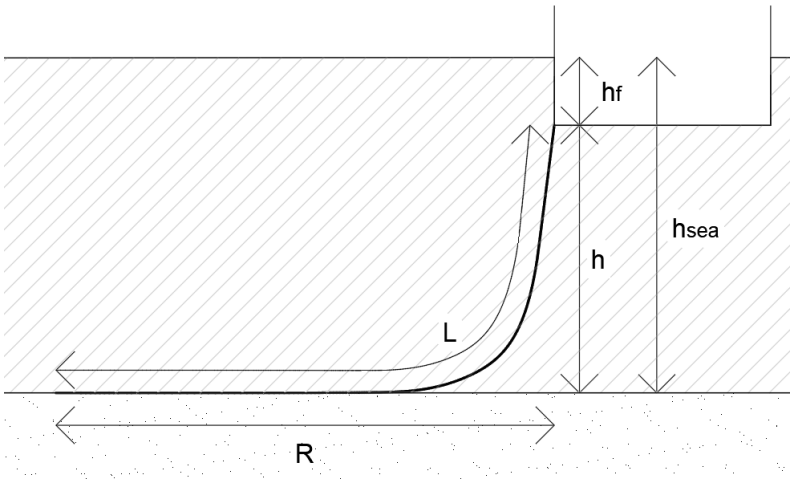

Figure 4.8. *Illustration of mooring lines and definition of line length (L), anchor radius (R_m), fairlead height (h_f), sea depth (h_{sea}) and sea depth between fairlead and seabed (h).*

Table 4.10. *Mooring line lengths for different sea depths (Xu & Michailides, 2015).*

Sea depth	Fairlead height (m)	Unstretched line length (m)
200 m	−18	873
150 m	−18	671
50 m	−18	567

Mooring lines in shallow waters are exposed to larger stresses and therefore it's suitable to use an anchor chain (Xu & Michailides, 2015). In deeper waters, the stresses on the mooring lines are smaller, and therefore a wire rope is suitable as used in the reference case OC4. The material parameters for the mooring lines are presented in Table 4.11.

Table 4.11. *Material parameters for wire rope (Robertson, Jonkman, Vorpahl, et al., 2014) and anchor chain mooring line (Xu & Michailides, 2015).*

Mooring line type	Nominal diameter (m)	Unit mass in water (kg/m)	Young's modulus (GPa)
Wire rope	0.0766	113.35	200
Anchor chain	0.18	648	200

From the given unstretched line length the shortest, longest, and mean anchor radius is calculated according to the equations below:

$$R_{min} = L - h \leq R_m \leq \sqrt{L^2 - h^2} = R_{max} \tag{4.3}$$

$$R_{mean} = \frac{R_{max} + R_{min}}{2} \tag{4.4}$$

In this thesis, the mean anchor radius is used to perform a linear extrapolation of the anchor radius for the studied sea depths of 30, 40, 50, and 60 m.

4.5.3 Design method

The flowchart in Figure 4.9 shows the design process for the semi-submersible substructure where requirements, design choices, and utilization are implemented and checked in MATLAB. The main controls are stability, structural resistance, and frequency. After each of these controls, the geometry is updated and then analyzed in the simulation software Ashes. Firstly, the semi-submersible substructure needs to be ensured enough volume to float. In the first run, this is regulated by the diameter of the offset columns. In the next runs, buoyancy is regulated with the ballast within the offset columns. The stability is regulated by the distance between the main column and the offset columns (CC-column offset). Lastly, the dimensions of the members will depend on the structural resistance. A more thorough description

of the steps is presented in the coming paragraphs.

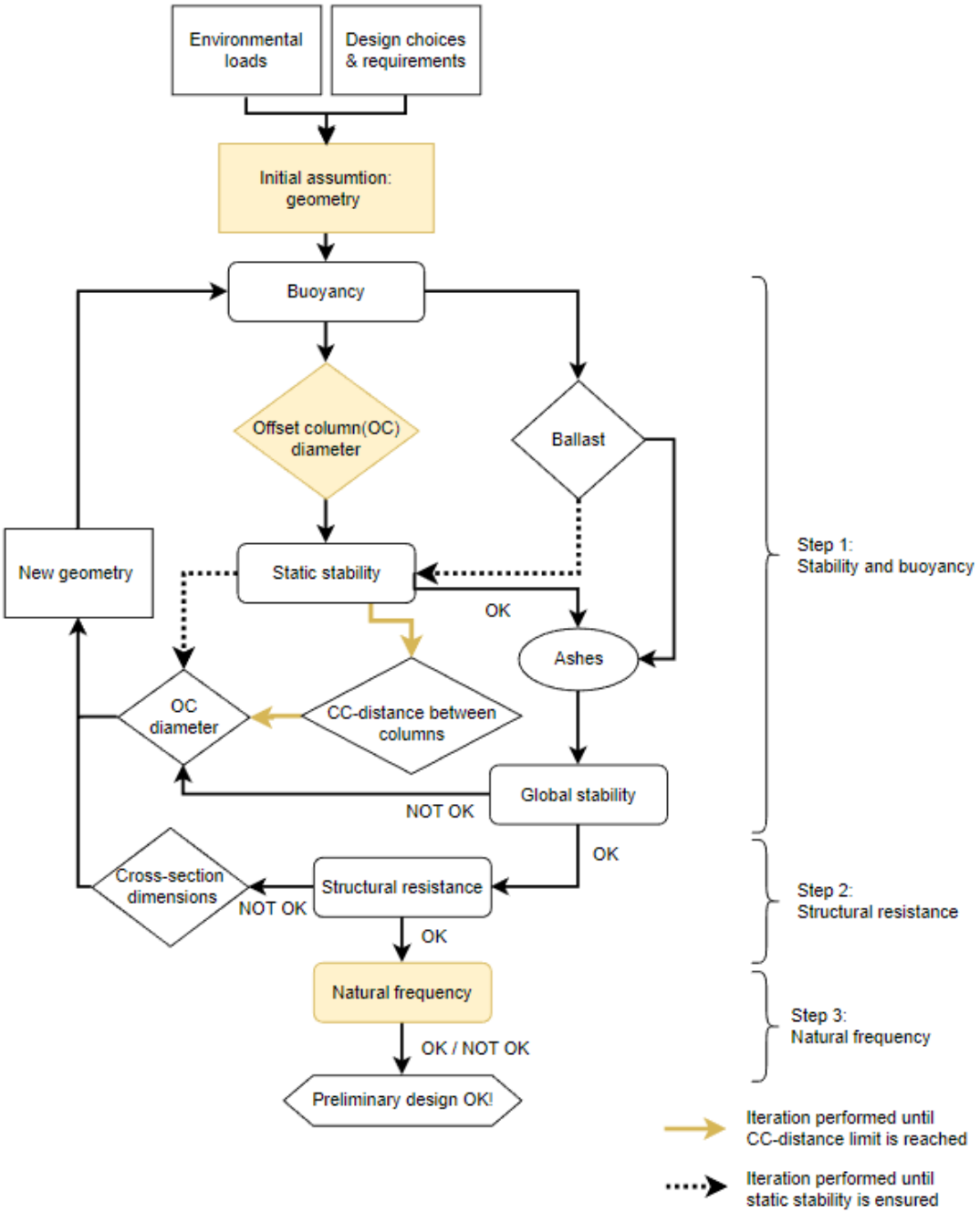

Figure 4.9. *Flowchart over the preliminary design of the semi-submersible substructure. Yellow marked boxes indicate that the event is done once.*

Step 1: buoyancy and stability

The first box in the flowchart in Figure 4.9 is the buoyancy function. Inside this function, the buoyancy condition is controlled according to the theory in Section

3.4.1 and Equation 3.23. In the first iteration, the input to the function is the assumed geometry and the output is the offset column diameter that is needed for the condition to be fulfilled.

The second box is the stability function which contains Equation 3.25 described in Section 3.4.2. In the first iteration, the input to the function is the assumed geometry and the offset column diameter from the buoyancy function. The output is the CC-distance and if the limit of this parameter is met the output is also an increased offset column diameter.

As seen in Figure 4.9 a new geometry is therefore defined which is the input to the buoyancy function in the second iteration. The difference in this iteration is that the output is the ballast mass instead of the offset column diameter. Therefore the input to the stability function is the ballast mass. The output of this function is then either a increased CC-distance or if this value already is met a increased offset column diameter. These iterations continue til the conditions in the two functions are fulfilled and an initial geometry can be sent to the simulation software Ashes.

After the simulation, the static stability is verified with the global stability from the simulation software. The simulated pitch angle is compared to the limit and if it overshoots, the offset column diameter is increased. This new geometry then goes back into the buoyancy function which outputs a new ballast mass that is sent into Ashes. A new simulation is performed and the iteration goes on til the pitch angle is below the limit.

Step 2: structural resistance

The last step in the iteration is the structural resistance box. The design method for structural resistance is based on the standard DNV-ST-0119. For design in the ultimate limit state, the members are divided into two types, tubular members and shell structures. The criterion to distinguish between these types is presented in Equation 4.5.

$$Tubular member \quad \frac{D}{t} \leq 120 < \frac{D}{t} \quad Shell structure \tag{4.5}$$

Where D is the diameter and t is the wall thickness of the member. Shell structures are designed according to DNV-RP-C202 and tubular members are designed according to SS-EN ISO 199902:2020. However, in SS-EN ISO 199202 the limit depends on the elastic modulus and the yield strength according to the following limit in Equation 4.6.

$$Tubular member \quad < \quad 0.2\frac{E}{fy} \tag{4.6}$$

Thereby it is a risk that some cross-sections end up in between the range defined by DNV and ISO, generating equations and limits that will not be applicable.

Shell structures are assessed for buckling according to DNV-RP-C202. Shells can be designed in four different configurations:

- Unstiffened circular cylinders
- Ring stiffened shells
- Longitudinally stiffened shells
- Orthogonally stiffened shells

As an initial check, the shells are designed as unstiffened circular cylinders. For this case, two buckling modes need to be checked, shell buckling and column buckling. The different steps needed for the calculation are presented in Appendix D.1. If the capacity is not enough, a second check is performed by adding stiffeners with the orthogonally stiffened shell configuration. The buckling modes for this configuration are shell buckling, panel stiffener buckling, panel ring buckling, general buckling, and column buckling and the steps are presented in Appendix D.4.

Tubular members are assessed for buckling and yielding according to SS-EN ISO 199902:2020. For the buckling analysis, two modes need to be checked, column buckling (including the effect of local buckling) and hoop buckling. The steps for the calculations are presented in Appendix D.2.

The assessment for tubular members against yield is based on a few different checks. These are axial tension, bending, beam shear, torsional shear, and a combination of these. The calculation steps are presented in Appendix D.3.

These controls are done for all members and if the utilization is over the limit, the dimension for the specific member type is changed. To be able to study the global behavior of the structure as well as locally within an element one parameter is changed at a time. This new geometry then goes back into the buoyancy function which outputs a new ballast mass that is sent into Ashes. A new simulation is performed and the iteration goes on til all the utilizations are below the limit.

Step 3: frequency

When the iterations in step one and two are fulfilled an assessment of the natural frequencies of the structure is performed in Ashes. The frequencies for the critical modes described in Section 3.3.2 are checked towards the target frequency domain. The preliminary design are considered completed after this step. Hence, there will not be executed further dimension changes post frequency check.

4.5.4 Sensitivity analysis of the model

In order to achieve convergence, a sensitivity analysis is conducted. The input data for the reference case is based on load case 3.2 from OC4 presented in Table 4.4. The non-linear algorithm used to solve the equation of motions needs to find a solution for every time step with a specific accuracy within a set number of iterations. There

are two members specifically sensitive to divergence issues: the rotor blades, and the mooring lines.

The blades can be modeled in two ways, with fully flexible elements or with stiff blade elements. Since it is not the purpose of this thesis to analyze the behavior of the blades it may be sufficient to model the blades as stiff to avoid non-convergence issues. In order to verify the choice of blade model, the two models are simulated to verify that the global behavior of the structure is acceptable compared to the results from OC4. When the blades are modeled as flexible structural damping is applied, in this case Rayleigh damping. The calculated mass (μ_R) and stiffness (λ_R) proportional damping coefficient used for the Rayleigh damping is presented in Appendix C. A damping coefficient of 1 % is used for the first and second frequency, at 0.009 Hz and 0.5 Hz respectively. The flexible rotor model is run with two different configurations:

- Flexible 1: stiffness damping only($\lambda_R = 6.254 \cdot 10^{-3}$, $\mu_R = 0$)
- Flexible 2: stiffness and mass damping($\lambda_R = 6.254 \cdot 10^{-3}$, $\mu_R = 1.111 \cdot 10^{-3}$)

The mooring lines can be modeled as non-linear or with linear springs with stiffness based on the mooring chains dimensions and modulus of elasticity, $k = \frac{EA}{L}$. The choice of model is assessed based on a comparison of the global behavior of the structure in surge, pitch, and bending moment at the bottom of the tower.

The equation of motions is solved with Newmark-Beta method with additional numerical damping using HHT method. In the non-linear analysis, the stiffness and tangent matrix are dependent on the displacement and therefore an error is introduced. From this residual error, residual energy can be established for a given time step and consider translational and rotational degrees of freedom. The sum of the residual energy can be reduced by using the Newton-Raphsson iteration scheme until it is smaller than a set criterion (10^{ϵ_a}). The exponent ϵ_a is the energy tolerance. The selection of suitable energy tolerance which will allow the solution to converge yet produce results close to the strictest criteria is done through a parametric study.

Furthermore, the number of iterations for each time step is set to 1000 and the time step is set to 0.025 s. These base settings are checked towards the results from the reference case. Since decreasing the time step will increase the computational time, this is only done if there is a non-converging problem with a certain load case. Appendix A.1 summarizes the input data for the convergence study used in the simulations.

4.6 Preliminary design of the jacket substructure

The configuration of lattice-based structures such as the jacket substructure can vary widely. Within this thesis, it is selected to use a similar configuration as in OC4 to enable verification of the design procedure to the reference model. This configuration consists of four main legs which are braced with X-braces in a number

of levels depending on the sea level. A mud brace is located near the sea floor and a transition piece of concrete is located at the top of the legs. All members are tubular shaped and have the possibility to be filled with either water or concrete. In this thesis, the legs are water filled and the braces are not.

4.6.1 Structural model

The jacket structure is modeled under the same principle as the semi-submersible with Euler-Bernoulli beams. The bottom of each main leg is provided with fixed support. The connection between the substructure and the tower is modeled with four beam members that are infinitely stiff. This connection is the concrete platform and since it is not a part of the preliminary dimensioning it is safe to assume this connection rigid enough to transfer the loads from the tower down to the substructure. The whole structural model can be seen in Figure 4.10. In Figure 4.10a the structural model including the turbine is presented and in Figure 4.10b a more detailed model of the substructure is presented including the four supports.

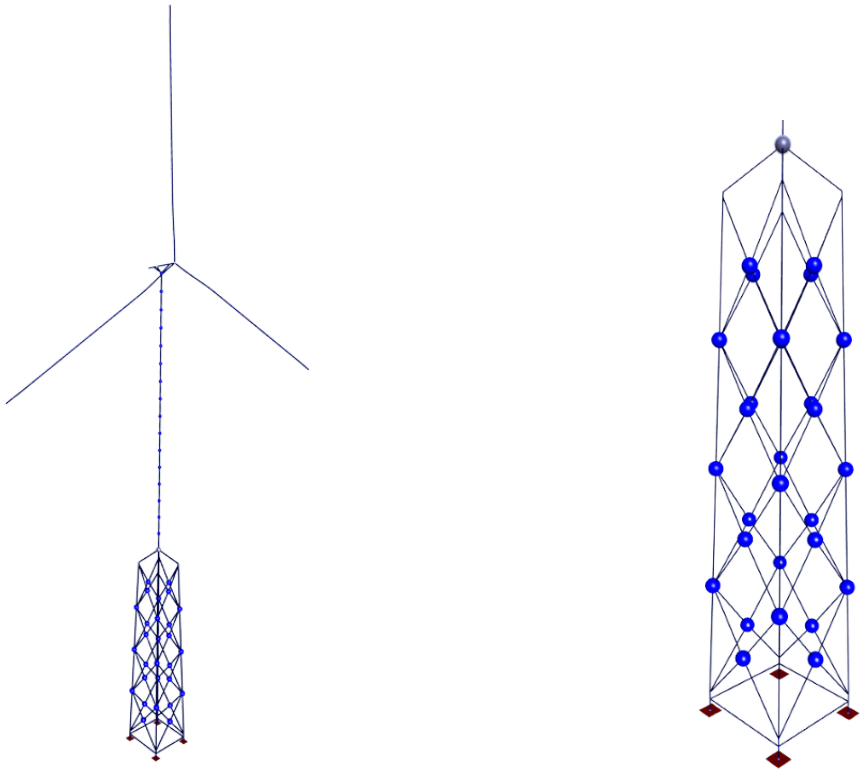

(a) *Illustration of the whole structural model for the jacket substructure.*

(b) *Detailed illustration of the structural model for the jacket substructure.*

Figure 4.10. *Structural models for the jacket substructure.*

4.6.2 Design choices and requirements

The jacket structures are designed from the connection of the tower and downwards. The transition piece (TP), a large block of concrete that transfers the forces from the tower to the jacket, has a given dimension depending on the tower's size. For a 5 MW turbine, the TP is 9.6 x 9.6 x 4 m, and for a 15 MW 13.6 x 13.6 x 4 m. The four legs have a specific batter and according to S. Ishwarya et al. (2016) 16 is the most optimal number in material efficiency. Although, to follow the design of the reference case as closely as possible a batter of 32 is used. The batter is described with the following equation:

$$Batter = \frac{Rise}{Run} \tag{4.7}$$

Where rise is the vertical height of the leg and run the horizontal length for one leg. The angle of the legs then decides the width of the jacket at the sea bottom. X-braces are evenly placed and the maximum vertical length of a cross brace is 16 m. The number of vertical bracing is therefore dependent on the sea depth. The height above the sea level is 20 m as in the OC4 project. The different parts that are analyzed and dimensioned are listed below and an illustration of where these are located in the structure is seen in Figure 4.11. The length of the top leg, mud brace leg, and bottom leg is fixed and set to 0.5 m, 0.875 m, and 1.5 m respectively. The length of the other members depends on the sea depth and number of levels of X-braces.

- Top leg, leg L-1-x, mud brace leg, and bottom leg: diameter and thickness
- X-brace L-1-x and mud brace: diameter and thickness

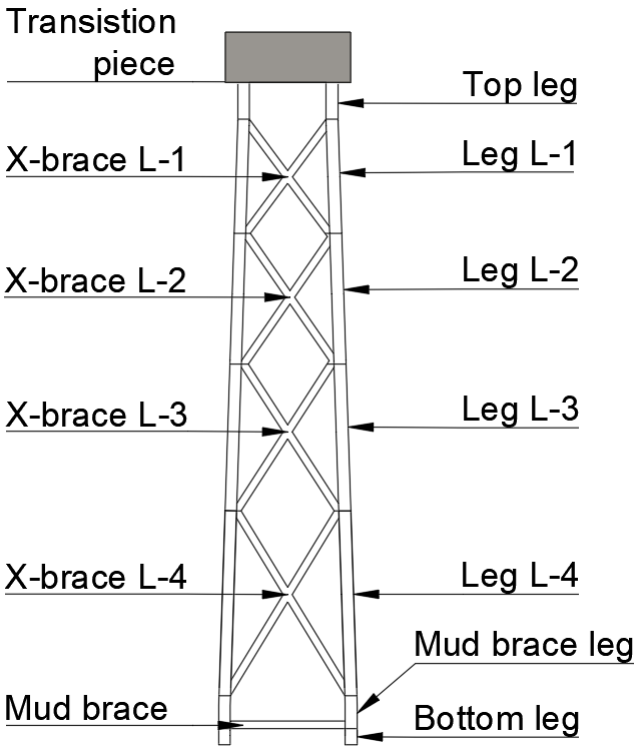

Figure 4.11. *Name of different structural parts for the jacket structure.*

The max structural resistance utilization is set to 90 % in the iteration procedure. Design requirements used in the preliminary design are stated by DNV (2021d) and are listed below.

- Yielding should be avoided
- Global and local buckling should be avoided
- Natural frequency should avoid the rotor induced frequency's with 10 %
- Maximum tilt angle < 0.5 °

4.6.3 Design method

The design procedure in the preliminary design of the jacket substructure is shown in Figure 4.12. During operation, the stability of the jacket substructure is ensured by the resistance of the foundation and is therefore not a part of the preliminary design. The main steps which are performed as an iteration in the flow chart are the control of the global stability and structural resistance.

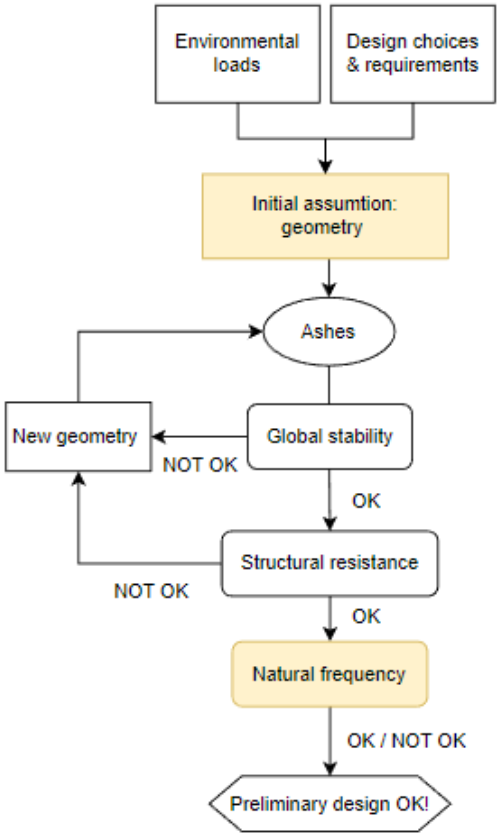

Figure 4.12. *Flowchart over the preliminary design of the jacket substructure. Yellow marked boxes indicate that the event is done once.*

The dimensions are found through an iterative process. The initial member dimensions are taken from the reference case as an initial assumption. A simulation is then performed to get the stresses on each member. After that, the global response is checked which for a jacket is the maximum tilt angle. The structural resistance which is described in Section 4.5.3 is then run to check if the utilization ratio is below the limit. If the utilization on one member is to high the dimension are revised and the structural resistance is rerun. The next step in the iteration procedure is to rerun the simulation with the new dimension and control global response and structural resistance again. The last step is to assess the natural frequencies in Ashes for the critical modes explained in Section 3.3.2. These frequencies are compared with the target frequency domain.

5
Results

In this chapter the results from the preliminary design will be presented. The first two sections contain the results from the preliminary design for the semi-submersible and the jacket respectively, supporting a 5 MW turbine for all intermediate sea depths. Section 5.3 present the results from the two substructure types supporting a 15 MW turbine at 40 m sea depth. The final section presents the comparison in structural mass and how much it contributes in CO_2.

5.1 Preliminary design of semi-submersible for a 5 MW turbine

The results from the preliminary design of the semi-submersible are presented in the following sections. Findings from the iteration process are explained as well as the critical sections and final design. The anchor radius for each intermediate sea depth is calculated according to Section 4.5.2 and is presented in Table 5.1.

Table 5.1. *Anchor radius for the intermediate sea depths.*

Sea depth	Fairlead height (m)	Anchor radius (m)
30 m	−14	528
40 m	−14	543
50 m	−14	558
60 m	−14	573

5.1.1 Model verification and validation

The subsequent section shows the results from the convergence study and includes the following:

- Sensitivity of the energy tolerance(ϵ_a)
- Modelling the mooring lines: linear or non-linear
- Modelling the rotor blades: stiff or flexible
- Using MacCamy-Fuchs or Morrison's wave algorithm

Sensitivity of energy tolerance

In the sensitivity analysis for the energy tolerance, the tower moment which varies with time is plotted for different energy tolerances, described in Section 4.5.4. The energy tolerances (ϵ_a) range from -8 to 8 which is illustrated in Figure 5.1. Results generated with an energy tolerance of 6 and above deviate significantly from the

strictest set energy tolerance of ϵ_a = -8. A smaller set of energy tolerances between -8 to 4 are presented in Figure 5.2. The deviation between the different energy tolerance is hardly noticeable when looking at a larger time span. However, when analyzing a small time interval as shown in Figure 5.3 an energy tolerance of 4 deviates from the other. An energy tolerance of 2 is thereby chosen to be an accurate enough tolerance to the residual error criteria. The signals in Figure 5.1, 5.2, and 5.3 are plotted with a signal-dampened low-pass filter. The setting in the filter is a cutoff frequency of 5 Hz.

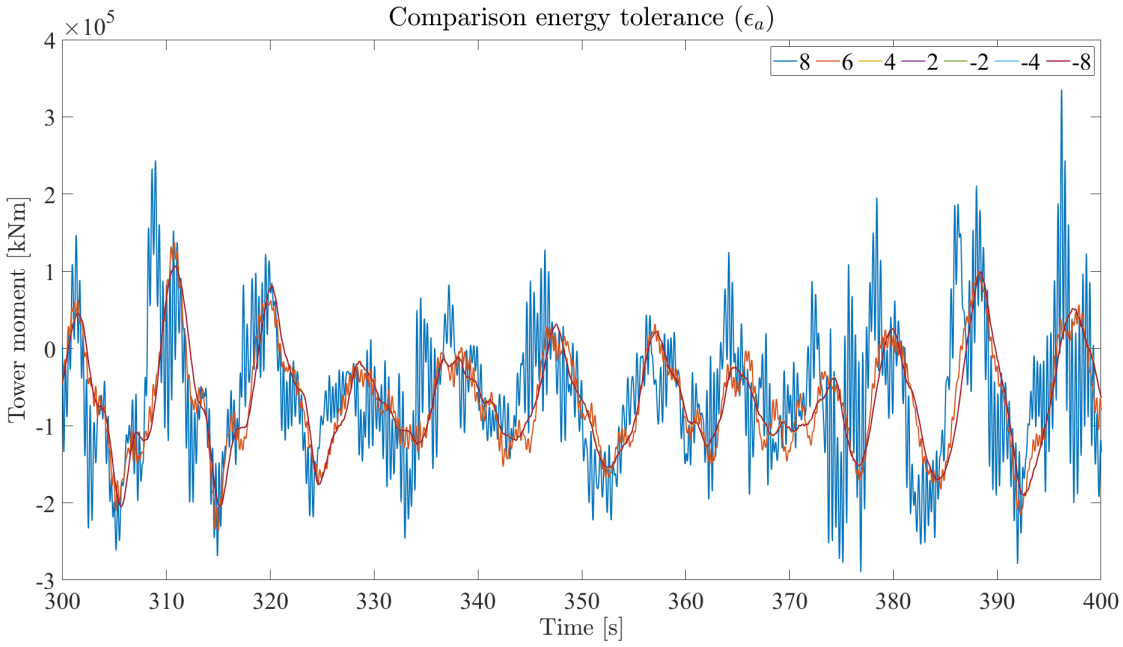

Figure 5.1. *Base tower moment over time for energy tolerances ranging between -8 to 8. Load case 3.2 from OC4, displaying time steps between 300 and 400 s. Plotted with a signal-dampened low-pass filter, with a cutoff frequency of 5 Hz.*

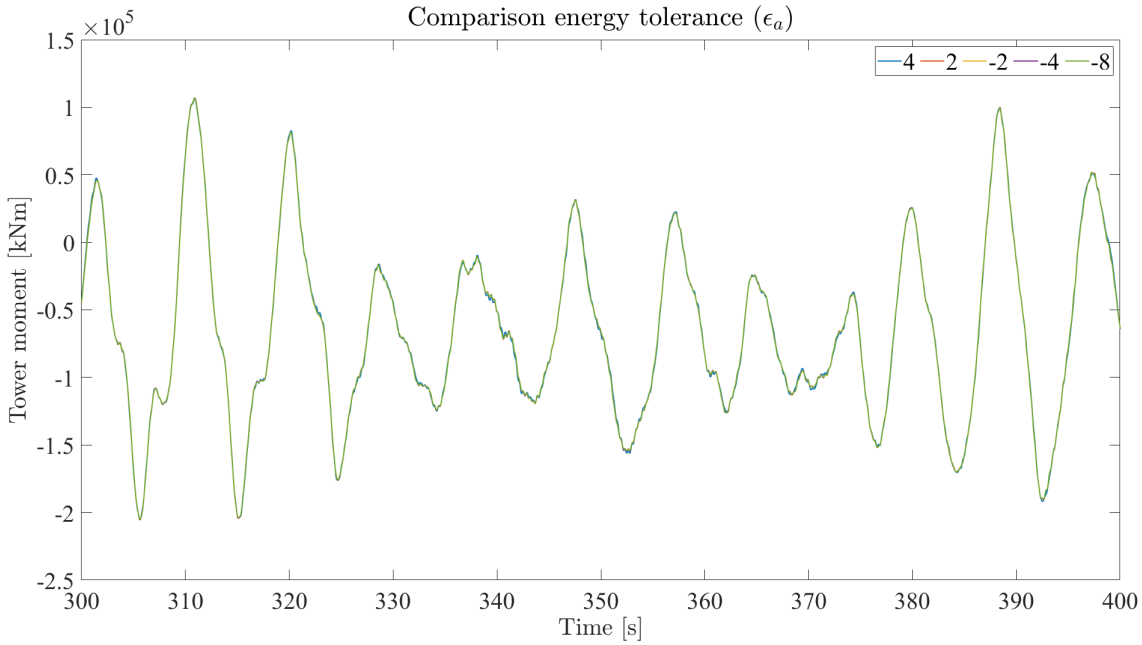

Figure 5.2. *Base tower moment over time for energy tolerances ranging between -8 to 4. Load case 3.2 from OC4, displaying time steps between 300 and 400 s. Plotted with a signal-dampened low-pass filter, with a cutoff frequency of 5 Hz.*

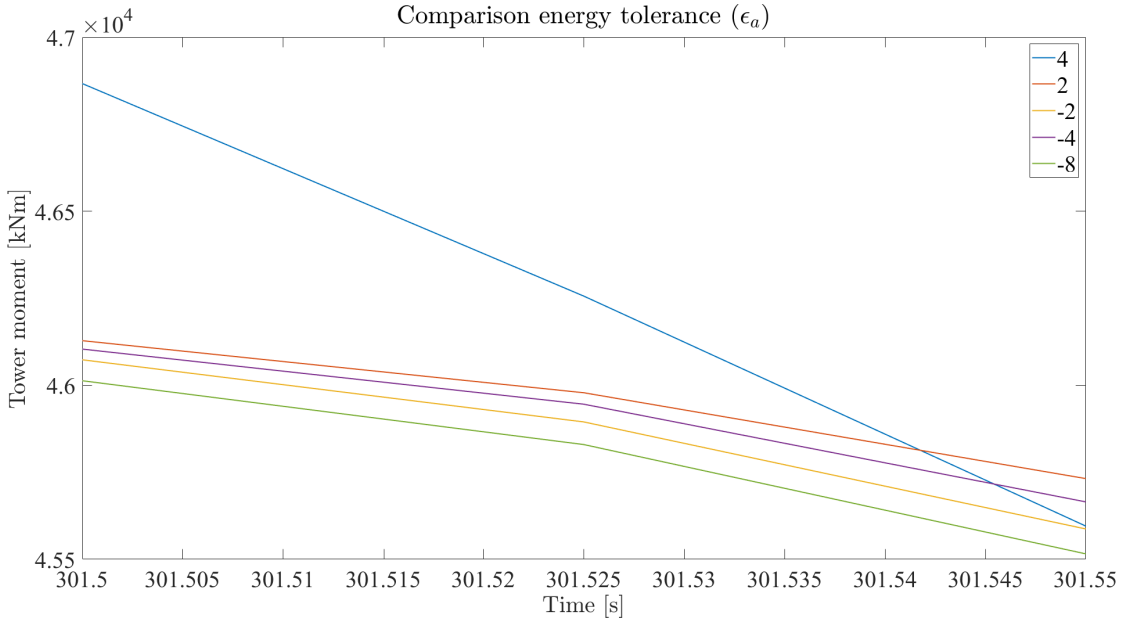

Figure 5.3. *Tower moment over a small time interval for energy tolerances ranging between -8 to 4. Load case 3.2 from OC4, displaying time steps between 301.5 and 301.55 s. Plotted with a signal-dampened low-pass filter, with a cutoff frequency of 5 Hz.*

Sensitivity of applied models and algorithms

The range of results obtained from the different simulation software's in the reference case in OC4 is displayed in Table 5.2 (Robertson, Jonkman, Vorpahl, et al., 2014). The results from the codes cover the mean value of the global responses (surge, pitch, and base tower moment). These results are used to validate the results from the FEM model built in Ashes. Furthermore, Table 5.3 presents the differences in results regarding different models used for mooring, rotor model, and wave algorithm.

Table 5.2. *Mean value range of global response (surge, pitch, and base tower moment) obtained from the different codes from the reference case in OC4 (Robertson, Jonkman, Vorpahl, et al., 2014).*

	Surge (m)	Pitch (°)	Base tower moment (MNm)
Min	6.1	2.7	62.0
Max	10.1	3.4	7.0

Table 5.3. *Results of the mean value of the global response (surge, pitch, and base tower moment) for; modeling mooring: lines linear or non-linear; modeling the rotor blades stiff or flexible; and using MacCamy-Fuchs or Morrison wave algorithm.*

	Surge (m)	Pitch (°)	Base tower moment (MNm)
Mooring: linear and non-linear			
Non linear	8.59	3.56	68.16
Linear	2.29	4.53	74.17
Diff.	−73.4%	27.4%	8.8%
Rotor model			
Stiff	8.59	3.56	68.16
Flexible 1	8.50	3.50	66.90
Flexible 2	8.57	3.53	67.57
Diff. 1	−1.1%	−1.7%	−1.8%
Diff. 2	−0.3%	−0.8%	−0.9%
Wave algorithm			
MacCamy-Fuchs	8.59	3.56	68.16
Morrisson	8.18	3.57	68.34
Diff.	−4.8%	0.4%	0.3%

Modeling the moorings with linear springs deviate significantly compared to using a non-linear model, shown in Table 5.3. Using linear springs also generate results outside the range from the reference case in all three global responses, therefore it is chosen to use a non-linear model for the mooring lines.

The different rotor models show a maximum difference of 1.8%. Based on these results it is chosen to use stiff blades to avoid divergence when simulating the model for the case study. This removes one of the non-linearities in the system and therefore increases the convergence rate. It is possible because the deformation of the blades isn't studied in this thesis.

Results from the comparison of the wave algorithms show similar results for the two algorithms. The MacCamy-Fuchs algorithm is chosen because it's more accurate according to the theory described in Section 3.2.2 and the pitch is closer to the range in the reference case.

With the final applied models and simulation settings, the surge and base tower moment are within the range of the reference case results. However the pitch is 4.6% above the maximum, since this will give conservative results, the chosen models are evaluated as acceptable. Appendix A summarize the settings used in Ashes for the convergence study and the final settings used for the case study.

5.1.2 Outcome of iterative preliminary design process for 40 m water depth

The results from the iterative process in finding the offset column diameter and the dimensions of the braces can be seen in Table 5.4. The simulation results with the batch name "B1" indicate that it is the offset column diameter that is changing, and "B2" is the simulations where the dimensions of the braces are changing. Furthermore, the results from the iterative process in finding the needed thickness for the structure's shell elements can be seen in Table 5.5, where the batch name "B3" refer to simulations where the offset column thickness is changed and batch names "B4" are when the thickness of the main column is checked.

The initial geometry of the offset column govern by the relation described in Section 3.4.2 gives 7.4 m in diameter, as can be seen in Table 5.4. However, this is not enough to maintain the design criteria of a maximum 10°. The resulting pitch is 34.2° from the simulation in Ashes. The column diameter of 10.1 m gives a pitch of 9.8° with the rest of the member's dimensions remaining unchanged from the reference case. One can also observe that the structural resistance and shell buckling utilization decreases except the hoop buckling which remains the same. The column diameter is used in further design iterations looking at braces.

When increasing the diameter of the braces one can notice that the structural controls including bending can decrease and increase. The structural controls for axial force decrease and the hoop buckling increases. When the thickness instead is increased one can observe that all controls decrease.

The final dimensions of the braces are found in batch B2.4 with a thickness of 225 mm and a diameter of 1.6 m which gives a maximum utilization of 88 % in the control of combined axial tension, bending, and hydrostatic pressure.

Table 5.4. *Results from batch runs analyzing the behavior when changing the column diameter, brace diameter, and brace thickness.*

Batch		B1.1	B1.2	B2.1	B2.2	B2.3	B2.4
Geometry brace							
Diameter, D	(m)	1.6	1.6	**1.8**	**2.0**	1.6	1.6
Thickness, t	(mm)	17.5	17.5	17.5	17.5	**20.0**	**22.5**
D/t	(-)	91.4	91.4	102.9	114.3	80.0	71.1
Geometry column							
Diameter	(m)	7.4	**10.1**	10.1	10.1	10.1	10.1
Thickness	(mm)	60.0	60.0	60.0	60.0	60.0	60.0
Geometry main column							
Diameter	(m)	6.5	6.5	6.5	6.5	6.5	6.5
Thickness	(mm)	30.0	30.0	30.0	30.0	30.0	30.0
Global response							
Pitch	(°)	34.2	9.8	9.7	9.6	9.4	9.5
Structural resistance SS-EN ISO 199202, utilization (%)							
Axial tension, A_t		71	31	24	20	29	29
Bending[1], B_{1st}		433	94	66	79	71	65
Bending[2], B_{2nd}		144	124	119	120	95	80
Beam shear, V_b		32	20	19	21	16	12
Torsional shear, V_b		32	20	19	21	16	12
Co[3] V_bV_t		41	20	19	21	15	12
Hoop buckling		8	8	10	13	7	5
Column buckling		82	31	26	23	32	31
Co[4] $A_tB_{1st,2nd}H$		466	128	129	136	110	88
Co[5] $A_cB_{1st,2nd}H1$		413	128	126	138	100	86
Co[6] $A_cB_{1st,2nd}H2$		399	127	126	137	98	86
Co[7] $A_cB_{1st}H$		539	197	149	208	95	47
Co[8] $A_cB_{2nd}H$		344	284	295	351	153	73
Shell buckling DNV-RP-C202, utilization (%)							
Offset column		11	4	5	6	4	5
Main column		110	52	53	49	51	50
Heave plate		4	3	3	2	3	3

Note.
[1]1st principal axis.
[2]2nd principal axis.
[3]Combined beam shear and torsional shear.
[4]Combined axial tension, bending, and hydrostatic pressure.
[5]Requirement 1: combined axial compression, bending, and hydrostatic pressure.
[6]Requirement 2: combined axial compression, bending, and hydrostatic pressure.
[7]Combined axial compression, bending, and hydrostatic pressure 1st principal axis.
[8]Combined axial compression, bending, and hydrostatic pressure 2nd principal axis.

The final thickness of the offset columns is 50 mm and the main column is 30 mm.

One can see in Table 5.5 the batch runs when the thickness for the main column and offset columns are changed respectively. When the thickness of the offset columns is decreased the shell buckling increases. One can also observe that the utilization of the braces decreases and increases for most of the controls. When the thickness of the main column is decreased, the shell buckling increases, and the utilization of the braces increase and decrease. The utilization changes with a lower range compared to when decreasing the thickness of the offset column. It should be noticed that small changes in a member geometry also change the global behavior, when looking at the pitch it alternates between 9 and 9.6° in between the different batches.

Table 5.5. *Results from batch runs analyzing the behavior when changing the thickness of the shell elements of the offset columns and main column.*

Batch	B2.4	B3.1	B3.2	B4.1	B4.2	B3/B4
Geometry brace						
Diameter (m)	1.6	1.6	1.6	1.6	1.6	1.6
Thickness (mm)	22.5	22.5	22.5	22.5	22.5	22.5
Geometry column						
Diameter (m)	10.1	10.1	10.1	10.1	10.1	10.1
Thickness (mm)	60.0	**50.0**	**40.0**	60.0	60.0	**50.0**
Geometry main column						
Diameter (m)	6.5	6.5	6.5	6.5	6.5	6.5
Thickness (mm)	30.0	30.0	30.0	**25.0**	**20.0**	25.0
Global response						
Pitch (°)	9.5	9.4	9	9.6	9.6	9.5
Structural resistance SS-EN ISO 199202, utilization (%)						
Axial tension, A_t	29	32	29	29	30	29
Bending[1], B_{1st}	65	62	133	64	68	65
Bending[2], B_{2nd}	80	78	138	80	74	83
Beam shear, V_b	12	12	15	12	11	12
Torsional shear, V_b	12	12	15	12	11	12
Co[3] V_bV_t	12	12	21	12	12	13
Hoop buckling	5	5	5	5	5	5
Column buckling	31	31	30	32	33	33
Co[4] $A_tB_{1st,2nd}H$	88	84	168	90	89	94
Co[5] $A_cB_{1st,2nd}H1$	86	82	160	85	89	90
Co[6] $A_cB_{1st,2nd}H2$	86	82	160	85	89	90
Co[7] $A_cB_{1st}H$	47	48	129	42	49	52
Co[8] $A_cB_{2nd}H$	73	69	178	72	61	78
Shell buckling DNV-RP-C202, utilization (%)						
Offset column	5	6	12	5	5	6
Main column	50	51	52	74	127	76
Heave plate	3	3	3	3	3	3

Note.
[1]1st principal axis.
[2]2nd principal axis.
[3]Combined beam shear and torsional shear.
[4]Combined axial tension, bending, and hydrostatic pressure.
[5]Requirement 1: combined axial compression, bending, and hydrostatic pressure.
[6]Requirement 2: combined axial compression, bending, and hydrostatic pressure.
[7]Combined axial compression, bending, and hydrostatic pressure 1st principal axis.
[8]Combined axial compression, bending, and hydrostatic pressure 2nd principal axis.

5.1.3 Critical sections

The critical sections for the braces due to structural resistance are shown in Figure 5.4. The brace members in these sections are exposed to a combination of axial force, bending, and hydrostatic pressure. The final design has a utilization of 88 % in the bottom brace element in the connection to the heave plate.

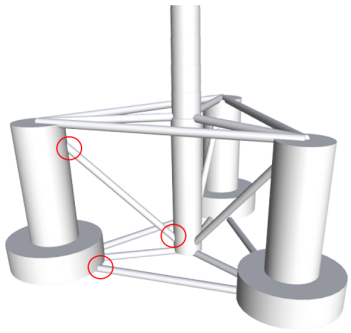

Figure 5.4. *Critical sections for the braces due to the structural resistance. Members are exposed to a combination of axial force, bending, and hydrostatic pressure.*

Another critical section is the bottom heave plate for the offset columns. The result from the iteration at 40 m sea depth in Section 5.1.2 results in a diameter of 20.2 m for the heave plate. The structural model described in Section 4.5.1 is analyzed for the initial dimensions given in Table 5.6.

Table 5.6. *Initial dimensions for bottom heave plate analysis.*

	Height (m)	Diameter (m)	Thickness (mm)
Offset column	24/30[1]	10.1	60
Heave plate	6	20.2	60

Note.
[1]24 m for configuration 1 and 30 m for configuration 2

The resulting von Mises stresses from the FE-analysis for configuration 1 are presented in Figure 5.5. One can see that the stresses in the bottom plate and also the top plate exceeds the material ultimate tensile strength. This means that a thickness of 60 mm is not sufficient.

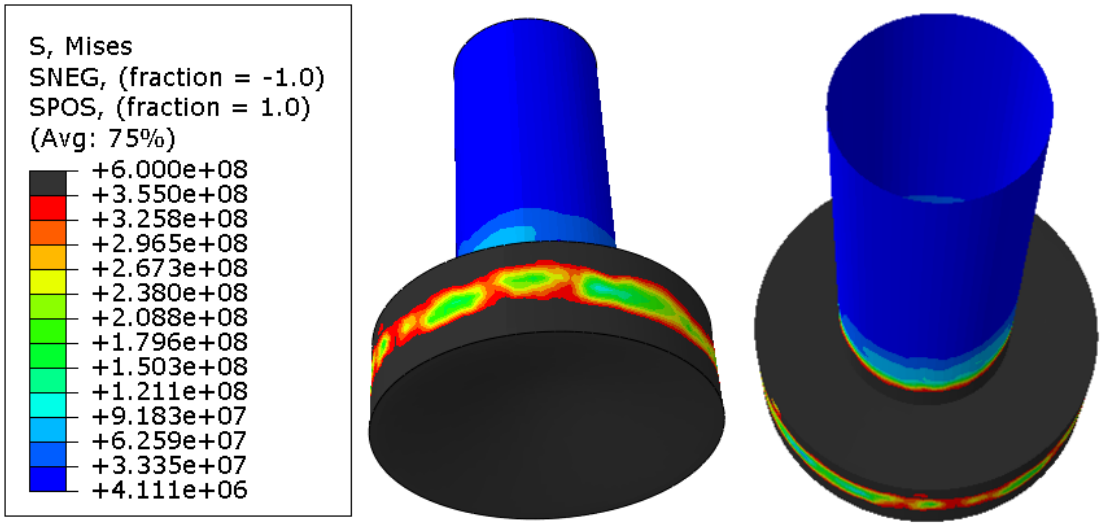

Figure 5.5. *Initial von Mises stresses (Pa) for bottom heave plate with configuration 1 according to Section 4.5.1.*

When the thickness is increased, the resulting von Mises stresses can be observed in Figure 5.6. The location of the maximum stresses is the connections between the two plates and the cylinder wall as well as the connection between the top plate and the offset column. With a thickness of 203 mm for the plates and a thickness of 185 mm for the heave plate wall, one can see that the stresses are below the yield limit in the heave plate. A thickness this large is though unrealistic. The higher stress seen in the label in the figure is in the column wall which is not considered in this analysis.

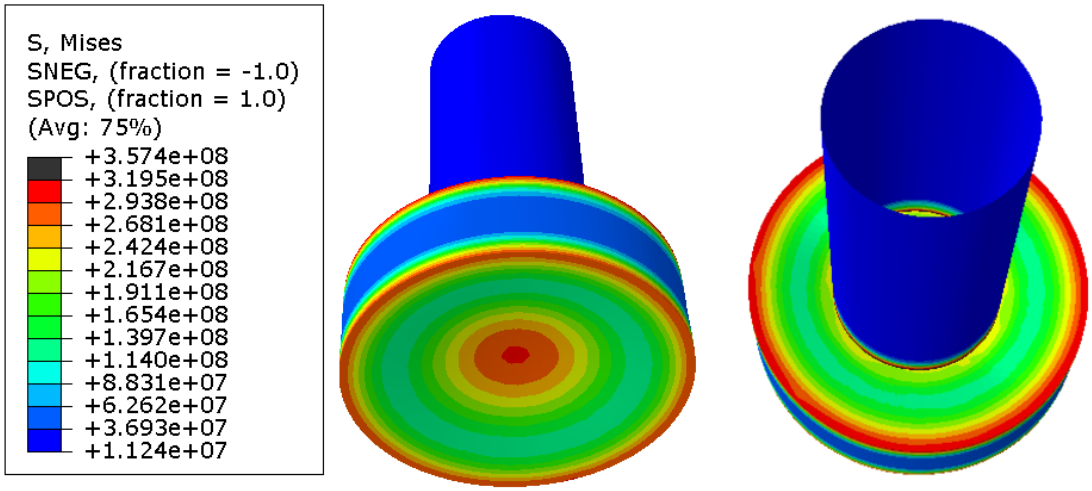

Figure 5.6. *Final von Mises stresses (Pa) for bottom heave plate with configuration 1 according to Section 4.5.1.*

The von Mises stresses for configuration 2 with the initial dimensions are presented in Figure 5.7. Compared to configuration 1 the stresses are lower than the ultimate tensile strength but still above the yield limit. The highest stresses are located at the center and where the offset column connects to the heave plate.

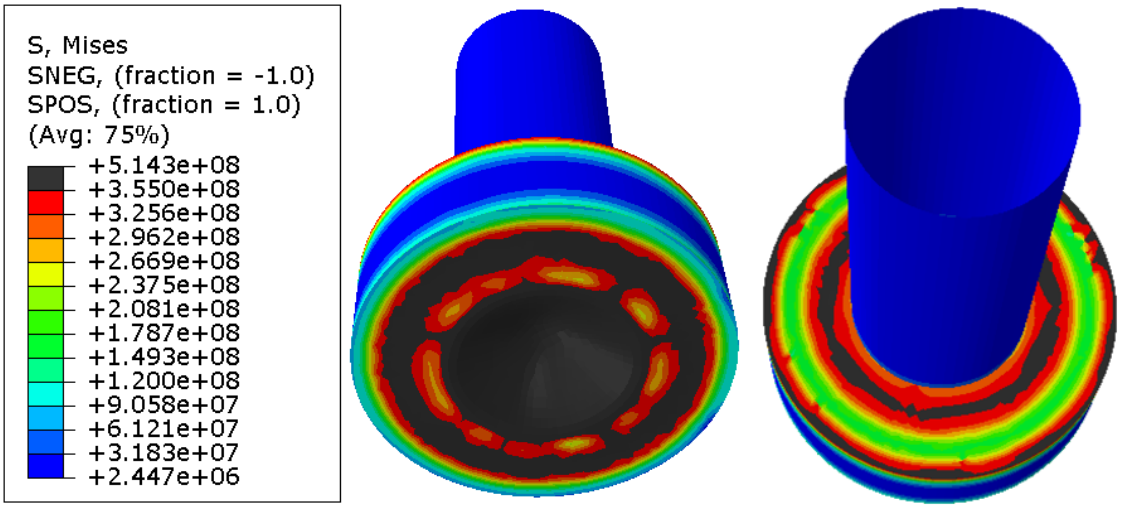

Figure 5.7. *Initial von Mises stresses (Pa) for bottom heave plate with configuration 2 according to Section 4.5.1.*

If the thickness is increased to 107 mm the stresses are less or equal to the yield strength. This can be seen in Figure 5.8. The location with the highest stresses is the connection between the offset column and the heave plate. Another location with high stresses is between the cylinder wall and the top plate. The result of this is that it is suitable to use this configuration without any internal construction.

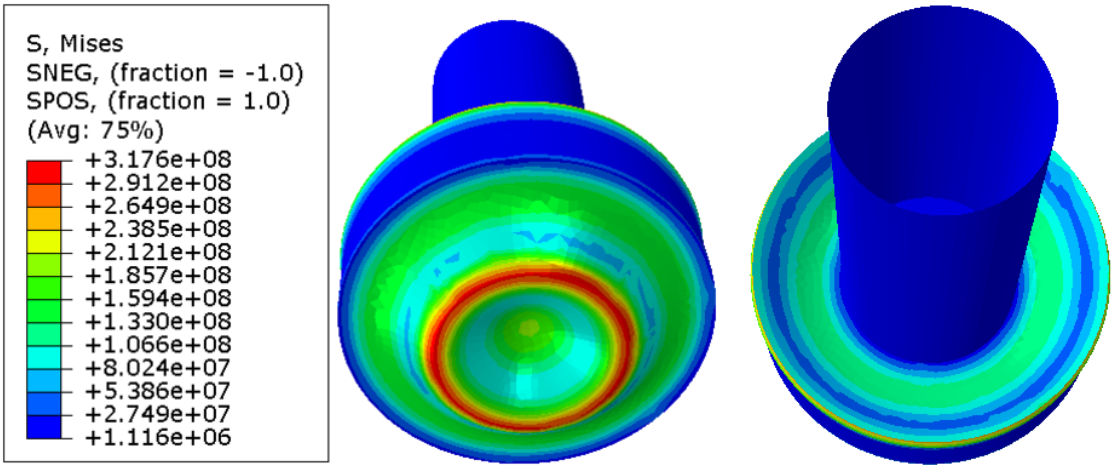

Figure 5.8. *Final von Mises stresses (Pa) for bottom heave plate with configuration 2 according to Section 4.5.1.*

The initial and final bottom heave plate utilization for the two configurations is presented in Table 5.7. With solely change of configuration the bottom heave plate goes from collapse to yielding state. It is therefore required twice as thick plate if no inner construction is implemented in order to avoid yielding.

Table 5.7. *Utilization for the two configurations and final needed thickness.*

	Heave plate thickness (mm)	Utilization (%)
	Configuration 1	
Initial	60	∞
Final	203	90
	Configuration 2	
Initial	60	145
Final	107	89

5.1.4 Result of preliminary design for intermediate sea depths

The global response and the utilization for structural resistance/shell buckling can be seen in 5.8 for intermediate sea depths. One can see that the highest pitch angle is for 50 m sea depths and the lowest for 30 m and 40 m. The dimensioning structural resistance control was the combined axial compression, bending, and hydrostatic pressure for the sea depth of 30 m and combined axial tension, bending, and hydrostatic pressure for the other depths.

Table 5.8. *Structural resistance and global response.*

Sea depth	30 m	40 m	50 m	60 m
Global response				
Pitch (°)	9.5	9.8	9.7	9.5
Structural resistance SS-EN ISO 199202, utilization (%)				
Axial tension, A_t	19	29	27	21
Bending[1], B_{1st}	63	63	66	75
Bending[2], B_{2nd}	80	80	81	76
Beam shear, V_b	10	12	12	10
Torsional shear, V_b	10	12	12	10
Co[3] V_bV_t	11	12	12	11
Hoop buckling	5	5	5	4
Column buckling	20	31	33	23
Co[4] $A_tB_{1st,2nd}H$	83	88	86	87
Co[5] $A_cB_{1st,2nd}H1$	83	87	86	81
Co[6] $A_cB_{1st,2nd}H2$	83	87	86	81
Co[7] $A_cB_{1st}H$	43	38	30	0
Co[8] $A_cB_{2nd}H$	77	72	42	1
Shell buckling DNV-RP-C202, utilization (%)				
Offset column	5	6	7	7
Main column	51	50	52	50
Heave plate	3	3	3	3

Note.
[1]1st principal axis.
[2]2nd principal axis.
[3]Combined beam shear and torsional shear.
[4]Combined axial tension, bending, and hydrostatic pressure.
[5]Requirement 1: combined axial compression, bending, and hydrostatic pressure.
[6]Requirement 2: combined axial compression, bending, and hydrostatic pressure.
[7]Combined axial compression, bending, and hydrostatic pressure 1st principal axis.
[8]Combined axial compression, bending, and hydrostatic pressure 2nd principal axis.

The final dimensions are presented in Table 5.9 for intermediate sea depths. One can observe that the diameter and thickness of the offset columns are the same for 40 m, 50 m, and 60 m. The thickness of the braces varies with the largest thickness for 30 m sea depth and the smallest for 30/40 m sea depth. Common for all designs is the thickness of the heave plate, the diameter of the braces, the CC-distance, and the dimensions of the main column.

Table 5.9. *Final dimensions of semi-submersible at intermediate sea depths.*

Part	Diameter (m)	Thickness (mm)	Length/Height (m)
Sea depth 30-60 m			
Main column	6.5	30.0	30.0
CC-distance[1]			29.0
Heave plate[2]		60.0	
Brace	1.6		
Sea depth 30 m			
Offset column	9.8	60.0	22.5
Heave plate	19.6		7.5
Brace		27.5	
Sea depth 40 m			
Offset column	10.0	50.0	24.0
Heave plate	20.0		6.0
Brace		22.5	
Sea depth 50 m			
Offset column	10.0	50.0	24.0
Heave plate	20.0		6.0
Brace		22.5	
Sea depth 60 m			
Offset column	10.0	50.0	24.0
Heave plate	20.0		6.0
Brace		25.0	

Note.
[1]Distance between the main column and offset column
[2]Thickness for the walls of the heave plate

The total structural mass is presented in Table 5.10. One can notice that the mooring system is a large portion, approximately one-third, of the total mass. The mass is highest for the semi-submersible at a sea depth of 30 m.

Table 5.10. *The mooring and the structural mass of the semi-submersible substructure for the four different sea depths.*

Sea depth	Mooring (ton)	Structural (ton)	Total (ton)
30 m	1014	2407	3421
40 m	1045	2083	3129
50 m	1078	2083	3162
60 m	1111	2112	3224

5.1.5 Frequency

The natural frequency of the semi-submersible designs is analyzed in Ashes and the frequency from the three critical modes: heave, side-side, and fore-aft is presented in Table 5.11. One can observe that the frequency for the three modes is similar for all sea depths. The heave mode is well-fitted in the range of the target frequency for soft-soft design, as shown in Figure 5.9. One can also see that the side-to-side mode and the fore-aft mode lie inside the 3P frequency range.

Table 5.11. *Frequency for the three critical modes.*

Sea depth	Heave (Hz)	nr^1	Side-side (Hz)	nr^1	Fore-aft (Hz)	nr^1
30 m	0.061	17	0.375	46	0.380	48
40 m	0.063	16	0.376	42	0.381	43
50 m	0.063	15	0.381	47	0.386	50
60 m	0.063	15	0.377	44	0.390	47

Note.
[1] Mode number with; 50 modes to find, search range in between 0-0.5 Hz, and search resolution of 0.001 Hz.

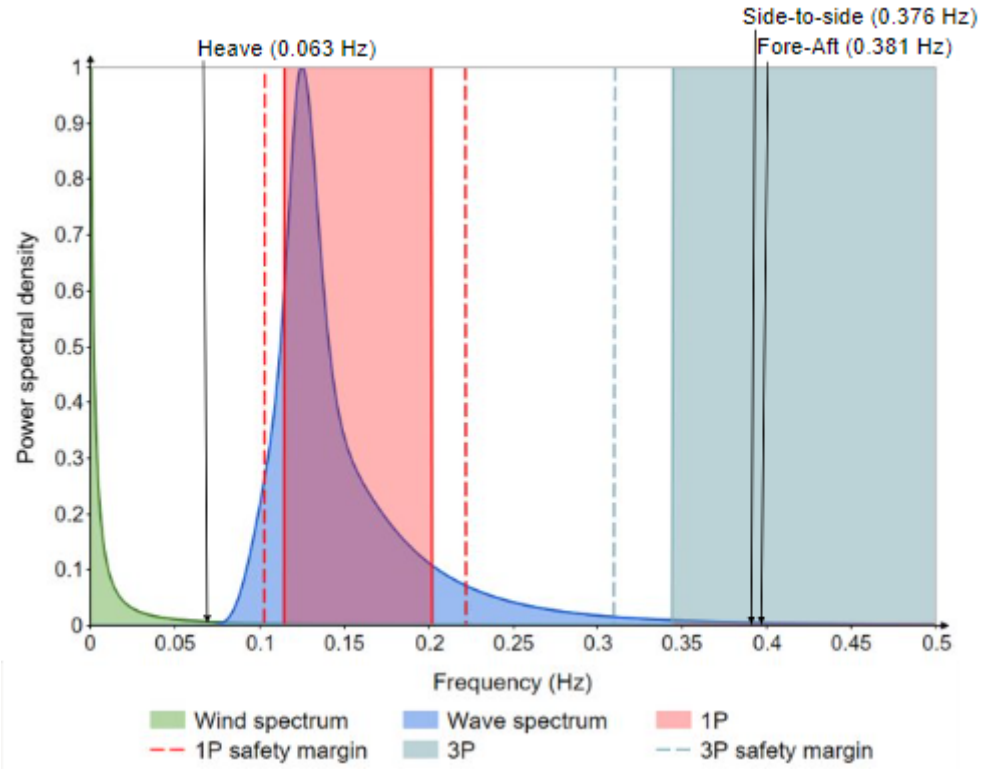

Figure 5.9. *The power spectral density spectrum showing the frequency of the loads, for the 5 MW wind turbine. The three critical modes and their frequency for the 40 m sea depth design are marked out.*

5.2 Preliminary design of jacket substructure for a 5 MW turbine

The results from the preliminary design are presented in the following sections. Findings from the iteration process are explained as well as the final design.

5.2.1 Outcome of iterative preliminary design process for 40 m water depth

The result from the iterative process of finding a solution for 40 m sea depth is presented in Table 5.12. As the initial dimensions are from the reference case at 50 m sea depth and with a very similar geometry only one iteration is needed. The combined axial tension, bending, and hydrostatic pressure are the critical control and the member type is the X-brace at the second level. The change in geometry to fulfill the control is to increase the thickness from 20 mm to 21 mm. One can see that the other controls are at low utilization rates. One can also see that the global response is the same for the two iterations and that most of the tilt is connected to the tower compared to the substructure.

Table 5.12. *Dimensions for jacket 40 m sea depth.*

	Element		
Thickness (mm)	X-brace 2	20	**21**
Global response			
Tilt angle[1] (°)	-	0.1	0.1
Tilt angle[2] (°)	-	0.4	0.4
Structural resistance SS-EN ISO 199202, utilization (%)			
Axial tension, A_t	Leg level 3	28	28
Bending[3], B_{1st}	Leg bottom	11	11
Bending[4], B_{2nd}	X-brace 2	24	24
Beam shear, V_b	Leg frame	9	9
Torsional shear, V_b	Leg frame	9	9
Combined[5] V_bV_t	Leg frame	9	9
Hoop buckling	Mud brace 3	12	12
Column buckling	Leg level 3	56	56
Combined[6] $A_tB_{1st,2nd}H$	Leg level 3	33	33
Combined[7] $A_cB_{1st,2nd}H1$	Leg level 3	42	42
Combined[8] $A_cB_{1st,2nd}H2$	X-brace 2	23	23
Combined[9] $A_cB_{1st}H$	-	0	0
Combined[10] $A_cB_{2nd}H$	X-brace 2	93	85

Note.
[1]Only including substructure.
[2]Including substructure and tower.
[3]1st principal axis.
[4]2nd principal axis.
[5]Combined beam shear and torsional shear.
[6]Combined axial tension, bending, and hydrostatic pressure.
[7] Requirement 1: combined axial compression, bending, and hydrostatic pressure.
[8] Requirement 2: combined axial compression, bending, and hydrostatic pressure.
[9] Combined axial compression, bending, and hydrostatic pressure 1st principal axis.
[10]Combined axial compression, bending, and hydrostatic pressure 2nd principal axis.

5.2.2 Result of preliminary design for intermediate sea depths

The dimensions for the jacket structure are presented in Table 5.13. One can see that the only member size that is changed is the thickness of the X-braces at level 2 for 40, 50, and 60 m sea depth. All the other dimensions are the initial assumptions and are therefore not optimized.

Table 5.13. *Dimensions jacket for 5 MW turbine.*

Part	Diameter (m)	Thickness (mm)	Length/Height (m)
Sea depth 30-60 m			
Top leg	1.2	40	0.5
Mud brace leg	1.2	50	0.9
Bottom leg	1.2	50	1.5
Leg level 1-x	1.2		
Mud brace	0.8	20	
X-brace level 1-x	0.8		
Sea depth 30 m			
Leg level 1-2		35	[1]14.4
Leg level 1-2		50	[1]14.4
Mud brace			[1]10.7
X-brace level 1-2		20	[1]16.5-16.9
Sea depth 40 m			
Leg level 1-3		35	[1]13.3
Leg level 4		50	[1]13.3
Mud brace			[1]11.4
X-brace level 2		21	[1]16.4
X-brace level 1, 3-4		20	[1]15.5-17.5
Sea depth 50 m			
Leg level 1-3		35	[1]15.8
Leg level 4		50	[1]15.8
Mud brace			[1]12.0
X-brace level 2		21	[1]18.7
X-brace level 1, 3-4		20	[1]18.2-19.8
Sea depth 60 m			
Leg level 1-4		35	[1]14.6
Leg level 5		50	[1]14.6
Mud brace			[1]12.6
X-brace level 2		21	[1]17.6
X-brace level 1, 3-5		20	[1]17.2-19.3

Note.
[1]The length presented is rounded off and the exact value is calculated according to Section 4.6.2.

The global response and the utilization rate for the structural resistance controls are presented in Table 5.14. One can notice that the tilt angle in the substructure is the same for intermediate sea depths. The utilization in the structural resistance controls is similar for all sea depths except the hoop buckling control which increases with the sea depth.

Table 5.14. *Structural resistance and global response.*

Sea depth	30 m	40 m	50 m	60 m
Global response (°)				
Tilt angle[1]	0.1	0.1	0.1	0.1
Tilt angle[2]	0.4	0.4	0.5	0.4
Structural resistance SS-EN ISO 199202, utilization (%)				
Axial tension, A_t	25	28	26	26
Bending[3], B_{1st}	12	11	11	10
Bending[4], B_{2nd}	25	24	24	23
Beam shear, V_b	9	9	9	7
Torsional shear, V_b	9	9	9	7
Co[5] V_bV_t	9	9	9	7
Hoop buckling	9	12	15	18
Column buckling	54	56	55	54
Co[6] $A_tB_{1st,2nd}H$	30	33	31	30
Co[7] $A_cB_{1st,2nd}H1$	38	42	41	38
Co[8] $A_cB_{1st,2nd}H2$	21	23	24	23
Co[9] $A_cB_{1st}H$	0	0	0	0
Co[10] $A_cB_{2nd}H$	80	85	87	81

Note.
[1]Only including substructure.
[2]Including substructure and tower.
[3]1st principal axis.
[4]2nd principal axis.
[5]Combined beam shear and torsional shear.
[6]Combined axial tension, bending, and hydrostatic pressure.
[7] Requirement 1: combined axial compression, bending, and hydrostatic pressure.
[8] Requirement 2: combined axial compression, bending, and hydrostatic pressure.
[9] Combined axial compression, bending, and hydrostatic pressure 1st principal axis.
[10]Combined axial compression, bending, and hydrostatic pressure 2nd principal axis.

The mass of the jacket structure is presented in Table 5.15. One can see that the weight of the transition piece is more than half of the total mass for all sea depths. The weight of the transition piece is constant and the weight of the steel increases by approximately 80 tons for each 10 m sea depth.

Table 5.15. *The concrete and the steel mass of the jacket substructure for the four different sea depths.*

Sea depth	Concrete (ton)	Steel (ton)	Total (ton)
30 m	666	420	1086
40 m	666	506	1172
50 m	666	579	1245
60 m	666	664	1330

5.2.3 Frequency

The natural frequencies for the critical modes in the jacket structure are presented in Table 5.16. One can see that the modes are almost equal for all sea depths and the difference between 30 and 60 m sea depth is approximately 0.03 Hz.

Table 5.16. *Frequency for the critical mode shapes.*

Sea depth	Side-side (Hz)	nr^1	Fore-aft (Hz)	nr^1
30 m	0.267	1	0.270	2
40 m	0.255	1	0.257	2
50 m	0.250	1	0.247	2
60 m	0.234	1	0.236	2

Note.
[1]Mode number with; 50 modes to find, search range in between 0-1 Hz, and search resolution of 0.001 Hz.

The critical natural frequencies for 40 m sea depth are marked out in a power spectral density spectrum where the load-imposed frequencies are plotted. One can see that the natural frequencies do not collide with the load-imposed frequencies in Figure 5.10. The frequencies corresponds to a soft-stiff design. Although, the natural frequencies for 60 m sea depth are close to the safety margin for P1.

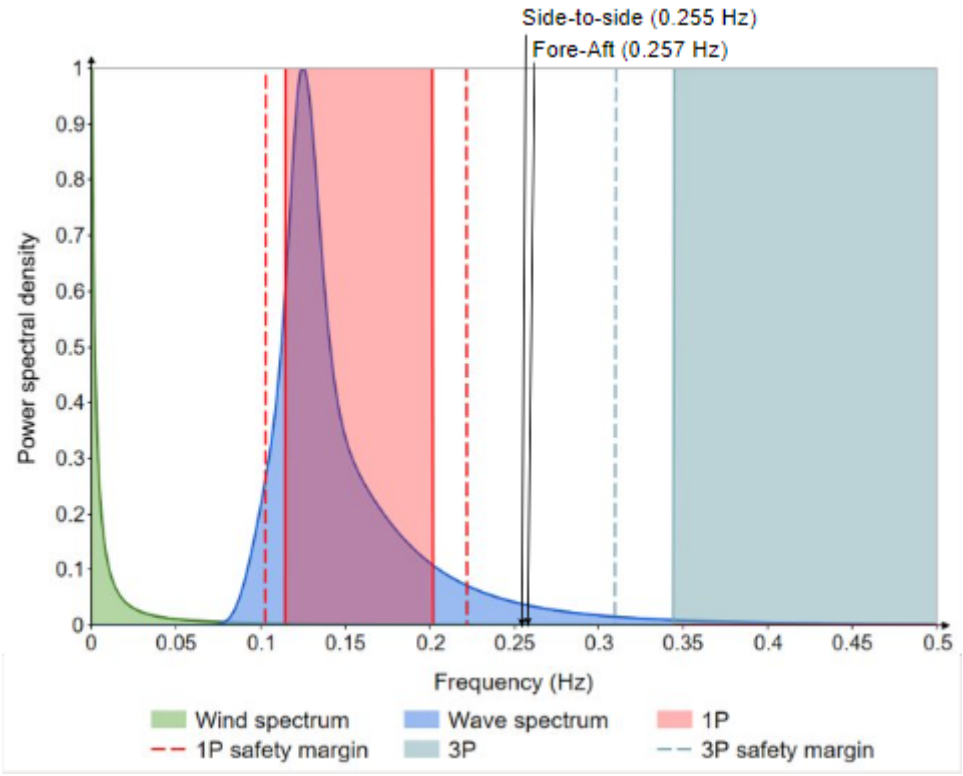

Figure 5.10. *The power spectral density spectrum showing the frequency of the loads, for the 5 MW wind turbine. The two critical modes and their frequency for the 40 m sea depth design is marked out.*

5.3 Preliminary design for semi-submersible and jacket substructure for a 15 MW turbine

The preliminary design of the floating and fixed substructure for the 15 MW turbine are done for 40 m sea depth. In this section the final designs for the two solutions are presented along with the results from the frequency analysis.

Semi-submersible

The dimensions of the semi-submersible for the 15 MW are presented in Table 5.17. One can see that the height of the substructure is 10 m higher and that the CC-distance is 31 m longer than for the 5 MW design. The main column is larger to support the 15 MW tower. Another observation is that the diameter of the braces is slightly larger and the thickness is markedly larger. The structural mass of the substructure is 6178 tons and the moorings are similar to the 5 MW design with 1037 tons.

Table 5.17. *Dimensions of the semi-submersible for a 15 MW turbine.*

Part	Diameter (m)	Thickness (mm)	Length/Height (m)
Main column	10.5	50	40
Heave plate[2]	26.0	60	10
Brace	2.2	45	
CC-distance[1]			60

Note.
[1]Distance between the main column and offset column
[2]Thickness for the wall of the heave plate

The global response and the utilization for structural resistance/shell buckling are presented in Table 5.18. One can see that the pitch is 10.3 degrees which are above the 10 ° limit. Another observation is that the highest utilization rate for structural resistance is 80 % for the control of combined axial compression, bending in 2nd principal axis, and hydrostatic pressure. The highest utilization for shell buckling is 48 % for the main column.

Table 5.18. *Structural resistance and global response for the semi-submersible with a 15 MW turbine.*

Sea depth	40 m
Global response	
Pitch (°)	10.3
Structural resistance SS-EN ISO 199202, utilization (%)	
Axial tension, A_t	34
Bending[1], B_{1st}	37
Bending[2], B_{2nd}	55
Beam shear, V_b	6
Torsional shear, V_b	6
Co[3] V_bV_t	6
Hoop buckling	6
Column buckling	54
Co[4] $A_tB_{1st,2nd}H$	73
Co[5] $A_cB_{1st,2nd}H1$	55
Co[6] $A_cB_{1st,2nd}H2$	55
Co[7] $A_cB_{1st}H$	0
Co[8] $A_cB_{2nd}H$	80
Shell buckling DNV-RP-C202, utilization (%)	
Offset column	19
Main column	48
Heave plate	12

Note.
[1]1st principal axis.
[2]2nd principal axis.
[3]Combined beam shear and torsional shear.
[4]Combined axial tension, bending, and hydrostatic pressure.
[5] Requirement 1: combined axial compression, bending, and hydrostatic pressure.
[6] Requirement 2: combined axial compression, bending, and hydrostatic pressure.
[7] Combined axial compression, bending, and hydrostatic pressure 1st principal axis.
[8] Combined axial compression, bending, and hydrostatic pressure 2nd principal axis.

Jacket

The dimensions for the jacket with a 15 MW turbine are presented in Table 5.19. One can see that the leg diameter is more than twice as large compared to the 5 MW design and the thicknesses are also considerably larger. The dimensions for the mud brace are the same as for the 5 MW design. The increase in dimensions for the X-braces is approximately one-third for the diameter and double for the thickness. The mass of the concrete is 1337 tons and 1599 tons for the steel.

Table 5.19. *Dimensions of the jacket with a 15 MW turbine.*

Part	Diameter (m)	Thickness (mm)	Length/Height (m)
Top leg	2.6	55	0.5
Mud brace leg	2.6	65	0.9
Bottom leg	2.6	70	1.5
Leg level 1-4	2.6	60	13.3
Mud brace	0.8	20	15.4
X-brace level 1	1.4	40	18.5
X-brace level 2	1.3	40	19.1
X-brace level 3	1.2	30	19.7
X-brace level 4	1.2	40	20.3

Note.
[1]The length presented is rounded off and the exact value is calculated according to Section 4.6.2.

The global response and the structural resistance for the jacket substructure are presented in Table 5.20. One can see that the tilt angle in the substructure is low at 0.1° but in the whole structure 1.1°. The highest utilization is 88 % in the X-brace at level 1 for the control of combined axial compression, bending in 2nd principal axis, and hydrostatic pressure.

Table 5.20. *Global response and utilization for a jacket with a 15 MW turbine.*

	Element	40 m
Global response (°)		
Tilt angle[1]		0.1
Tilt angle[2]		1.1
Structural resistance SS-EN ISO 199202, utilization (%)		
Axial tension, A_t	Leg top	58
Bending[3], B_{1st}	Leg bottom	15
Bending[4], B_{2nd}	X-brace 2	30
Beam shear, V_b	Leg mud brace	22
Torsional shear, V_b	Leg mud brace	22
Combined[5] V_bV_t	Leg mud brace	22
Hoop buckling	Leg level 4	15
Column buckling	Leg top	77
Combined[6] $A_tB_{1st,2nd}H$	Leg top	72
Combined[7] $A_cB_{1st,2nd}H1$	Leg top	83
Combined[8] $A_cB_{1st,2nd}H2$	X-brace 2	30
Combined[9] $A_cB_{1st}H$	Leg level 4	30
Combined[10] $A_cB_{2nd}H$	X-brace 1	88

Note.
[1]Only including substructure.
[2]Including substructure and tower.
[3]1st principal axis.
[4]2nd principal axis.
[5]Combined beam shear and torsional shear.
[6]Combined axial tension, bending, and hydrostatic pressure.
[7] Requirement 1: combined axial compression, bending, and hydrostatic pressure.
[8] Requirement 2: combined axial compression, bending, and hydrostatic pressure.
[9] Combined axial compression, bending, and hydrostatic pressure 1st principal axis.
[10]Combined axial compression, bending, and hydrostatic pressure 2nd principal axis.

Frequency

The natural frequencies for the two substructures are summarized in Table 5.21. One can see that all modes have a lower frequency than the 5 MW designs. Another observation is that the side-to-side and fore-aft modes are lower for the jacket than for the semi-submersible.

Table 5.21. *Frequency for the critical modes.*

Substructure	Heave (Hz)	nr^1	Side-side (Hz)	nr^1	Fore-aft (Hz)	nr^1
Semi-submersible	0.052	17	0.251	35	0.257	36
Jacket	-	-	0.204	1	0.209	2

Note.
[1]Mode number with; 50 modes to find, search range in between 0-0.5 or 0-1 Hz, and search resolution of 0.001 Hz.

The natural frequencies presented in Table 5.21 are plotted together with the power spectral density spectrum for the load-imposed frequencies and visualized in Figure 5.11. One can see the heave mode is in the soft-soft design area and the two modes for the jacket lie in the soft-stiff design area. The side-to-side and fore-aft modes for the semi-submersibles lie inside the 3P spectrum but are closer to the soft-stiff design area compared to the 5 MW design.

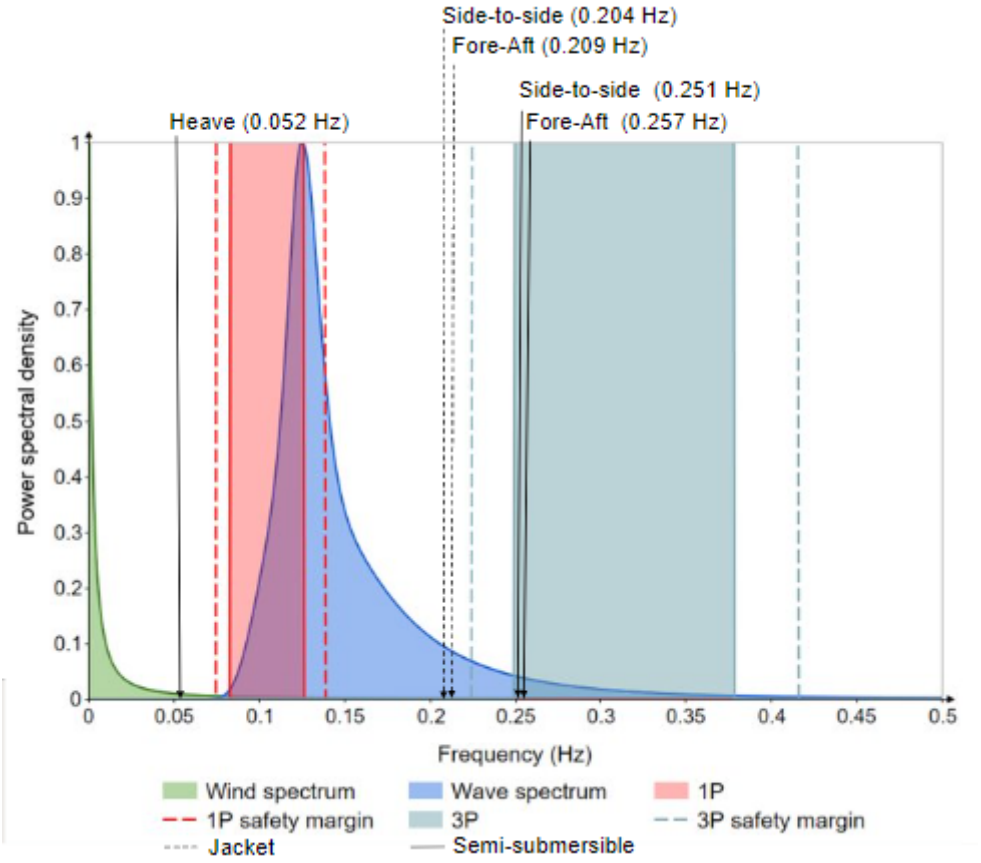

Figure 5.11. *The power spectral density spectrum showing the frequency of the loads, for the 15 MW wind turbine. The critical modes and their frequency for the jacket and the semi-submersible at 40 m sea depth.*

5.4 Comparison between semi-submersible and jacket

Following sections contains a comparison in material consumption for the floating and fixed substructures as well as how it contributes in CO_2. The comparison is done for sea depths of 30, 40, 50, and 60 m for the preliminary designs when a 5 MW turbine is applied. The comparison when the 15 MW turbine is applied is solely for 40 m sea depth.

5.4.1 5 MW turbine for intermediate sea depths

The main comparison between the floating and the fixed substructure is based on the structural mass and is visulized in Figure 5.12. One can see that the mass of the jacket is approximate one-third of the semi-submerisble. Another observation is that more than half of the mass for the jacket is the TP. One can also see that the mooring mass is approximate one-third of the semi-submersibles total mass. When the depth is increasing one can also see that the mass of the jacket increases faster.

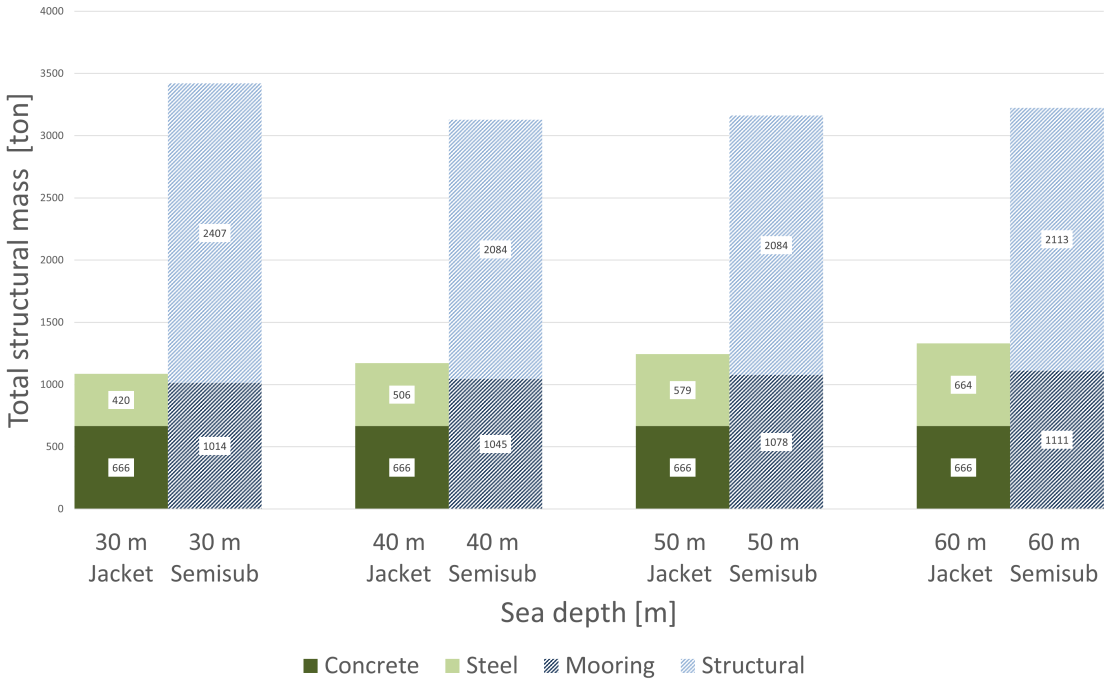

Figure 5.12. *Comparison of structural mass for floating and fixed substructure.*

The second comparison is the mass of CO_2 emissions which is presented in Figure 5.13. One can see that the mass the mass CO_2 increases more for the semi-submersible because the CO_2 equivalent is higher for steel than for concrete.

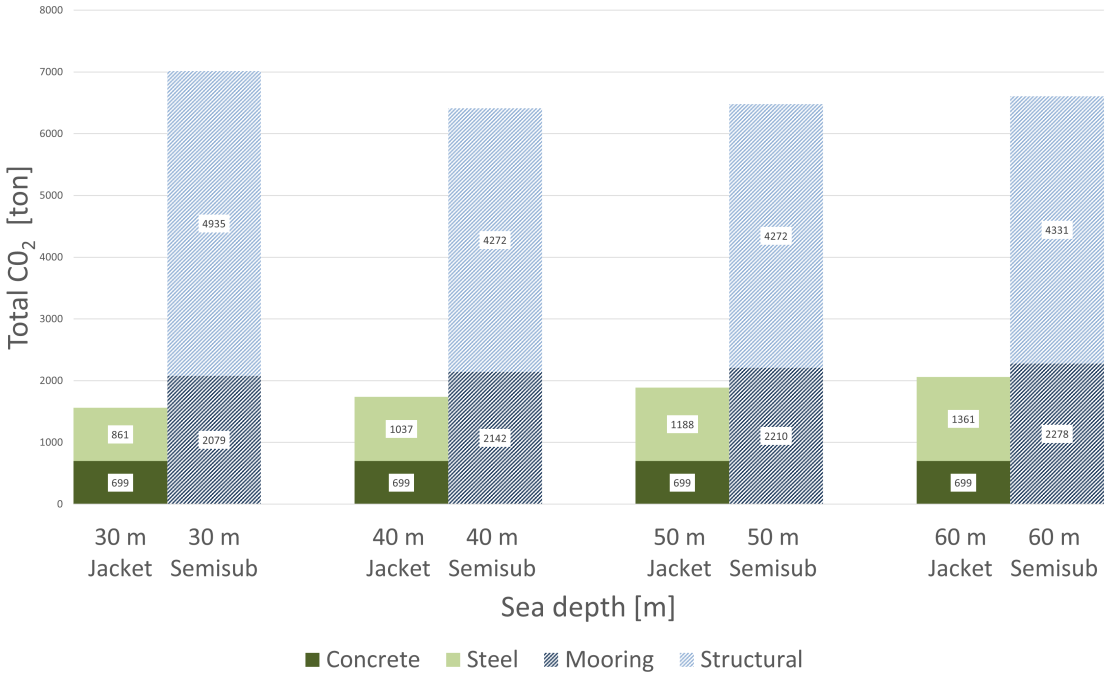

Figure 5.13. *Comparison of CO_2 for floating and fixed substructure.*

5.4.2 15 MW turbine for 40 m sea depth

The comparison of structural mass between the floating and fixed substructure is visualized in Figure 5.14. One can see a similar result as for the 5 MW solutions. The jacket is markedly lighter than the semi-submersible. One can observe that the relation between them is approximately 2.5 times instead of 3 times as for the 5 MW solutions. The cause of this is that the mooring mass is the same for 5 MW and 15 MW solutions.

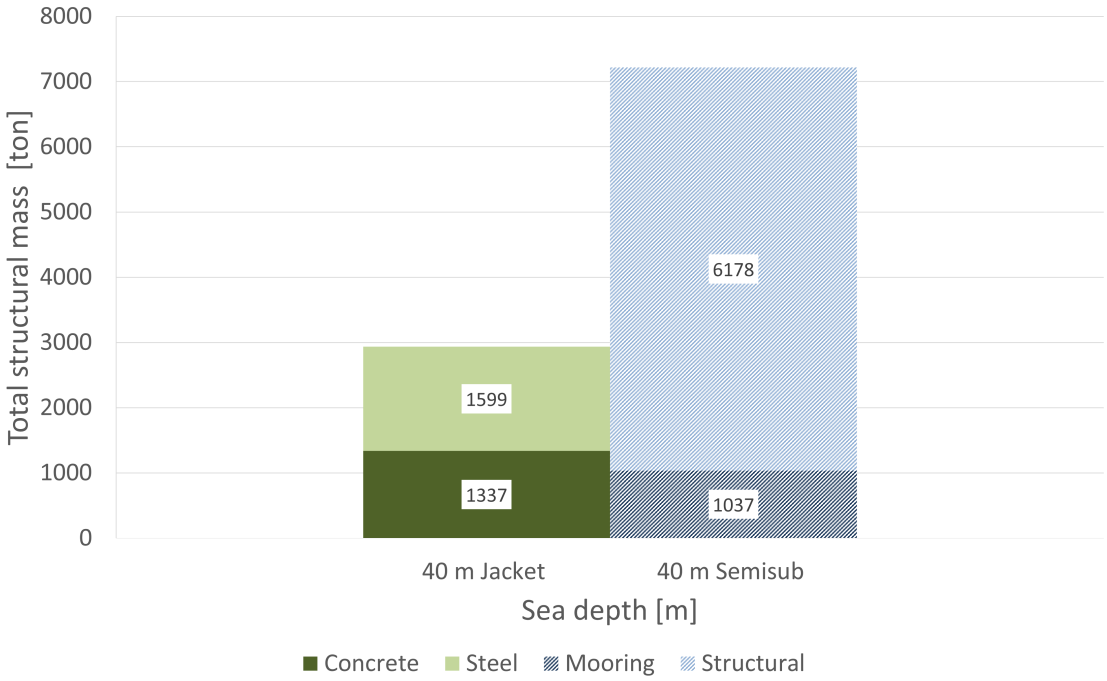

Figure 5.14. *Comparison of structural mass for floating and fixed substructure.*

The second comparison of the CO_2 emissions presented in 5.15 shows the same result as for the 5 MW case. This is due to the same reason that the CO_2 equivalent is larger for steel than concrete.

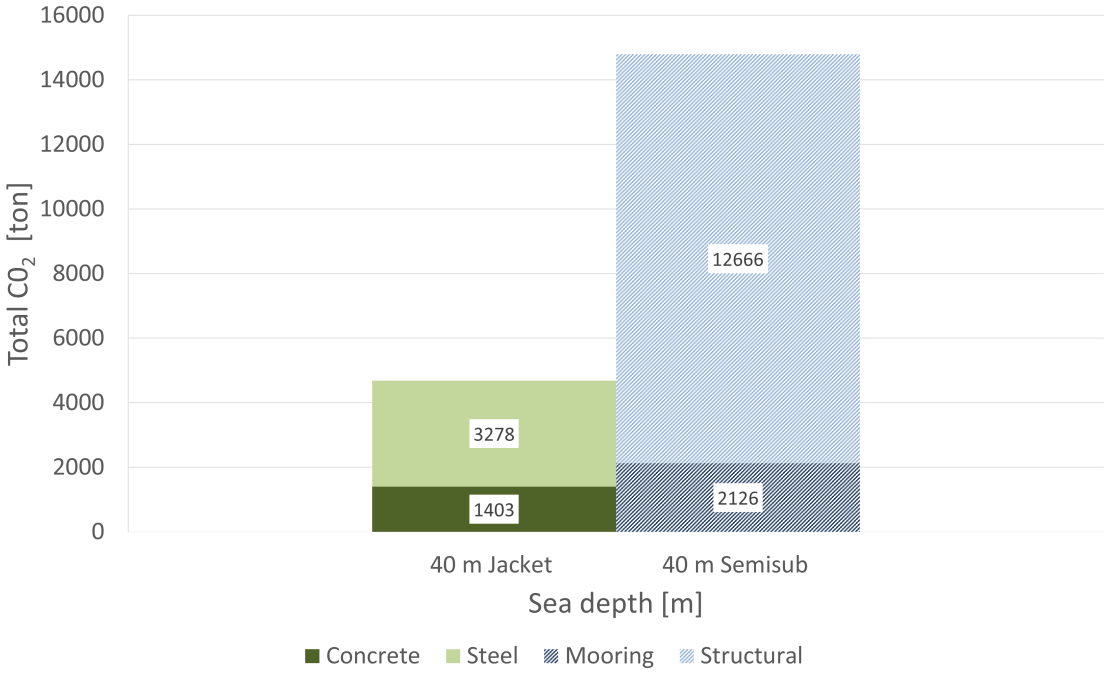

Figure 5.15. *Comparison of CO_2 for floating and fixed substructure.*

6
Discussion and conclusion

In this chapter the findings from the thesis will be discussed. Firstly, the design methods conducted for this thesis is discussed. Containing reflections of all the design methods steps and measures taken during the project. Furthermore, the comparison related to the material consumption is discussed followed by thoughts of the semi-submersible substructure at intermediate sea depths. Finally, some subjects for future work are presented.

6.1 Design method

For the purpose of this thesis, the design method was developed to modify the geometry of the reference case. The aim was to investigate if the modified geometry could be suitable for intermediate sea depths. It is therefore neither a complete optimization nor a parametrization.

The designs are preliminary and it is important to consider that they are designed for simplified load cases and do not include the design for fatigue or accidental loads. Furthermore, it was not possible to apply separate safety factors on each load in Ashes. This was instead done in MATLAB by applying the safety factors on the section forces, with the conservative option of a high safety factor. The final dimensions of the design may be impacted as a result of these simplifications and limitations.

Numerical models

The semi-submersible substructure is modeled with beam elements. Due to the large cylinder elements such as the columns and the heave plates a more accurate model would be to use shell elements for these members. However, this type of element is not implemented in the simulation software Ashes used in this project. Using shell elements would enable a direct connection between the column walls and braces and thereby catch the concentrated stresses these connections generate. Secondly, this would generate the correct shorter length of the braces. However, the beam elements provide a less computationally expensive model. An improvement of the model built in this project could be to apply infinitely stiff elements from the center of the column to the brace attachment point. This would better resemble the actual length of the braces but at the same time generate a fully fixed connection.

Furthermore, the water pressure acting on the bottom heave plate is not captured in the numerical model due to the beam elements. Through the separate static FEM analysis in Abaqus, this load situation showed that major design adjustments were required in order to handle the load. The options were either to increase the

thickness or to add an inner support structure. With this in mind, it might be beneficial to rather restrict the column diameter and ultimately also the heave plate diameter instead of the CC-distance between the columns. This would avoid a large span for the water pressure to act on in the first design process iteration. A large bottom heave plate diameter is disadvantageous in material consumption and in production. On the other hand, a large bottom heave plate diameter increases the stability and dampens the movements in the vertical direction. In the simplified Abaqus analysis, adding a simple inner support structure decreased the thickness of the bottom plate by approximately 50 %. A further study of how this internal structure should be designed could probably lead to a more material-efficient design.

Convergence study

When simulating the semi-submersible for intermediate sea depths in Ashes, the FEM model encountered issues to reach a numerical solution. The nonlinearities were backtracked to the blades and the mooring lines. Since neither the blades nor the mooring lines were within the scope of the thesis, it was studied if simplified models were applicable. Modeling the blades as stiff did not influence the results of the global response. However, modeling the mooring lines with linear springs affected the results markedly. For the intermediate sea depths the stiffness of the lines needed to be increased. To uphold the schedule of the project it was chosen to use a mooring chain instead as explained in Section 4.5.2, which solved the problem. However, in the design for the 30 m sea depth, the same numerical issue came across again. Since the focus lies at the substructure it was chosen not to change the design of the moorings. Interestingly, it was found that increasing the height of the heave plate helped the numerical calculation to find a solution. One can elaborate on why the heave plate height solves the problem and one thought could be that the mooring line is attached higher. This also goes in line with the need for mooring lines with higher strength at lower sea depths as described in Section 4.5.2. As the anchor radius is extrapolated from sea depths at 50 m, 100, m, and 200 m one can suspect that this may not be the most optimal solution. This is a subject that would need to be further investigated if floating substructures should be designed at intermediate sea depths, especially since the final designs show that one-third of the total amount of steel is coming from the mooring lines.

Stability and buoyancy

The first step in the design method loop for the semi-submersible aimed to ensure buoyancy and stability. It is clear that the stability mainly depends on the CC-distance between the columns and the diameter of the offset columns. Since the CC-distance was chosen to be restrained to a maximum, only the diameter of the offset column was free to change and so also subsequently the heave plate due to their set codependency. The resulting geometry did however not fulfill the required pitch limit when simulated in Ashes. The main reason for this would be that the static model is only considering the thrust force, whilst all loads and load cases are

applied in the simulations. However, it is found suitable to use the static model for an initial first guess that can be iterated further.

Structural resistance

The next step in the design method loop was to ensure the structural resistance of all members. The results from the iterative process showed that the global response of the substructure and the structural resistance of braces were the parameters that govern the design.

In a static load situation, the design due to structural resistance is rather straightforward. However, when designing substructures in offshore conditions the structural resistance should be able to handle multiple different seeds of the wind and wave loading when analyzed in the FEM simulations. This makes it difficult to catch the differences and how the structure responds locally and globally when changing one dimension parameter without producing several simulations of each change, creating a band spread. Due to the limited time frame, it was therefore chosen in a simplified manner to apply the same seed to all simulations. In order to verify the results and conclusions drawn from the iterative structural resistance design analysis it is recommended to do multiple simulations of each design parameter change with different seeds.

Since the simulations were performed with the simplification of the same wind and wave seed, it would be expected that the semi-submersible design for one sea depth that has exactly the same load condition, would generate the same results independent of changing the water depth. However, the results show that a depth change of 10 m can change the utilization of a specific control up to 42 %. Furthermore, the analysis shows that small changes in the dimensions of a member type affect the global behavior of the substructure. An increased diameter of the brace showed increased axial and bending capacity, which were expected. However, the resulting combination with hydrostatic pressure highlights that this loading parameter is of importance. So the benefits of a larger diameter are neutralized or even worsened by the effect of hydrostatic pressure acting on a larger surface. It can be concluded that an increased brace thickness is more effective in this case. Because the ratio between the diameter and thickness is high from the initial geometry, it is rather close to a shell element. Therefore a reduction in thickness will more rapidly reduce the ratio resulting in a member further away from a shell element. Reducing the thickness of the offset columns has a minor effect on shell buckling. However, the reduction is highly affecting the response of the braces. It is analyzed that the braces first increase in capacity with a reduction of 10 mm in the thickness offset column and then elevate to failure when it is decreased by a further 10 mm. The unexpected increase in brace capacity is probably due to the fact that a change in one parameter can influence how the substructure moves globally during the simulation and in this case result in a favorable loading situation. When the thickness is decreased further the global stiffness is too low resulting in high stresses in the braces.

There were encountered some contradictions in the structural design of the floating substructure when following the guidelines of DNV. This was due to the combination of different guidelines and standards. This is especially a concern for the definition if a member is a shell structure or a tubular. The limit from DNV is higher than the limit in the ISO standard for tubular members and therefore for certain dimensions there is a gap where no code is applicable without having to do assumptions and corrections.

Frequency

The final step in the design method loop was to evaluate the natural frequency. As expected, the result shows that the natural frequency of the jacket substructure lies in the range of soft-stiff design. The first critical mode does not intersect with the frequencies from the loads and therefore there is a low risk of resonance. The design for the semi-submersible shows that the critical heave mode is within the soft-soft design range. However, for all semi-submersible designs, the critical modes side-to-side and fore-aft are in the range of the 3P loading. Therefore there should be added a dynamic amplification factor on this particular load. However, since it was not possible to add safety factors on the separate loads in Ashes, the only possibility would be to apply the generated dynamic amplification factors at all section forces. It was chosen not to change dimensions for further iterations in the design since these results probably would generate a design too conservative.

6.2 Comparison material consumption

When comparing solely the material consumption of the two different solutions for the 5 MW turbine, the jacket substructure is by magnitude the most suited selection for all intermediate sea depths. However, since the solutions have different resultant forces at the mud line, both in magnitude and direction, the selection of the needed foundation will affect the final material consumption. This might lead to a smaller difference in the total material consumption between the two solutions. The jacket substructure are modeled with fixed boundary condition in the connection to the sea bed, since no foundation solution can provide this in reality it should be regarded that it could affect the final dimensions.

The comparison with the larger turbine of 15 MW reflects the same conclusion, the jacket substructure demands less material than the semi-submersible. The larger dead weight also needs more submerged volume for the semi-submersible, which either will require larger columns or deeper draught which will make it difficult or almost impossible to design for the lower depth of 30 m sea without oversize the columns.

It should be highlighted that the large deviation in the comparison of the material consumption is between these two particular substructure types. Other substructure types for example gravity, monopile, or tension-leg might generate other conclusions. Furthermore, other configurations of the semi-submersible such as different stabilizing structure, or reduction of the plate thickness with the implementation of stiffeners, and other optimizing measures might provide a solution more competitive in comparison to the fixed jacket substructure.

6.3 Floating substructures at intermediate water depths

There are a lot of other aspects that have not been analyzed in this thesis that also might affect the relevance of floating substructures on intermediate sea depths. Aspects such as ease of production and maintenance are values that can have a large influence in regard to the overall cost. For example, the anchor solution for the semi-submersible is less time-consuming in installation, and less sensitive to the soil condition. Therefore, it is reasonable to assume that the solution is less expensive than for example piling for the jacket substructure. One other benefit of the floating solution is that it can be towed to the harbor for maintenance, which could ease work and reduce work site risks.

It would be reasonable to assume that the dimensions of the members would remain the same for the semi-submersible substructure for all sea depths between 30-60 m. However, the result from the simulations showed that the same dimensions provided deviating sectional forces in the members for the different sea depths, despite that

they all were simulated with the same seed. Since the only difference between the different cases is the length of the mooring lines, this shows that they have a key influence on the motions of the substructure. It was also discovered that the numerical model had a problem finding a solution for the 30 m sea depth, which also is tracked back to the mooring lines. Therefore, it is doubtful if the mooring line design is adaptable to this low sea depth.

6.4 Future work

The following subjects are proposed as further work.

- Include the contribution of the foundation in the comparison of structural mass between fixed and floating substructures.
- Design of internal structure for the heave plates.
- Further investigation of mooring lines at intermediate depths.
- Analyse another type of stabilizing solution, such as beams instead of bracing between the columns. Investigate geometry changes that would increase material efficiency.
- Continue preliminary design including fatigue limit state and accidental limit state.
- Proceed evaluation in the selection between floating and fixed substructure based on other aspects, such as maintenance, production, logistics, and life cycle cost.

Bibliography

Ambrosio, J. A. C. (2001). Quasi-Static Behavior. *In: Ambrosio, J.A.C. (eds) Crashworthiness. International Centre for Mechanical Sciences*, *vol 423*(Springer, Vienna), 19–31. https://doi.org/10.1007/978-3-7091-2572-4{_}2

Arany, L., Bhattacharya, S., Macdonald, J., & Hogan, S. J. (2015). Simplified critical mudline bending moment spectra of offshore wind turbine support structures. *Wind Energy*, *18*(12), 2171–2197. https://doi.org/10.1002/WE.1812

Bhattacharya, S. (2019). *Design of Foundations for Offshore*. John Wiley & Sons, Incorporated.

Britannica. (2023). Bessel function | Definition, Equation, Uses, & Facts | Britannica. https://www.britannica.com/science/Bessel-function

Bülow Jørgensen Ljjj, L., & Gravesen, H. (2009). *Kriegers Flak Offshore Wind Farm Site Assessment* (tech. rep.). Vattenfall.

Bureau of Ocean Energy Management. (2023). Renewable Energy on the Outer Continental Shelf | Bureau of Ocean Energy Management. https://www.boem.gov/renewable-energy/renewable-energy-program-overview

Chella, M. A., Mayilvahanan, A. C., & Selvam, R. P. (2010). *Static Stability and Dynamic Analysis of Semi-submersible Floaters for an Offshore Wind Turbine* (tech. rep.). Indian Institute of Technology Madra. India. https://www.researchgate.net/publication/282131616

Cronin, Y., Cummins, V., & Wolsztynski, E. (2021). Public perception of offshore wind farms in Ireland. *Marine Policy*, *134*, 104814. https://doi.org/10.1016/J.MARPOL.2021.104814

Crowle, A., & Thies, P. (2022). Floating offshore wind turbines port requirements for construction. *Proceedings of the Institution of Mechanical Engineers, Part M: Journal of Engineering for the Maritime Environment*, *236*(4), 1047–1056. https://doi.org/10.1177/14750902221078425

Dingley, A. (2012). *Offshore wind turbines at Barrow Offshore Wind off Walney Island in the Irish Sea Unusually good weather for April!* (Photography). (CC BY SA 3.0). https://commons.wikimedia.org/wiki/File:Barrow_Offshore_wind_turbines_edit1.jpg

DNV. (2021a). *Environmental conditions and environmental loads*. https://standards.dnv.com/explorer/document/01C72BD89E90416C89C4CA942694391E/6

DNV. (2021b). *Floating wind turbine structures*. https://standards.dnv.com/explorer/document/72990A2C4023405DA43C92C46D02950C/6

DNV. (2021c). *Loads and site conditions for wind turbines*. https://standards.dnv.com/explorer/document/FB825A24288648309DA012E2A6D84E00/2

DNV. (2021d). *Support structures for wind turbines*. https://standards.dnv.com/explorer/document/251EFC70A476419D8FC41CC0B86888C5/4

Equinor. (2022). Hywind Scotland - the world's first floating wind farm - Equinor. https://www.equinor.com/energy/hywind-scotland

ETIPWind Executive Committee. (2020). *Floating offshore wind delivering climate neutrality* (tech. rep.). Bruxelles.

Faltinsen, O. (1990). *Sea loads on ships and offshore structures* (tech. rep.). Cambridge University Press. Cambridge.

Gaertner, E., Rinker, J., Sethuraman, L., Zahle, F., Anderson, B., Barter, G., Abbas, N., Meng, F., Bortolotti, P., Skrzypinski, W., Scott, G., Feil, R., Bredmose, H., Dykes, K., Shields, M., Allen, C., & Viselli, A. (2020). *Definition of the IEA Wind 15-Megawatt Offshore Reference Wind Turbine Technical Report* (tech. rep.). www.nrel.gov/publications.

Gilloteaux, J.-C., & Bozonnet, P. (2014). *Parametric Analysis of a Cylinder-Like Shape Floating Platform Dedicated to Multi-Mega Watt Wind Turbine* (tech. rep.). Applied Mechanics division. Rueil-Malmaison, France. https://www.researchgate.net/publication/263099654_Parametric_Analysis_of_a_Cylinder-Like_Shape_Floating_Platform_Dedicated_to_Multi-Mega_Watt

Hartman, L. (2022). Wind Turbines: the Bigger, the Better. https://www.energy.gov/eere/articles/wind-turbines-bigger-better

Huijs, F., De Bruijn, R., & Savenije, F. (2014). Concept Design Verification of a Semi-submersible Floating Wind Turbine Using Coupled Simulations. *Energy Procedia*, *53*(100), 2–12. https://doi.org/10.1016/J.EGYPRO.2014.07.210

ICF. (2020). *Comparison of Environmental Effects from Different Offshore Wind Turbine Foundations* (tech. rep.). U.S. Dept. of the Interior, Bureau of Ocean Energy Management, Headquarters. Sterling.

International Electrotechnical Commission. (2019a). *Wind energy generation systems - Part 1: Design requirements*. (IEC 61400-1:2019). https://webstore.iec.ch/publication/26423

International Electrotechnical Commission. (2019b). *Wind energy generation systems - Part 3-1: Design requirements for fixed offshore wind turbines*. (IEC 61400-3-1:2019). https://webstore.iec.ch/publication/29360

International Energy Agency. (2019). World Energy Outlook. https://iea.blob.core.windows.net/assets/98909c1b-aabc-4797-9926-35307b418cdb/WEO2019-free.pdf

International Renewable Energy Agency. (2019a). Wind energy. https://www.irena.org/Energy-Transition/Technology/Wind-energy

International Renewable Energy Agency, I. (2019b). *Future of wind*. www.irena.org/publications.

Jonkman, B. J., & Kilcher, L. (2012). *TurbSim User's Guide: Version 1.06.00* (tech. rep.). National Renewable Energy Laboratory. Golden, CO. http://www.osti.gov/bridge

Jonkman, J., Butterfield, S., Musial, W., & Scott, G. (2009). *Definition of a 5-MW Reference Wind Turbine for Offshore System Development* (tech. rep.).

National Renewable Energy Laboratory. Golden, CO. http://www.osti.gov/bridge

Lamy, J., Bruine de Bruin, W., Azevedo, I. M., & Morgan, M. G. (2020). Keep wind projects close? A case study of distance, culture, and cost in offshore and onshore wind energy siting. *Energy Research & Social Science*, *63*, 101377. https://doi.org/10.1016/J.ERSS.2019.101377

Lee, B. S. (2019). Hydrostatics and Stability of Marine Vehicles. *7*. https://doi.org/10.1007/978-981-13-2682-0

Li, C., Mogollón, J. M., Tukker, A., Dong, J., von Terzi, D., Zhang, C., & Steubing, B. (2022). Future material requirements for global sustainable offshore wind energy development. *Renewable and Sustainable Energy Reviews*, *164*. https://doi.org/10.1016/J.RSER.2022.112603

Lindblom, A., & Ånger, E. (2022). *Assessment of ice loads on piled structures based on local conditions* (tech. rep.). KTH Royal Institute of Technology. Stockholm.

Malhotra, S. (2007). Design and construction considerations for offshore wind turbine foundations. *Proceedings of the International Conference on Offshore Mechanics and Arctic Engineering - OMAE*, *5*, 635–647. https://doi.org/10.1115/OMAE2007-29761

Musial, W., Spitsen, P., Duffy, P., Beiter, P., Marquis, M., Hammond, R., & Shields, M. (2022a). *Offshore Wind Market Report: 2022 Edition* (tech. rep.). United States. https://doi.org/10.2172/1883382

Musial, W., Spitsen, P., Duffy, P., Beiter, P., Marquis, M., Hammond, R., & Shields, M. (2022b). *Offshore Wind Market Report: 2022 Edition* (tech. rep.).

Mutungi, H., & Faruk Halici, Ö. (2016). *Assessment of simulation codes for offshore wind turbine foundations* (tech. rep.). Chalmers University of Technology. Göteborg.

Reuters Events. (2019). Equinor cuts floating wind costs by 40% in design revamp | Reuters Events | Renewables. https://www.reutersevents.com/renewables/wind-energy-update/equinor-cuts-floating-wind-costs-40-design-revamp

Robertson, A., Jonkman, J., Masciola, M., Song, H., Goupee, A., Coulling, A., & Luan, C. (2014). Definition of the Semisubmersible Floating System for Phase II of OC4. www.nrel.gov/publications.

Robertson, A., Jonkman, J., Vorpahl, F., Popko, W., Qvist, J., Frøyd, L., Chen, X., Azcona, J., Uzunoglu, E., Soares, C. G., Luan, C., Yutong, H., Pengcheng, F., Yde, A., Larsen, T., Nichols, J., Buils, R., Lei, L., Nygard, T. A., … Guérinel, M. (2014). *Offshore Code Comparison Collaboration, Continuation within IEA Wind Task 30: Phase II Results Regarding a Floating Semisubmersible Wind System: Preprint* (tech. rep.). www.nrel.gov/publications.

Rogers, A. L., Manwell, J. F., & McGowan, J. G. (2010). *Wind energy explained : Theory, design and application*. John Wiley & Sons, Incorporated.

S. Ishwarya, M. Arockiasamy, & R. Senthil. (2016). Inelastic Nonlinear Pushover Analysis of Fixed Jacket-Type Offshore Platform with Different Bracing Systems Considering Soil-Structure Interaction. *Journal of Shipping and Ocean Engineering*, *6*(4). https://doi.org/10.17265/2159-5879/2016.04.006

Speight, J. G. (2015). Offshore Platforms. *Subsea and Deepwater Oil and Gas Science and Technology*, 71–106. https://doi.org/10.1016/B978-1-85617-558-6.00003-9

Stehly, T., Beiter, P., & Duffy, P. (2019). *2019 Cost of Wind Energy Review* (tech. rep.). National Renewable Energy Laboratory. Golden. https://www.nrel.gov/docs/fy21osti/78471.pdf

van der Tempel, J., Zaaijer, M., & Subroto, H. (2019). *The effects of Scour on the design of Offshore Wind Turbines* (tech. rep.). Delft University of Technology. Delft.

Vázquez, A., Izquierdo, U., Enevoldsen, P., Andersen, F. H., & Blanco, J. M. (2022a). A macroscale optimal substructure selection for Europe's offshore wind farms. *Sustainable Energy Technologies and Assessments*, *53*. https://doi.org/10.1016/j.seta.2022.102768

Vázquez, A., Izquierdo, U., Enevoldsen, P., Andersen, F. H., & Blanco, J. M. (2022b). A macroscale optimal substructure selection for Europe's offshore wind farms. *Sustainable Energy Technologies and Assessments*, *53*, 102768. https://doi.org/10.1016/J.SETA.2022.102768

Vorpahl, F., Popko, W., & Kaufer, D. (2011). *Description of a basic model of the "UpWind reference jacket" for code comparison in the OC4 project under IEA Wind Annex XXX* (tech. rep.). www.iwes.fraunhofer.de

Wang, X., Zeng, X., Li, J., Yang, X., & Wang, H. (2018). A review on recent advancements of substructures for offshore wind turbines. *Energy Conversion and Management*, *158*, 103–119. https://doi.org/10.1016/J.ENCONMAN.2017.12.061

Wayman, E. N., Sclavounos, P. D., Butterfield, S., Jonkman, J., Musial, W., & Butterfield, ; S. (2006). *Coupled Dynamic Modeling of Floating Wind Turbine Systems Preprint OTC Paper Number 18287 Coupled Dynamic Modeling of Floating Wind Turbine Systems* (tech. rep.). http://www.osti.gov/bridgeonlineordering:http://www.ntis.gov/ordering.htm

wpd. (2021). *Fyrskeppet Samrådsunderlag* (tech. rep.).

Xu, K., & Michailides, C. (2015). *Design and Analysis of Mooring System for Semi-submersible Floating Wind Turbines in Shallow Water* (tech. rep.). Department of Marine Technology. Trondheim.

Zhou, S., Müller, K., Li, C., Xiao, Y., & Cheng, P. W. (2021). Global sensitivity study on the semisubmersible substructure of a floating wind turbine: Manufacturing cost, structural properties and hydrodynamics. *Ocean Engineering*, *221*. https://doi.org/10.1016/j.oceaneng.2021.108585

A

Appendix - Input data for simulations

Table A.1. *Input data for convergence study.*

Duration	[s]	600
Rec. time step		1
Analysis	Timestep [s]	0.025
	Rotor model	Stiff/Flexible
	Numerical integration method	HHT-alpha
	HHT-alpha factor	-0.025
	Structural damping	Reyleigh
	Mass coefficient(μ)	$1.111 \cdot 10^{-3}$
	Stiffness coefficient(λ)	$6.254 \cdot 10^{-3}$
	Energy tolerance (absolute)	Evaluated: -8 to 8
	Maximum iterations	1000
Atmosphere	Type	Turbulent
	Turbulence model	Mann
Seabed	Depth [m]	200
Sea	Type	Irregular - single spectrum
Hydrodynamics	Spectrum	JONSWAP
	Algorithm for perpendicular loading	MacCamy-Fuchs/ Morrison
Mooring line	Model type	Lines (linear/non-linear)
	Number of elements	30
Rotor	Blade type	NREL 5-MW

Table A.2. *Input data for case study.*

Duration	[s]	600
Rec. time step		4
Analysis	Timestep [s]	0.025
Analysis	Rotor model []	Stiff
Analysis	Numerical integration method []	HHT-alpha
Analysis	HHT-alpha factor []	-0.025
Analysis	Energy tolerance (absolute) []	-8
Analysis	Maximum iterations []	1000
Atmosphere	Type []	Turbulent
Hydrodynamics	Algorithm for perpendicular loading []	MacCamy-Fuchs
Mooring line	Model type []	Lines (nonlinear)
Mooring line	Line diameter [m]	0.0766
Mooring line	Length scheme []	Relative length
Mooring line	Anchor distance [m]	853.87
Mooring line	Number of elements []	30
Mooring line	Distributed mass [kg/m]	113.35
Rotor	Blade type []	NREL 5-MW
Sea	Type []	Irregular - single spectrum
Seabed	Depth [m]	200
Waves: Irregular 1	Input file []	"filename"
Waves: Irregular 1	Principal angle [Â°]	0
Wind: Turbulent	Source []	"filename"

B

Appendix - Wave height, wave period and wave number

Load case 1 wave W1

ESS (Extreme sea state)

Input:
Principal angle
Peak period
Significant wave height (HS1)

$T_{p.1} := 8\ s$ — Peak period 1 year

$H_{s.1} := 3.6\ m$ — Significant wave height 1 year

Peak-enhancement factor
DNV-ST-0437 2.4.5.1 eq 2.13

$$\gamma_{p.1} := \begin{cases} 5 & \text{if } \dfrac{\frac{T_{p.1}}{s}}{\sqrt{\frac{H_{s.1}}{m}}} \le 3.6 \\ \exp\left(5.75 - 1.15 \cdot \dfrac{\frac{T_{p.1}}{s}}{\sqrt{\frac{H_{s.1}}{m}}}\right) & \text{else} \\ 1 & \text{else if } \dfrac{\frac{T_{p.1}}{s}}{\sqrt{\frac{H_{s.1}}{m}}} \ge 5 \end{cases} = 2.462$$

$S := 50\ m$ — Sea depth

$\omega_{1.p.1} := \dfrac{2 \cdot \pi}{T_{p.1}} = 0.785\ \dfrac{1}{s}$

Wave angular frequency
DNV-RP-C205 3.1.2

Solve Constraints Guess Values

$k_1 := 1 \cdot \dfrac{1}{m}$ — Initial guess

$\omega_{1.p.1}{}^2 = g \cdot k_1 \cdot tanh\left(k_1 \cdot S\right)$ — Dispersion relationship
DNV-RP-C205 3.2.2.3

$k_{p.1} := \mathbf{find}\left(\mathbf{k_1}\right) = 0.063\ \dfrac{1}{m}$ — Wave number

Load case 3 wave W2

EWH (Extreme wave height)

Principal angle

Peak period

Significant wave height (HM1)

$$T_{z.p.1} := T_{p.1} \cdot \sqrt{\frac{5+\gamma_{p.1}}{11+\gamma_{p.1}}} = 5.956\ s$$

Zero-upcrossing period
DNV-ST-0437 2.4.5.1 eq 2.12

$$T_{s.p.1} := 3 \cdot 60 \cdot 60\ s = \left(1.08 \cdot 10^4\right)\ s$$

Sea state of duration (3 hours)
DNV-ST-0437 2.4.5.3

$$N_{.p.1} := \frac{T_{s.p.1}}{T_{z.p.1}} = 1.813 \cdot 10^3$$

Number of waves
DNV-ST-0437 2.4.5.3

$$H_{m.1} := H_{s.1} \cdot \sqrt{\frac{1}{2} \ln\left(N_{.p.1}\right)} = 6.973\ m$$

Maximum wave height 1 year
DNV-ST-0437 2.4.5.3 eq 2.19

$$T_{m.1} := 11.1 \cdot \sqrt{\frac{H_{m.1}}{g}} = 9.36\ s$$

Peak period 1 year
DNV-ST-0437 2.4.4.4 eq 2.10

$$\gamma_{m.1} := \begin{cases} 5 & \text{if } \dfrac{\frac{T_{m.1}}{s}}{\sqrt{\frac{H_{m.1}}{m}}} \le 3.6 \\ 1 & \text{else if } \dfrac{\frac{T_{m.1}}{s}}{\sqrt{\frac{H_{m.1}}{m}}} \ge 5 \\ \exp\left(5.75 - 1.15 \cdot \dfrac{\frac{T_{m.1}}{s}}{\sqrt{\frac{H_{m.1}}{m}}}\right) & \text{else} \end{cases} = 5$$

Peak-enhancement factor
DNV-ST-0437 2.4.5.1 eq 2.13

$$\omega_{1.m.1} := \frac{2 \cdot \pi}{T_{m.1}} = 0.671\ \frac{1}{s}$$

Wave angular frequency
DNV-RP-C205 3.1.2

Solve Constraints Guess Values

$k_1 := 1 \cdot \frac{1}{m}$

Initial guess

$\omega_{1.m.1}{}^2 = g \cdot k_1 \cdot tanh\left(k_1 \cdot S\right)$

Dispersion relationship
DNV-RP-C205 3.2.2.3

$k_{m.1} := \text{find}\left(k_1\right) = 0.047 \ \frac{1}{m}$

Wave number

Load case - wave W3

ESS (Extreme sea state)

Principal angle

Peak period

Significant wave height (HS50)

$H_{s.50} := 5.2 \ m$

Significant wave height 50 year

$T_{p.50} := 9.7 \ s$

Peak period 50 year

$$\gamma_{p.50} := \text{if} \left(\frac{\frac{T_{p.50}}{s}}{\sqrt{\frac{H_{s.50}}{m}}} \le 3.6 \ , 5 \ , \text{if} \left(\frac{\frac{T_{p.50}}{s}}{\sqrt{\frac{H_{s.50}}{m}}} \ge 5 \ , 1 \ , \exp\left(5.75 - 1.15 \cdot \frac{\frac{T_{p.50}}{s}}{\sqrt{\frac{H_{s.50}}{m}}}\right) \right) \right) = 2.359$$

Peak-enhancement factor
DNV-ST-0437 2.4.5.1 eq 2.13

$\omega_{1.p.50} := \frac{2 \cdot \pi}{T_{p.50}} = 0.648 \ \frac{1}{s}$

Wave angular frequency
DNV-RP-C205 3.1.2

Solve Constraints Guess Values

$$k_1 := 1 \cdot \frac{1}{m}$$

$$\omega_{1.p.50}{}^2 = g \cdot k_1 \cdot tanh\left(k_1 \cdot S\right)$$

$$k_{p.50} := \mathbf{find}\left(k_1\right) = 0.044 \ \frac{1}{m}$$

Initial guess

Dispersion relationship
DNV-RP-C205 3.2.2.3

Wave number

Load case 2, 4, 5 wave W4

EWH (Extreme wave height)

Principal angle

Peak period

Significant wave height (HM50)

$$T_{z.p.50} := T_{p.1} \cdot \sqrt{\frac{5 + \gamma_{p.50}}{11 + \gamma_{p.50}}} = 5.938 \ s$$

Zero-upcrossing period
DNV-ST-0437 2.4.5.1 eq 2.12

$$T_{s.p.50} := 3 \cdot 60 \cdot 60 \ s = \left(1.08 \cdot 10^4\right) \ s$$

Sea state of duration (3 hours)
DNV-ST-0437 2.4.5.3

$$N_{.p.50} := \frac{T_{s.p.50}}{T_{z.p.50}} = 1.819 \cdot 10^3$$

Number of waves
DNV-ST-0437 2.4.5.3

$$H_{m.50} := H_{s.50} \cdot \sqrt{\frac{1}{2} \ln\left(N_{.p.50}\right)} = 10.074 \ m$$

Maximum wave height 50 year
DNV-ST-0437 2.4.5.3 eq 2.19

$$T_{m.50} := 11.1 \cdot \sqrt{\frac{H_{m.50}}{g}} = 11.25 \ s$$

Peak period 50 year
DNV-ST-0437 2.4.4.4 eq 2.10

$$\gamma_{m.50} := \begin{cases} 5 & \text{if } \dfrac{\dfrac{T_{m.50}}{s}}{\sqrt{\dfrac{H_{m.50}}{m}}} \le 3.6 \\ 1 & \text{else if } \dfrac{\dfrac{T_{m.50}}{s}}{\sqrt{\dfrac{H_{m.50}}{m}}} \ge 5 \\ \exp\left(5.75 - 1.15 \cdot \dfrac{\dfrac{T_{m.50}}{s}}{\sqrt{\dfrac{H_{m.50}}{m}}}\right) & \text{else} \end{cases} = 5$$

Peak-enhancement factor
DNV-ST-0437 2.4.5.1 eq 2.13

$$\omega_{1.m.50} := \frac{2 \cdot \pi}{T_{m.50}} = 0.558 \ \frac{1}{s}$$

Wave angular frequency
DNV-RP-C205 3.1.2

Solve Constraints Guess Values

$$k_1 := 1 \cdot \frac{1}{m}$$

Initial guess

$$\omega_{1.m.50}{}^2 = g \cdot k_1 \cdot \tanh\left(k_1 \cdot S\right)$$

Dispersion relationship
DNV-RP-C205 3.2.2.3

$$k_{m.50} := \text{find}\left(k_1\right) = 0.034 \ \frac{1}{m}$$

Wave number

C

Appendix - Rayleigh damping

Reyleigh damping

$C = \mu \cdot M + \lambda \cdot K$

C = Damping matrix
M = Mass matrix
K = Stiffness matrix
μ = Mass proportional coefficient
λ = Stiffness proportional coefficient

Reyleigh damping coefficients

$\varepsilon_1 := 0.01$ Damping ratio 1
$\varepsilon_2 := 0.01$ Damping ratio 2

$f_1 := 0.009$ 1st frequency
$f_2 := 0.5$ 2st frequency

Constraints Guess Values

$\mu := 1$
$\lambda := 1$

$0.5 \cdot \left(\frac{\mu}{2 \cdot \pi \cdot f_1} + \lambda \cdot 2 \cdot \pi \cdot f_1 \right) = \varepsilon_1$

$0.5 \cdot \left(\frac{\mu}{2 \cdot \pi \cdot f_2} + \lambda \cdot 2 \cdot \pi \cdot f_2 \right) = \varepsilon_2$

Solver

$R := \mathbf{find}(\mu, \lambda) = \begin{bmatrix} 0.001 \\ 0.006 \end{bmatrix}$

$\mu := R_0 = 0.001111$

$\lambda := R_1 = 0.006254$

D

Appendix - Calculation steps for structural resistance

D.1 Unstiffened circular cylinder

Calculation steps to check shell buckling. (DNV-RP-C202)

- Calculate relevant stresses (Section 2.2)
- Calculate the elastic buckling strength of an unstiffened circular cylinder (Section 3.4)
- Calculate characteristic buckling strength (Section 3.2)
- Control the stability requirement (Section 3.1)
- If the stability requirement is not fulfilled, add stiffener (Section 3.5, 3.6, 3.7)

Calculation steps to check column buckling. (DNV-RP-C202)

- Control the stability requirement (Section 3.8.1)
- If the stability requirement is not fulfilled, calculate column buckling strength (Section 3.8.2)

D.2 Buckling tubular member

Calculation steps to check column buckling. (SS-EN ISO 19902:2020)

- Calculate local buckling strength (Section 13.2.3.3)
- Calculate axial compression strength (Section 13.2.3.2)
- Calculate axial compression capacity (Section 13.2.3.1)
- If the utilization rate is too high, increase member size or decrease buckling length

Calculation steps to check hoop buckling. (SS-EN ISO 19902:2020)

- Calculate the hydrostatic pressure (Section 13.2.6.1)
- Calculate the hoop buckling capacity (Section 13.2.6.2)
- If the utilization rate is too high add ring stiffener (Section 13.2.6.3)

D.3 Yielding tubular member

Calculation steps to check yielding. (SS-EN ISO 19902:2020)

- Calculate the axial tension capacity (Section 13.2.2)
- Calculate the bending capacity (Section 13.2.4)
- Calculate the beam shear capacity (Section 13.2.5.1)
- Calculate the torsional shear capacity (Section 13.2.5.2)
- Calculate the combined shear capacity (Section 13.2.5.3)

- Calculate the combined axial tension, bending, and hydrostatic capacity (Section 13.4.2)
- Calculate the combined axial compression, bending, and hydrostatic capacity (Section 13.4.3)
- If the utilization rate is too high increase member size

D.4 Orthogonally stiffened shell

Calculation steps to check shell buckling. (DNV-RP-C202)

- Calculate relevant stresses (Section 2.2)
- Calculate the elastic buckling strength of an unstiffened curved panel (Section 3.3)
- Calculate characteristic buckling strength (Section 3.2)
- Control the stability requirement (Section 3.1)
- If the stability requirement is not fulfilled, decrease the distance between stiffeners

Calculation steps to check panel stiffener buckling. (DNV-RP-C202)

- Calculate relevant stresses (Section 2.2)
- Calculate the elastic buckling strength of the longitudinal stiffener (Section 3.6)
- Calculate characteristic buckling strength (Section 3.2)
- Control the stability requirement (Section 3.1)
- If the stability requirement is not fulfilled, increase longitudinal stiffener size

Calculation steps for panel ring buckling, general buckling, and local buckling. (DNV-RP-C202)

- Check ring stiffener capacity (Section 3.5)
- If ring stiffener capacity is enough general buckling capacity is also enough (Section 3.7.4)
- Check local buckling of stiffener (Section 3.10)
- If capacity is not enough, increase stiffener size

Calculation steps to check column buckling. (DNV-RP-C202)

- Control the stability requirement (Section 3.8.1)
- If the stability requirement is not fulfilled, calculate column buckling strength (Section 3.8.2)

E

Appendix - Target frequency for 5 MW turbine

General input

$f := 1 \cdot 10^{-6} \cdot Hz, 0.0001\ Hz .. 1.5\ Hz =$ $\begin{bmatrix} 1 \cdot 10^{-6} \\ \vdots \end{bmatrix} \frac{1}{s}$ Frequency range

$i := \text{ORIGIN} .. \text{last}(f)$

Turbine 5 MW

$n_{rpm.min} := 6.9$ $n_{rpm.max} := 12.1$ Range in rpm

$n := 3$ Number of blades

Environmental input

Wind

$U_{10} := 9.3\ \frac{m}{s}$ Mean wind speed(10-min)

$z_{hub} := 90\ m$ Height above sea level to hub

$z_0 := 0.01\ m$ Terrain roughness
Open sea z_0 =with waves(0.01) - without waves(0.0001)
DNV-RP-C205 tab.2.1

$I := 0.14$ Turbulence intensity
Varys(OA=0.14, OB=0.12, OC=0.10)
DNV-ST-0437

Wave

$H_s := 3.6\ m$ Significant(Average) wave height
Average height of the highest one-third of the waves

$T_p := 8\ s$ Peak period
wave period determined by the inverse of the frequency at which a wave energy spectrum has its maximum value

Wind: Kaimal spectrum

DNV-RP-C205 2.3.4.7

$$L_u := \left(300 \cdot \left(\frac{z_{hub}}{m} \cdot \frac{1}{300} \right)^{0.46 + 0.074 \cdot \ln\left(\frac{z_0}{m}\right)} \right) \cdot m = 259.887\ m$$

Integral length scale
3.2.4.7
Corresponds to specification in Eurocode 1

$$\sigma_U := I \cdot U_{10} = 1.302\ \frac{m}{s}$$

Standard deviation of wind speed

$$S_U := \sigma_U{}^2\ \frac{6.868 \cdot \frac{L_u}{U_{10}}}{\left(1 + 10.32 \cdot \frac{f \cdot L_u}{U_{10}}\right)^{\frac{5}{3}}} = \begin{bmatrix} 325.196 \\ 310.295 \\ \vdots \end{bmatrix} \frac{m^2}{s}$$

Spectral density for wind
2.3.4.7

$$S_{U.n_i} := \frac{S_{U_i} - min\left(S_U\right)}{\max\left(S_U\right) - min\left(S_U\right)}$$

Normalized wind spectrum

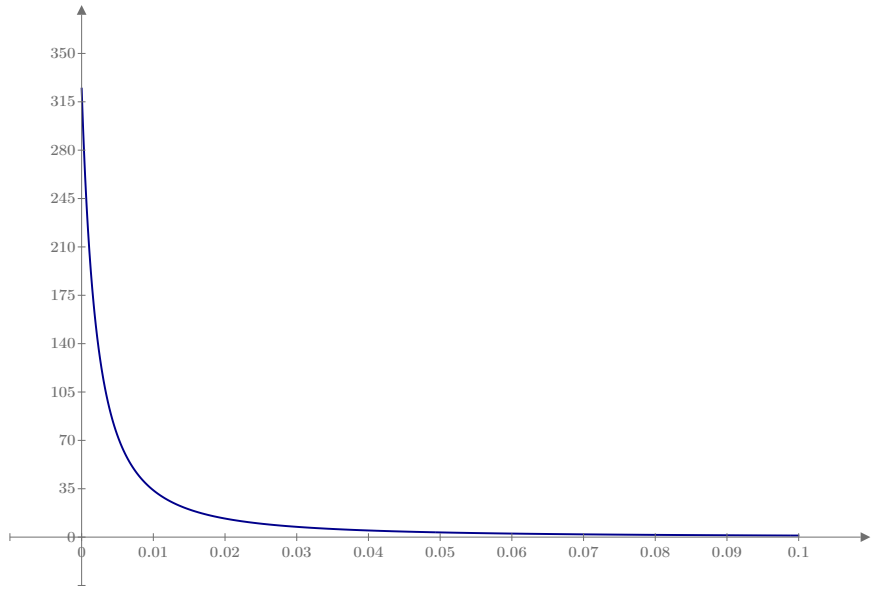

Wave: JONSWAP spectrum

DNV-RP-C205 3.5.5

$$\omega_p := \frac{2 \cdot \pi}{T_p} = 0.785 \ \frac{1}{s}$$

Angular spectral peak frequency
3.5.5.1

$$T := \frac{1}{f}$$

Wave period
3.1.2

$$\omega := \frac{2 \cdot \pi}{T} = \begin{bmatrix} 6.283 \cdot 10^{-6} \\ \vdots \end{bmatrix} \frac{1}{s}$$

Wave angular frequency
3.1.2

$$S_{PM_i} := \frac{5}{16} \cdot {H_s}^2 \cdot {\omega_p}^4 \cdot {\omega_i}^{-5} \cdot \exp\left(-\frac{5}{4} \cdot \left(\frac{\omega_i}{\omega_p}\right)^{-4}\right)$$

Pierson-Moscovitz spectrum
3.5.5.1

$$\gamma := \begin{cases} 5 & \text{if } \dfrac{\frac{T_p}{s}}{\sqrt{\frac{H_s}{m}}} \le 3.6 \\ 1 & \text{else if } \dfrac{\frac{T_p}{s}}{\sqrt{\frac{H_s}{m}}} \ge 5 \\ \exp\left(5.75 - 1.15 \cdot \dfrac{\frac{T_p}{s}}{\sqrt{\frac{H_s}{m}}}\right) & \text{else} \end{cases} = 2.462$$

Non-dimensional peak shape parameter
3.5.5.5

$$A_\gamma := \frac{0.2}{0.065 \cdot \gamma^{0.803} + 0.135} = 0.743$$

Normalizing factor
3.5.5.2

$\sigma_a := 0.07$ for $\omega \le \omega_p$

$\sigma_b := 0.09$ for $\omega > \omega_p$

Spectral width parameter
3.5.5.2

$$\sigma_i := \text{if } \omega_i \le \omega_p \;\|\; \sigma \leftarrow \sigma_a \;\text{else}\; \|\; \sigma \leftarrow \sigma_b = \begin{bmatrix} 0.07 \\ \vdots \end{bmatrix}$$

$$S_{J_i} := A_\gamma \cdot S_{PM_i} \cdot \gamma^{\exp\left(-0.5 \cdot \left(\frac{\omega_i - \omega_p}{\sigma_i \cdot \omega_p}\right)^2\right)} = \begin{bmatrix} 0 \\ \vdots \end{bmatrix} m^2 \cdot s$$

JONSWAP spectrum
3.5.5.2
Modified Pierson-Moskowitz spectrum to considers sea that is not fully developed

$$S_{J.n_i} := \frac{S_{J_i} - min(S_J)}{\max(S_J) - min(S_J)} = \begin{bmatrix} 0 \\ \vdots \end{bmatrix}$$

Normalized wave spectrum

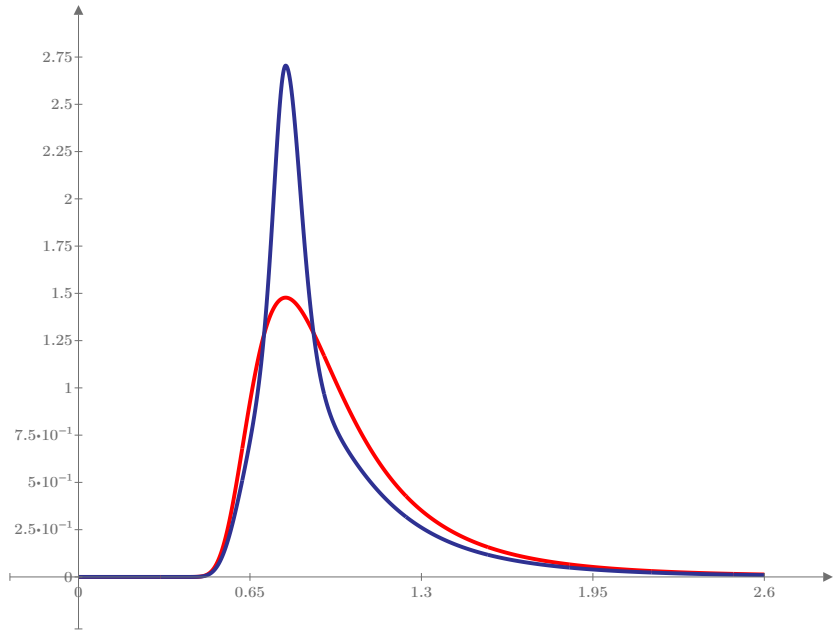

1P

$rpm_{min} := n_{rpm.min} \cdot \frac{1}{60}\ \boldsymbol{Hz}$

$rpm_{max} := n_{rpm.max} \cdot \frac{1}{60}\ \boldsymbol{Hz}$

$f_{1Pmin} := rpm_{min} = 0.115\ \boldsymbol{Hz}$ Frequency range

$f_{1Pmax} := rpm_{max} = 0.202\ \boldsymbol{Hz}$

Safety region

$s_1 := 0.9 \qquad s_2 := 1.1$ 10%

$f_{1Pmin.s} := s_1 \cdot rpm_{min} = 0.104\ \boldsymbol{Hz}$ Frequency range with safety margin

$f_{1Pmax.s} := s_2 \cdot rpm_{max} = 0.222\ \boldsymbol{Hz}$

$S_{1P_i} := \text{if } f_{1Pmin} < f_i < f_{1Pmax} \mid = \begin{bmatrix} 0 \\ \vdots \end{bmatrix}$ 1P spectrum

$\quad \mid\mid S_{1P_i} \leftarrow 1$

$\quad \text{else}$

$\quad \mid\mid 0$

$S_{1P.S_i} := \text{if } f_{1Pmin.s} < f_i < f_{1Pmax.s} \mid = \begin{bmatrix} 0 \\ \vdots \end{bmatrix}$ 1P spectrum(Safety margin)

$\quad \mid\mid S_{1P.S_i} \leftarrow 1$

$\quad \text{else}$

$\quad \mid\mid 0$

3P

$$rpm_{min3} := n \cdot n_{rpm.min} \cdot \frac{1}{60}\ \boldsymbol{Hz}$$

$$rpm_{max3} := n \cdot n_{rpm.max} \cdot \frac{1}{60}\ \boldsymbol{Hz}$$

$f_{3Pmin} := rpm_{min3} = 0.345\ \boldsymbol{Hz}$ Frequency range

$f_{3Pmax} := rpm_{max3} = 0.605\ \boldsymbol{Hz}$

Safety region

$f_{3Pmin.s} := s_1 \cdot rpm_{min3} = 0.311\ \boldsymbol{Hz}$ Frequency range with safety margin

$f_{3Pmax.s} := s_2 \cdot rpm_{max3} = 0.666\ \boldsymbol{Hz}$

$S_{3P_i} := \text{if } f_{3Pmin} < f_i < f_{3Pmax} \left| \begin{array}{l} S_{3P_i} \leftarrow 1 \\ \text{else} \\ 0 \end{array} \right. = \begin{bmatrix} 0 \\ \vdots \end{bmatrix}$ 3P spectrum

$S_{3P.S_i} := \text{if } f_{3Pmin.s} < f_i < f_{3Pmax.s} \left| \begin{array}{l} S_{3P.S_i} \leftarrow 1 \\ \text{else} \\ 0 \end{array} \right. = \begin{bmatrix} 0 \\ \vdots \end{bmatrix}$ 3P spectrum(Safety margin)

Normalized frequency spectrum of the dynamic loads

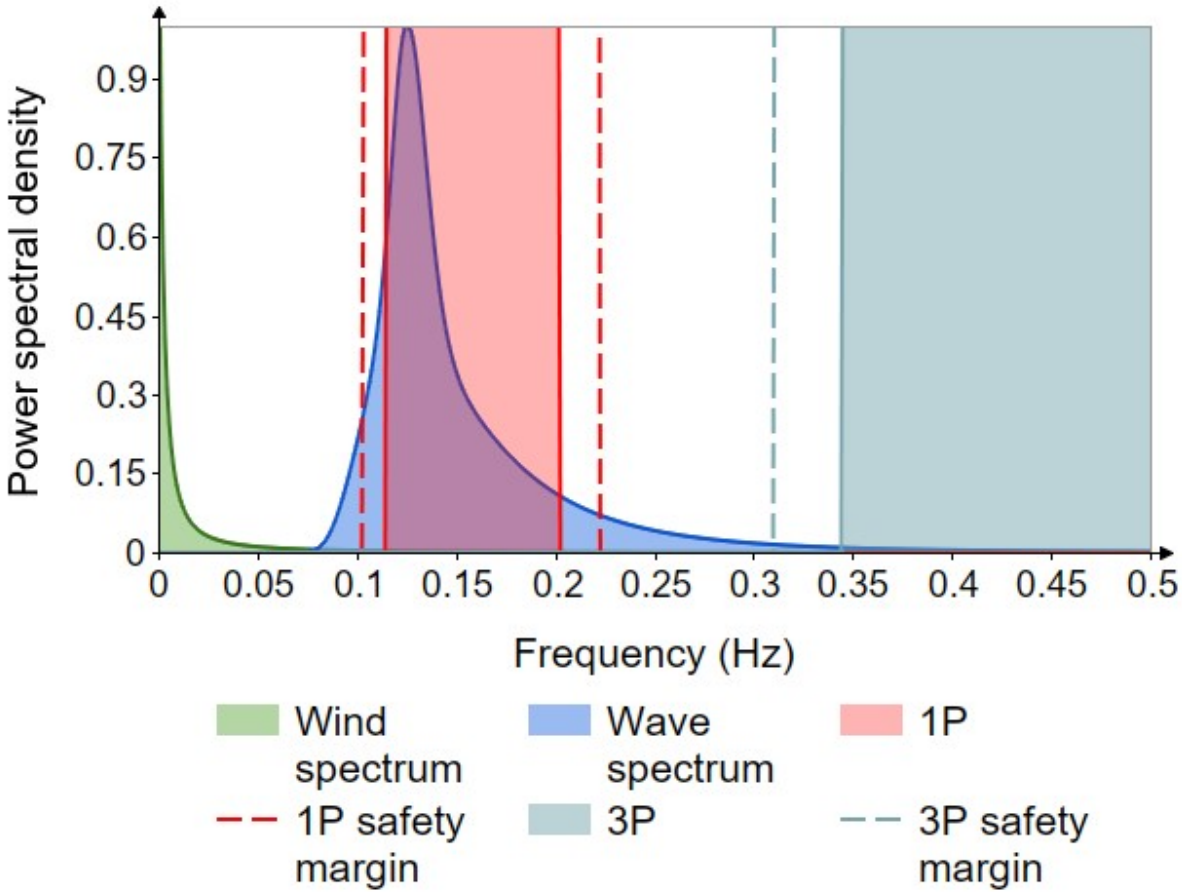

F

Appendix - Target frequency for 15 MW turbine

General input:

$f := 1 \cdot 10^{-6} \cdot Hz, 0.0001\ Hz .. 1.5\ Hz =$ $\begin{bmatrix} 1 \cdot 10^{-6} \\ \vdots \end{bmatrix} \frac{1}{s}$ Frequency range

$i := ORIGIN .. last(f)$

Turbine 15 MW

$n_{rpm.min} := 5$ $n_{rpm.max} := 7.56$ Range in rpm

$n := 3$ Number of blades

Environmental input

Wind

$U_{10} := 9.3\ \frac{m}{s}$ Mean wind speed(10-min)

$z_{hub} := 150\ m$ Height above sea level to hub

$z_0 := 0.01\ m$ Terrain roughness
Open sea z_0 =with waves(0.01) - without waves(0.0001)
DNV-RP-C205 tab.2.1

$I := 0.14$ Turbulence intensity
Varys(OA=0.14, OB=0.12, OC=0.10)
DNV-ST-0437

Wave

$H_s := 3.6\ m$ Significant(Average) wave height
Average height of the highest one-third of the waves

$T_p := 8\ s$ Peak period
wave period determined by the inverse of the frequency at which a wave energy spectrum has its maximum value

Wind: Kaimal spectrum

DNV-RP-C205 2.3.4.7

$$L_u := \left(300 \cdot \left(\frac{z_{hub}}{m} \right)^{0.46 + 0.074 \cdot \ln\left(\frac{z_0}{m}\right)} \right) \cdot m = 276.206\ m$$

Integral length scale
3.2.4.7
Corresponds to specification in Eurocode 1

$$\sigma_U := I \cdot U_{10} = 1.302\ \frac{m}{s}$$

Standard deviation of wind speed

$$S_U := {\sigma_U}^2\ \frac{6.868 \cdot \frac{L_u}{U_{10}}}{\left(1 + 10.32 \cdot \frac{f \cdot L_u}{U_{10}}\right)^{\frac{5}{3}}} = \begin{bmatrix} 345.606 \\ 328.814 \\ \vdots \end{bmatrix} \frac{m^2}{s}$$

Spectral density for wind
2.3.4.7

$$S_{U.n_i} := \frac{S_{U_i} - min\left(S_U\right)}{\max\left(S_U\right) - min\left(S_U\right)}$$

Normalized wind spectrum

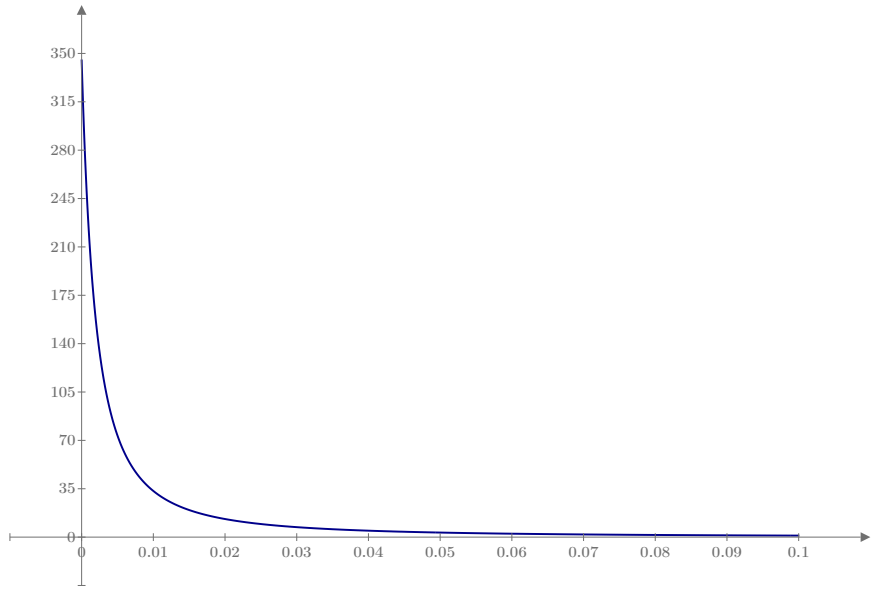

Wave: JONSWAP spectrum

DNV-RP-C205 3.5.5

$$\omega_p := \frac{2 \cdot \pi}{T_p} = 0.785 \ \frac{1}{s}$$

Angular spectral peak frequency
3.5.5.1

$$T := \frac{1}{f}$$

Wave period
3.1.2

$$\omega := \frac{2 \cdot \pi}{T} = \begin{bmatrix} 6.283 \cdot 10^{-6} \\ \vdots \end{bmatrix} \frac{1}{s}$$

Wave angular frequency
3.1.2

$$S_{PM_i} := \frac{5}{16} \cdot {H_s}^2 \cdot {\omega_p}^4 \cdot {\omega_i}^{-5} \cdot \exp\left(-\frac{5}{4} \cdot \left(\frac{\omega_i}{\omega_p}\right)^{-4}\right)$$

Pierson-Moscovitz spectrum
3.5.5.1

$$\gamma := \begin{cases} 5 & \text{if } \dfrac{\frac{T_p}{s}}{\sqrt{\frac{H_s}{m}}} \le 3.6 \\ 1 & \text{else if } \dfrac{\frac{T_p}{s}}{\sqrt{\frac{H_s}{m}}} \ge 5 \\ \exp\left(5.75 - 1.15 \cdot \dfrac{\frac{T_p}{s}}{\sqrt{\frac{H_s}{m}}}\right) & \text{else} \end{cases} = 2.462$$

Non-dimensional peak shape parameter
3.5.5.5

$$A_\gamma := \frac{0.2}{0.065 \cdot \gamma^{0.803} + 0.135} = 0.743$$

Normalizing factor
3.5.5.2

$\sigma_a := 0.07$ for $\omega \le \omega_p$

$\sigma_b := 0.09$ for $\omega > \omega_p$

Spectral width parameter
3.5.5.2

$$\sigma_i := \text{if } \omega_i \le \omega_p \;\; \sigma \leftarrow \sigma_a \;\; \text{else} \;\; \sigma \leftarrow \sigma_b = \begin{bmatrix} 0.07 \\ \vdots \end{bmatrix}$$

$$S_{J_i} := A_\gamma \cdot S_{PM_i} \cdot \gamma^{\exp\left(-0.5 \cdot \left(\frac{\omega_i - \omega_p}{\sigma_i \cdot \omega_p}\right)^2\right)} = \begin{bmatrix} 0 \\ \vdots \end{bmatrix} \; m^2 \cdot s$$

JONSWAP spectrum
3.5.5.2
Modified Pierson-Moskowitz spectrum to considers sea that is not fully developed

$$S_{J.n_i} := \frac{S_{J_i} - min(S_J)}{\max(S_J) - min(S_J)} = \begin{bmatrix} 0 \\ \vdots \end{bmatrix}$$

Normalized wave spectrum

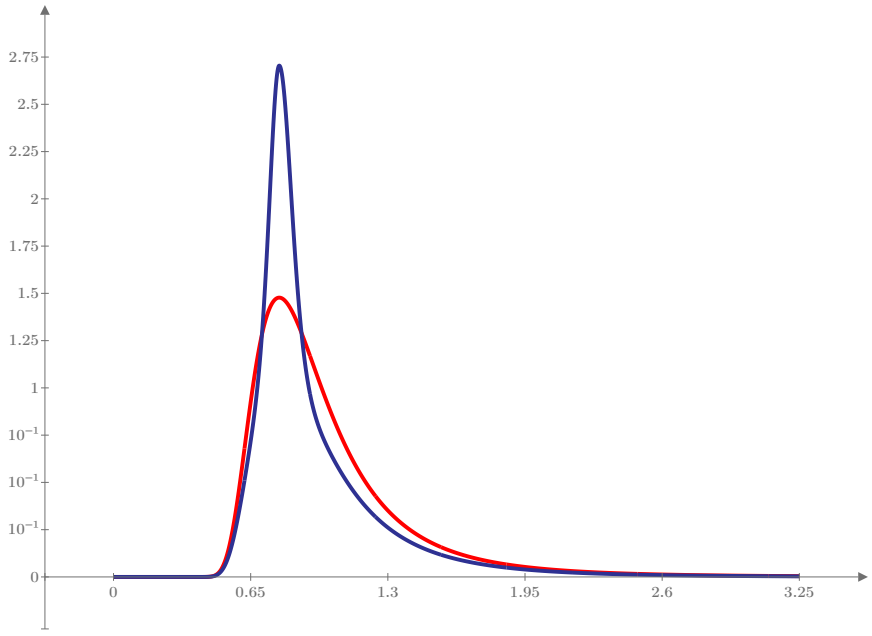

1P

$rpm_{min} := n_{rpm.min} \cdot \frac{1}{60}\ \boldsymbol{Hz}$

$rpm_{max} := n_{rpm.max} \cdot \frac{1}{60}\ \boldsymbol{Hz}$

$f_{1Pmin} := rpm_{min} = 0.083\ \boldsymbol{Hz}$ Frequency range

$f_{1Pmax} := rpm_{max} = 0.126\ \boldsymbol{Hz}$

Safety region

$s_1 := 0.9 \qquad s_2 := 1.1$ 10%

$f_{1Pmin.s} := s_1 \cdot rpm_{min} = 0.075\ \boldsymbol{Hz}$ Frequency range with safety margin

$f_{1Pmax.s} := s_2 \cdot rpm_{max} = 0.139\ \boldsymbol{Hz}$

$S_{1P_i} := \text{if } f_{1Pmin} < f_i < f_{1Pmax} \quad \text{then } S_{1P_i} \leftarrow 1 \quad \text{else } 0 = \begin{bmatrix} 0 \\ \vdots \end{bmatrix}$ 1P spectrum

$S_{1P.S_i} := \text{if } f_{1Pmin.s} < f_i < f_{1Pmax.s} \quad \text{then } S_{1P.S_i} \leftarrow 1 \quad \text{else } 0 = \begin{bmatrix} 0 \\ \vdots \end{bmatrix}$ 1P spectrum(Safety margin)

3P

$$rpm_{min3} := n \cdot n_{rpm.min} \cdot \frac{1}{60}\ \boldsymbol{Hz}$$

$$rpm_{max3} := n \cdot n_{rpm.max} \cdot \frac{1}{60}\ \boldsymbol{Hz}$$

$f_{3Pmin} := rpm_{min3} = 0.25\ \boldsymbol{Hz}$ Frequency range

$f_{3Pmax} := rpm_{max3} = 0.378\ \boldsymbol{Hz}$

Safety region

$f_{3Pmin.s} := s_1 \cdot rpm_{min3} = 0.225\ \boldsymbol{Hz}$ Frequency range with safety margin

$f_{3Pmax.s} := s_2 \cdot rpm_{max3} = 0.416\ \boldsymbol{Hz}$

$S_{3P_i} := \text{if } f_{3Pmin} < f_i < f_{3Pmax} \left| \begin{array}{l} S_{3P_i} \leftarrow 1 \\ \text{else} \\ 0 \end{array} \right. = \begin{bmatrix} 0 \\ \vdots \end{bmatrix}$ 3P spectrum

$S_{3P.S_i} := \text{if } f_{3Pmin.s} < f_i < f_{3Pmax.s} \left| \begin{array}{l} S_{3P.S_i} \leftarrow 1 \\ \text{else} \\ 0 \end{array} \right. = \begin{bmatrix} 0 \\ \vdots \end{bmatrix}$ 3P spectrum(Safety margin)

Normalized frequency spectrum of the dynamic loads

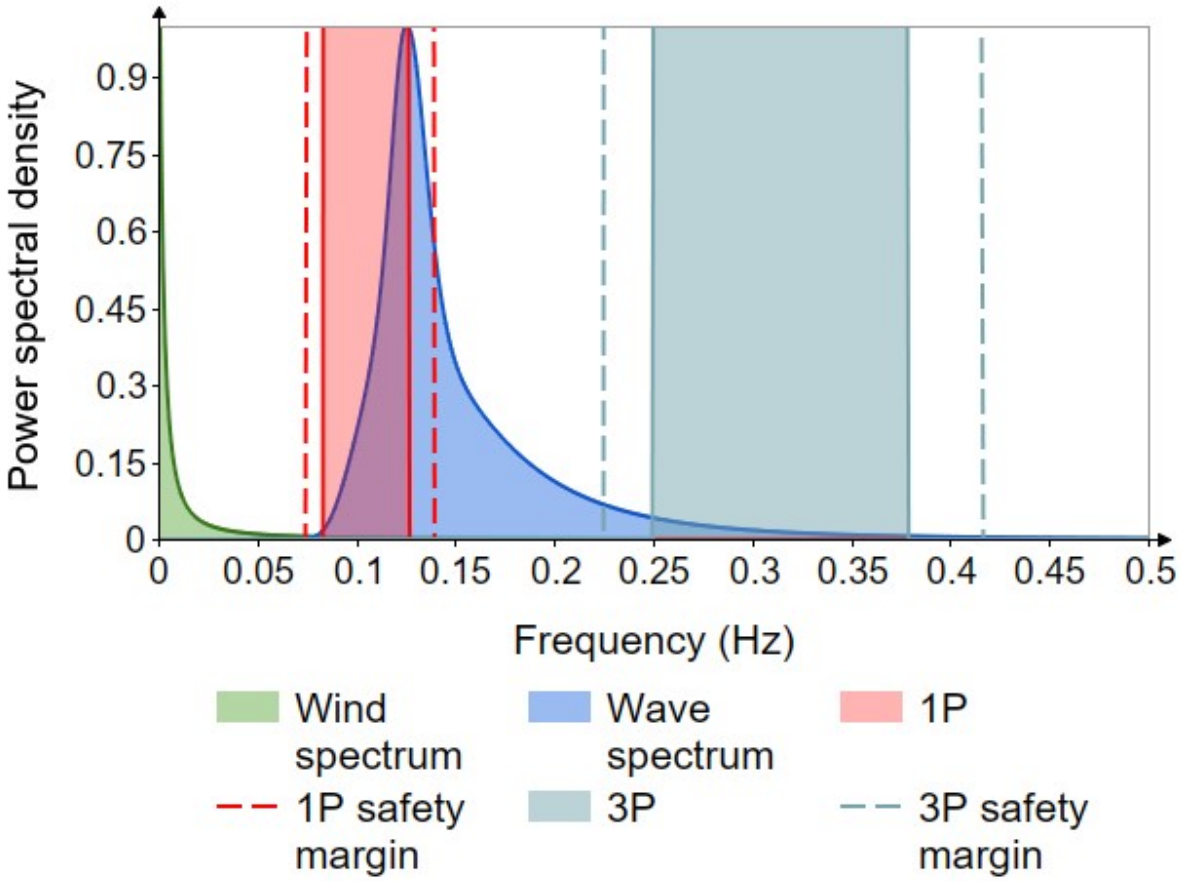

G

Appendix - Input files for Turbsim

G.1 Normal turbulence model for 5 MW turbine

```
1   ---------TurbSim v2.00.* Input File------------------------
2   Example input file for TurbSim.
3   ---------Runtime Options-----------------------------------
4   False     Echo            - Echo input data to <RootName>.ech (flag)
5   2318573   RandSeed1       - First random seed  (-2147483648 to 2147483647)
6   RANLUX    RandSeed2       - Second random seed (-2147483648 to 2147483647) for
    intrinsic pRNG, or an alternative pRNG: "RanLux" or "RNSNLW"
7   False     WrBHHTP         - Output hub-height turbulence parameters in binary form?
    (Generates RootName.bin)
8   False     WrFHHTP         - Output hub-height turbulence parameters in formatted
    form?  (Generates RootName.dat)
9   False     WrADHH          - Output hub-height time-series data in AeroDyn form?
    (Generates RootName.hh)
10  False     WrADFF          - Output full-field time-series data in TurbSim/AeroDyn
    form? (Generates RootName.bts)
11  True      WrBLFF          - Output full-field time-series data in BLADED/AeroDyn
    form?  (Generates RootName.wnd)
12  False     WrADTWR         - Output tower time-series data? (Generates RootName.twr)
13  False     WrFMTFF         - Output full-field time-series data in formatted
    (readable) form?  (Generates RootName.u, RootName.v, RootName.w)
14  False     WrACT           - Output coherent turbulence time steps in AeroDyn form?
    (Generates RootName.cts)
15  True      Clockwise       - Clockwise rotation looking downwind? (used only for
    full-field binary files - not necessary for AeroDyn)
16   0        ScaleIEC        - Scale IEC turbulence models to exact target standard
     deviation? [0=no additional scaling; 1=use hub scale uniformly; 2=use individual
     scales]
17
18  --------Turbine/Model Specifications-----------------------
19  32        NumGrid_Z       - Vertical grid-point matrix dimension
20  32        NumGrid_Y       - Horizontal grid-point matrix dimension
21  0.03      TimeStep        - Time step [seconds]
22  600       AnalysisTime    - Length of analysis time series [seconds] (program will
    add time if necessary: AnalysisTime = MAX(AnalysisTime,
    UsableTime+GridWidth/MeanHHWS) )
23  600       UsableTime      - Usable length of output time series [seconds] (program
    will add GridWidth/MeanHHWS seconds unless UsableTime is "ALL")
24  90        HubHt           - Hub height [m] (should be > 0.5*GridHeight)
25  179       GridHeight      - Grid height [m]
26  252       GridWidth       - Grid width [m] (should be >= 2*(RotorRadius+ShaftLength))
27  0         VFlowAng        - Vertical mean flow (uptilt) angle [degrees]
28  0         HFlowAng        - Horizontal mean flow (skew) angle [degrees]
29
30  --------Meteorological Boundary Conditions-------------------
31  "IECKAI"  TurbModel       - Turbulence model
    ("IECKAI","IECVKM","GP_LLJ","NWTCUP","SMOOTH","WF_UPW","WF_07D","WF_14D","TIDAL","API"
    ,"USRINP","TIMESR", or "NONE")
32  "unused"  UserFile        - Name of the file that contains inputs for user-defined
    spectra or time series inputs (used only for "USRINP" and "TIMESR" models)
33  "1-Ed3"   IECstandard     - Number of IEC 61400-x standard (x=1,2, or 3 with optional
    61400-1 edition number (i.e. "1-Ed2") )
34  "18"      IECturbc        - IEC turbulence characteristic ("A", "B", "C" or the
    turbulence intensity in percent) ("KHTEST" option with NWTCUP model, not used for
    other models)
35  "NTM"     IEC_WindType    - IEC turbulence type ("NTM"=normal, "xETM"=extreme
    turbulence, "xEWM1"=extreme 1-year wind, "xEWM50"=extreme 50-year wind, where x=wind
    turbine class 1, 2, or 3)
36  default   ETMc            - IEC Extreme Turbulence Model "c" parameter [m/s]
37  "PL"      WindProfileType - Velocity profile type ("LOG";"PL"=power
    law;"JET";"H2L"=Log law for TIDAL model;"API";"USR";"TS";"IEC"=PL on rotor disk, LOG
    elsewhere; or "default")
38  "unused"  ProfileFile     - Name of the file that contains input profiles for
    WindProfileType="USR" and/or TurbModel="USRVKM" [-]
39  150       RefHt           - Height of the reference velocity (URef) [m]
40  9.3       URef            - Mean (total) velocity at the reference height [m/s] (or
    "default" for JET velocity profile) [must be 1-hr mean for API model; otherwise is
    the mean over AnalysisTime seconds]
41  default   ZJetMax         - Jet height [m] (used only for JET velocity profile, valid
    70-490 m)
42  0.2       PLExp           - Power law exponent [-] (or "default")
43  default   Z0              - Surface roughness length [m] (or "default")
44
45  --------Non-IEC Meteorological Boundary Conditions------------
```

```
default   Latitude        - Site latitude [degrees] (or "default")
0.05      RICH_NO         - Gradient Richardson number [-]
default   UStar           - Friction or shear velocity [m/s] (or "default")
default   ZI              - Mixing layer depth [m] (or "default")
default   PC_UW           - Hub mean u'w' Reynolds stress [m^2/s^2] (or "default" or
"none")
default   PC_UV           - Hub mean u'v' Reynolds stress [m^2/s^2] (or "default" or
"none")
default   PC_VW           - Hub mean v'w' Reynolds stress [m^2/s^2] (or "default" or
"none")

--------Spatial Coherence Parameters----------------------------
default   SCMod1           - u-component coherence model ("GENERAL", "IEC", "API",
"NONE", or "default")
default   SCMod2           - v-component coherence model ("GENERAL", "IEC", "NONE",
or "default")
default   SCMod3           - w-component coherence model ("GENERAL", "IEC", "NONE",
or "default")
default   InCDec1          - u-component coherence parameters for general or IEC
models [-, m^-1] (e.g. "10.0  0.3e-3" in quotes) (or "default")
default   InCDec2          - v-component coherence parameters for general or IEC
models [-, m^-1] (e.g. "10.0  0.3e-3" in quotes) (or "default")
default   InCDec3          - w-component coherence parameters for general or IEC
models [-, m^-1] (e.g. "10.0  0.3e-3" in quotes) (or "default")
default   CohExp           - Coherence exponent for general model [-] (or "default")

--------Coherent Turbulence Scaling Parameters-------------------
"C:/Yiwork_NREL/OffshoreWind/Turbsim/Test/EventData"  CTEventPath     - Name of the
path where event data files are located
"Random"  CTEventFile     - Type of event files ("LES", "DNS", or "RANDOM")
true      Randomize       - Randomize the disturbance scale and locations?
(true/false)
 1.0      DistScl         - Disturbance scale [-] (ratio of event dataset height to
 rotor disk). (Ignored when Randomize = true.)
 0.5      CTLy            - Fractional location of tower centerline from right [-]
 (looking downwind) to left side of the dataset. (Ignored when Randomize = true.)
 0.5      CTLz            - Fractional location of hub height from the bottom of the
 dataset. [-] (Ignored when Randomize = true.)
30.0      CTStartTime     - Minimum start time for coherent structures in
RootName.cts [seconds]

===================================================
! NOTE: Do not add or remove any lines in this file!
===================================================
```

G.2 Extreme turbulence model for 5 MW turbine

```
1   ---------TurbSim v2.00.* Input File------------------------
2   Example input file for TurbSim.
3   ---------Runtime Options-----------------------------------
4   False     Echo            - Echo input data to <RootName>.ech (flag)
5   2318573   RandSeed1       - First random seed  (-2147483648 to 2147483647)
6   RANLUX    RandSeed2       - Second random seed (-2147483648 to 2147483647) for
    intrinsic pRNG, or an alternative pRNG: "RanLux" or "RNSNLW"
7   False     WrBHHTP         - Output hub-height turbulence parameters in binary form?
    (Generates RootName.bin)
8   False     WrFHHTP         - Output hub-height turbulence parameters in formatted
    form?  (Generates RootName.dat)
9   False     WrADHH          - Output hub-height time-series data in AeroDyn form?
    (Generates RootName.hh)
10  False     WrADFF          - Output full-field time-series data in TurbSim/AeroDyn
    form? (Generates RootName.bts)
11  True      WrBLFF          - Output full-field time-series data in BLADED/AeroDyn
    form?  (Generates RootName.wnd)
12  False     WrADTWR         - Output tower time-series data? (Generates RootName.twr)
13  False     WrFMTFF         - Output full-field time-series data in formatted
    (readable) form?  (Generates RootName.u, RootName.v, RootName.w)
14  False     WrACT           - Output coherent turbulence time steps in AeroDyn form?
    (Generates RootName.cts)
15  True      Clockwise       - Clockwise rotation looking downwind? (used only for
    full-field binary files - not necessary for AeroDyn)
16   0        ScaleIEC        - Scale IEC turbulence models to exact target standard
     deviation? [0=no additional scaling; 1=use hub scale uniformly; 2=use individual
     scales]
17
18  --------Turbine/Model Specifications-----------------------
19  32        NumGrid_Z       - Vertical grid-point matrix dimension
20  32        NumGrid_Y       - Horizontal grid-point matrix dimension
21  0.03      TimeStep        - Time step [seconds]
22  600       AnalysisTime    - Length of analysis time series [seconds] (program will
    add time if necessary: AnalysisTime = MAX(AnalysisTime,
    UsableTime+GridWidth/MeanHHWS) )
23  600       UsableTime      - Usable length of output time series [seconds] (program
    will add GridWidth/MeanHHWS seconds unless UsableTime is "ALL")
24  90        HubHt           - Hub height [m] (should be > 0.5*GridHeight)
25  179       GridHeight      - Grid height [m]
26  252       GridWidth       - Grid width [m] (should be >= 2*(RotorRadius+ShaftLength))
27  0         VFlowAng        - Vertical mean flow (uptilt) angle [degrees]
28  0         HFlowAng        - Horizontal mean flow (skew) angle [degrees]
29
30  --------Meteorological Boundary Conditions-------------------
31  "IECKAI"  TurbModel       - Turbulence model
    ("IECKAI","IECVKM","GP_LLJ","NWTCUP","SMOOTH","WF_UPW","WF_07D","WF_14D","TIDAL","API"
    ,"USRINP","TIMESR", or "NONE")
32  "unused"  UserFile        - Name of the file that contains inputs for user-defined
    spectra or time series inputs (used only for "USRINP" and "TIMESR" models)
33  "1-Ed3"   IECstandard     - Number of IEC 61400-x standard (x=1,2, or 3 with optional
    61400-1 edition number (i.e. "1-Ed2") )
34  "A"       IECturbc        - IEC turbulence characteristic ("A", "B", "C" or the
    turbulence intensity in percent) ("KHTEST" option with NWTCUP model, not used for
    other models)
35  "1ETM"    IEC_WindType    - IEC turbulence type ("NTM"=normal, "xETM"=extreme
    turbulence, "xEWM1"=extreme 1-year wind, "xEWM50"=extreme 50-year wind, where x=wind
    turbine class 1, 2, or 3)
36  default   ETMc            - IEC Extreme Turbulence Model "c" parameter [m/s]
37  "PL"      WindProfileType - Velocity profile type ("LOG";"PL"=power
    law;"JET";"H2L"=Log law for TIDAL model;"API";"USR";"TS";"IEC"=PL on rotor disk, LOG
    elsewhere; or "default")
38  "unused"  ProfileFile     - Name of the file that contains input profiles for
    WindProfileType="USR" and/or TurbModel="USRVKM" [-]
39  150       RefHt           - Height of the reference velocity (URef) [m]
40  9.3       URef            - Mean (total) velocity at the reference height [m/s] (or
    "default" for JET velocity profile) [must be 1-hr mean for API model; otherwise is
    the mean over AnalysisTime seconds]
41  default   ZJetMax         - Jet height [m] (used only for JET velocity profile, valid
    70-490 m)
42  0.2       PLExp           - Power law exponent [-] (or "default")
43  default   Z0              - Surface roughness length [m] (or "default")
44
45  --------Non-IEC Meteorological Boundary Conditions------------
```

```
default   Latitude        - Site latitude [degrees] (or "default")
0.05      RICH_NO         - Gradient Richardson number [-]
default   UStar           - Friction or shear velocity [m/s] (or "default")
default   ZI              - Mixing layer depth [m] (or "default")
default   PC_UW           - Hub mean u'w' Reynolds stress [m^2/s^2] (or "default" or
"none")
default   PC_UV           - Hub mean u'v' Reynolds stress [m^2/s^2] (or "default" or
"none")
default   PC_VW           - Hub mean v'w' Reynolds stress [m^2/s^2] (or "default" or
"none")

--------Spatial Coherence Parameters----------------------------
default   SCMod1           - u-component coherence model ("GENERAL", "IEC", "API",
"NONE", or "default")
default   SCMod2           - v-component coherence model ("GENERAL", "IEC", "NONE",
or "default")
default   SCMod3           - w-component coherence model ("GENERAL", "IEC", "NONE",
or "default")
default   InCDec1          - u-component coherence parameters for general or IEC
models [-, m^-1] (e.g. "10.0  0.3e-3" in quotes) (or "default")
default   InCDec2          - v-component coherence parameters for general or IEC
models [-, m^-1] (e.g. "10.0  0.3e-3" in quotes) (or "default")
default   InCDec3          - w-component coherence parameters for general or IEC
models [-, m^-1] (e.g. "10.0  0.3e-3" in quotes) (or "default")
default   CohExp           - Coherence exponent for general model [-] (or "default")

--------Coherent Turbulence Scaling Parameters-------------------
"C:/Yiwork_NREL/OffshoreWind/Turbsim/Test/EventData"  CTEventPath     - Name of the
path where event data files are located
"Random"  CTEventFile     - Type of event files ("LES", "DNS", or "RANDOM")
true      Randomize       - Randomize the disturbance scale and locations?
(true/false)
 1.0      DistScl         - Disturbance scale [-] (ratio of event dataset height to
 rotor disk). (Ignored when Randomize = true.)
 0.5      CTLy            - Fractional location of tower centerline from right [-]
 (looking downwind) to left side of the dataset. (Ignored when Randomize = true.)
 0.5      CTLz            - Fractional location of hub height from the bottom of the
 dataset. [-] (Ignored when Randomize = true.)
30.0      CTStartTime     - Minimum start time for coherent structures in
RootName.cts [seconds]

===================================================
! NOTE: Do not add or remove any lines in this file!
===================================================
```

H

Appendix - Input for wave files

The wave files are created with the settings presented in Figure H.1. The principal angle, peak period, significant wave height, and peakedness are changed according to the correct load case.

Irregular waves	
1.23 Principal angle	0 °
☰ Spectrum	JONSWAP
1.23 Peak period	8 s
1.23 Significant wave heig...	3.6 m
☰ Seed scheme	Random
☰ Simulation scheme	Equal energy
1.23 Frequency delta limit	10
123 N	100
1.23 Error estimate	1
☰ Peakedness scheme	User defined
1.23 Peakedness	2.462
☰ Wave spreading	None
Extreme wave search	
123 Number of extremes	10
1.23 Search duration	600 s
1.23 Time step	1 s
1.23 Time buffer	15 s

Figure H.1. Input for wave files where the principal angle, peak period, significant wave height, and peakedness are changed according to the correct load case.

DEPARTMENT OF ARCHITECTURE AND CIVIL ENGINEERING
CHALMERS UNIVERSITY OF TECHNOLOGY
Gothenburg, Sweden 2023
www.chalmers.se

CHALMERS
UNIVERSITY OF TECHNOLOGY